Factors Governing Oxygen Reduction in Solid Oxide Fuel Cell Cathodes†

Stuart B. Adler

Department of Chemical Engineering, University of Washington, Box 351750, Seattle, Washington 98195-1750

Received March 30, 2004

Contents

† Dedicated to Brian Steele, 1929−2003. Researcher, Entrepreneur, Consensus Seeker.

1. Introduction

Recent worldwide interest in building a decentralized, hydrogen-based energy economy has refocused attention on the solid oxide fuel cell (SOFC) as a potential source of efficient, environmentally friendly, fuel-versatile electric power. Due to its high operating temperature, the SOFC offers several potential advantages over polymer-based fuel cells, including reversible electrode reactions, low internal resistance, high tolerance to typical catalyst poisons, production of high-quality waste heat for (among other uses) reformation of hydrocarbon fuels, as well as the possibility of burning hydrocarbon fuels directly.

Today, SOFCs are much closer to commercial reality than they were 20 years ago, due largely to technological advances in electrode material composition, microstructure control, thin-film ceramic fabrication, and stack and system design. These advances have led to dozens of active SOFC development programs in both stationary and mobile power and contributed to commercialization or development in a number of related technologies, including gas sensors,[1] solid-state electrolysis devices,[2] and ion-transport membranes for gas separation and partial oxidation.[3] Many reviews are available which summarize the technological advances made in SOFCs over the last 15−35 years—readers who are primarily interested in knowing the state-of-the art in materials, design, and fabrication (including the electrodes) are encouraged to consult these reviews.[4−12]

This review focuses on the factors governing SOFC cathode performance—advances we have made over

10.1021/cr020724o CCC: $48.50
Published on Web 10/13/2004

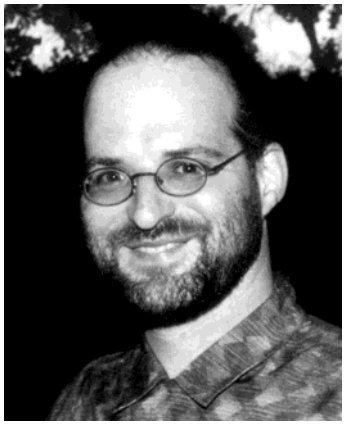

Stuart B Adler received his Ph.D. degree in Chemical Engineering in 1993 from the University of California, Berkeley, where he used high-temperature nuclear magnetic resonance (NMR) to probe microstructure, atomic motion, and electronic structure in electrochemical ceramics. His work in ionic materials continued at Imperial College (NATO–NSF fellow), where he developed continuum mechanical theories for high-temperature electrodes. In 1994 he moved to Ceramatec, Inc., where he led research supporting commercialization of ion transport membranes and other oxygen production and removal processes. After rejoining academia in 1999 (CWRU), he moved in 2002 to the University of Washington, Department of Chemical Engineering. There his work in electrochemical ceramics has continued, including advanced measurement and modeling techniques for solid-state electrodes and independent studies of kinetic, transport, and thermodynamic properties of solids. Professor Adler's awards include the NSF–NATO postdoctoral Fellowship (1993), and NSF Career Award (2001), and most recently he is the inaugural recipient of the biennial Charles W. Tobias Young Investigator Award of the Electrochemical Society (2004).

the last 20 years in our scientific understanding of oxygen reduction mechanisms, how these mechanisms vary for different materials and conditions, and remaining questions and challenges that have been generated by this large volume of work.

For the purposes of review, Figure 1 illustrates the basic function of the cathode in a solid oxide fuel cell. Whether acting alone or as part of a stack of cells, each cell consist of a free-standing or supported membrane of an oxygen-ion-conducting electrolyte, often yttria-stabilized zirconia (YSZ). Oxygen, which is fed (usually as air) to one side of the membrane, is reduced by the cathode to oxygen ions via the overall half-cell reaction

$$2e^- + \frac{1}{2}O_2 \rightarrow O^{2-} \qquad (1)$$

Oxygen ions thus created migrate selectively through the membrane to the anode, where they undergo a similar half-cell reaction with a gaseous fuel (either H_2, syngas, or a hydrocarbon) to produce H_2O and CO_2. The flow of electrons liberated and consumed at the anode and cathode, respectively, deliver some portion of the reversible work of the reaction to the external circuit. The percentage of reversible work converted to electrical work depends on (among other things) the internal losses in the cell, including the ohmic resistance of the electrolyte, as well as the overpotential losses at the anode and cathode.

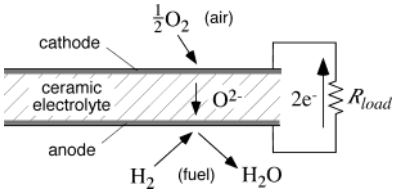

Figure 1. Schematic showing the roles of anode, cathode, and electrolyte in a solid oxide fuel cell (SOFC).

While ohmic losses in oxide electrolytes are largely understood today, the physics governing the electrode overpotential losses remain an enormous focus of research, with substantial progress being made only in the last 15−20 years. This shift in emphasis from the electrolyte to the electrodes has been driven (in part) by an ability to make increasingly thinner, less resistive, electrolyte films as well as a drive toward lower operating temperatures where the electrodes are a higher percentage of the voltage loss (due to higher activation energy). Much of this work has focused on the cathode, largely because oxygen reduction is generally thought to be the more difficult reaction to activate on SOFCs operating at commercially relevant temperatures. Workers have tried to not only understand electrode mechanisms, but also explore new electrode materials and microstructures, elucidate structure−property−performance relationships, and understand how and why electrode performance changes with time, temperature, thermal cycling, operating conditions, impurities, or other factors that may be pertinent in the design of multicell stacks and systems.

This review attempts to summarize the advances made in our understanding of SOFC cathodes since approximately the early 1980s, when there was a surge in worldwide SOFC research activity. According to the ISI Web-Of-Science *Science Citation Index*, more than 1000 refereed articles pertinent to the topic of SOFC cathodes and cathode materials have been published since 1980. Regrettably, it is not possible to cover this enormous volume of work in uniform detail. Also, new insights regarding SOFC cathodes have not occurred in a vacuum−they have benefited substantially from advances in electrochemical measurement and modeling techniques, improved understanding of cathode materials properties, and new fabrication and characterization techniques which allow control and measurement of electrode microstructure. These enabling developments can only be tangentially reviewed here.

Rather this review focuses on how new approaches have been used by workers to better understand cathode mechanisms and how these mechanisms relate to materials properties and microstructure. This review also attempts to identify ongoing critical questions that will likely be the focus of cathode research and development over the next 10−15 years. In highlighting and discussing in detail the most influential and important work in the field, this review also hopes to summarize the general trends and consensus understanding that has developed in parallel with these key insights. In telling the story of these new developments and challenges, it is the sincere hope of the author to do justice to the many scientists and engineers who have spent their careers contributing to this fascinating and potentially important area of research.

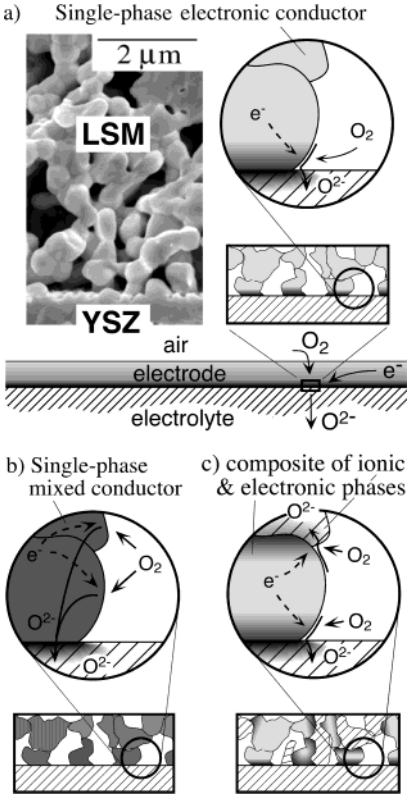

Figure 2. Common strategies for SOFC cathodes: (a) porous single-phase electronically conductive oxide such as $(La,Sr)MnO_3$ (LSM); (b) porous single-phase mixed conductor; (c) porous two-phase composite. The SEM micrograph of LSM on YSZ in a is adapted from ref 84. (Adapted with permission from ref 84. Copyright 1997 Swiss Federal Institute of Technology.)

2. Understanding the Three-Phase Boundary—A Long History of Inquiry

As illustrated in Figure 2, a SOFC cathode typically consists of a porous single phase or two-phase composite matrix cast onto an oxide ion conducting electrolyte substrate using a low-cost slurry-based process involving powder precursors, such as screen printing. The oxygen, which we wish to reduce to O^{2-}, diffuses into the open pores of the electrode and is reduced somewhere within this matrix. For a traditional porous electronic conducting electrode material such as Pt or $(La,Sr)MnO_3$ (LSM) (Figure 2a), reduction of oxygen is generally thought to be confined close to the electrode/electrolyte interface, where the gas has simultaneous access to both the electronically and ionically conductive phases (illustrated as the shaded active region).

One strategy for trying to improve performance has been to replace LSM with a single-phase *mixed conductor* (material which conducts both oxygen ions and electrons), such as $La_{1-x}Sr_xCo_{1-y}Fe_yO_{3-\delta}$ (LSCF) (Figure 2b). By introducing bulk ionic transport, oxygen can be reduced to O^{2-} over a significant portion of the electrode surface, thereby extending the size of the active region and improving the kinetics at temperatures below 800 °C.[9,13−28] Electronically conductive LSM can also be combined with an ionically conducting oxide (YSZ itself or rare-earth-doped ceria) in a porous composite microstructure (Figure 2c), thereby increasing the contact area between electronically and ionically conductive phases.[29−34] These strategies can also be combined wherein a composite electrode contains both ionic and mixed conducting phases.[29,35,36]

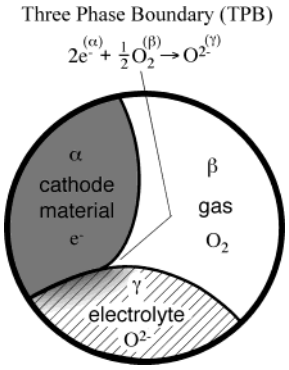

Figure 3. Phenomenological roles of the electronically conducting (electronic) phase (α), gas phase (β), and ionically conducting (ionic) phase (γ) in accomplishing oxygen reduction.

While the various strategies described above have proven promising, SOFC electrodes remain largely empirically understood and far from optimized and suffer from numerous short- and long-term degradation problems.[16,37,38] Reported performances vary tremendously with many unknown variables at work and limited understanding as to how materials properties and microstructure relate to performance and long-term stability.[39,40]

At the risk of oversimplification, Figure 3 illustrates the phenomenological role of the cathode material, electrolyte material, and gas in accomplishing the reaction in eq 1. Regardless of the microstructure, a common feature of all cathodes is that the cathode material itself (α) (an electronic conductor) makes intimate contact with an electrolyte phase (γ) (an oxygen-ion conductor) along an interface, this interface also being exposed at its edge to the gas phase (β) (where O_2 is available). Phase α is connected at some point away from the interface to a source of electronic current, providing a conduction path for electrons to the interface. Likewise, the electrolyte phase γ is either itself the electrolyte membrane or connected by a continuous ionic path to the electrolyte membrane, providing a sink for the oxygen ions produced in the reaction. The oxygen gas (which diffuses from outside the electrode through interconnected pores or channels) is reduced somewhere in the vicinity of this $\alpha/\beta/\gamma$ interface.

Since this reaction involves ions, electrons, and gas molecules in three separate phases, the edge of the α/γ interface that makes contact with the gas phase β is often described as the three-phase (or triple-phase) boundary (TPB). The concept of the TPB actually dates to the 1920s,[41] when workers studying the oxidation of H_2 on platinum introduced this concept to explain why Pt must be exposed simultaneously to both solution and gas to get significant reaction. This type of electrode, which Schmid called "die diffusiongaselektrode"[41] or gas-diffusion electrode (GDE), is still called this today by workers studying solution- or polymer-based fuel cells. As

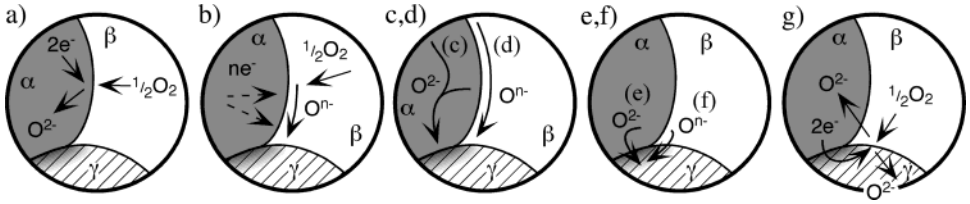

Figure 4. Some mechanisms thought to govern oxygen reduction in SOFC cathodes. Phases α, *β*, and *γ* refer to the electronic phase, gas phase, and ionic phase, respectively: (a) Incorporation of oxygen into the bulk of the electronic phase (if mixed conducting); (b) adsorption and/or partial reduction of oxygen on the surface of the electronic phase; (c) bulk or (d) surface transport of O^{2-} or O^{n-}, respectively, to the α/γ interface, (e) Electrochemical charge transfer of O^{2-} or (f) combinations of O^{n-} and e^-, respectively, across the α/γ interface, and (g) rates of one or more of these mechanisms wherein the electrolyte itself is active for generation and transport of electroactive oxygen species.

implied by the name, all GDE reactions share the common feature of involving gas-phase molecules and thus represent a fundamental departure from traditional electrochemical kinetics governing charge transfer across a 2-dimensional interface.[42]

In the case of SOFCs, a large volume of work shows that for many SOFC electrodes, overall performance scales with the 1D geometric length of this three-phase boundary. As such, the TBP concept and electrode performance models based on it have proven to be some of the most useful phenomenological concepts for guiding design and fabrication of SOFC cathodes, particularly the microstructure.

However, in trying to develop a deeper understanding of the physics and chemistry governing the SOFC cathode reaction, the concept of the three-phase boundary somewhat begs the question as to what specific physical processes actually occur in the vicinity of the three-phase interface and how these processes depend on materials properties, microstructure, etc. Workers studying aqueous gas-diffusion electrodes in the mid-1960s recognized the limitations of the three-phase boundary concept.[43,44] As an alternative, they began to break down the electrode reaction into individual steps, including the dissolution and diffusion of H_2 in solution and the oxidation of dissolved H_2 at the Pt/solution interface. These and subsequent studies contributed significantly to our fundamental and practical understanding of solution and polymer GDEs, including how molecular diffusion processes contribute to the overall $i-V$ characteristics and how best to arrange the electrolyte inside a flooded electrode. Of particular note is the observation that diffusion processes can often co-limit electrode performance far below limiting current and can mimic activated behavior.[45] Thus, the phenomenological observation that a GDE obeys Tafel (or Butler−Volmer) kinetics provides no assurance that the electrode is, in fact, activation limited.

Although the SOFC community has generally maintained an empirical approach to the three-phase boundary longer than the aqueous and polymer literature, the last 20 years have seen a similar transformation of our understanding of SOFC cathode kinetics. Few examples remain today of solid-state electrochemical reactions that are not known to be at least partially limited by solid-state or surface diffusion processes or chemical catalytic processes remote from the electrochemical−kinetic interface.

Figure 4 outlines some of the mechanisms either known or theorized in the literature to be important in determining the rate of the oxygen reduction in SOFC cathodes. Oxygen molecules are generally thought to adsorb somewhere onto one or more solid surface(s), where they undergo catalytic and/or electrocatalytic reduction steps to form partially reduced ionic/atomic species (sometimes called "electroactive species"[46]). Before, after, or between partial reduction steps, these species must transport along surfaces, interfaces, or inside the bulk of the electrode material(s) to the electrolyte, where they are fully and formally incorporated as electrolytic O^{2-}. If, how, and where any of these processes happen and what step(s) are rate determining for a particular electrode is often only partially understood.

As evidenced by the cases reviewed below, no single mechanism has been discovered which explains all electrodes. Furthermore, arguments in the literature concerning which theory is correct for a given cathode system usually end in a standoff of equally legitimate interpretations of limited data on dubiously comparable samples. Which step(s) are rate determining, and thus which factors are important for cathode performance, depends strongly on the material(s), microstructure, and processing of the electrode as well as the conditions under which the electrode is tested, including temperature, atmosphere, polarization, time, or other factors, some of which may not be known.

Given these uncertainties, the approach taken here is to review the asymptotic behavior of well-characterized and studied systems, where enough scientific evidence exists to reach a reasonable consensus. Perhaps then it becomes easier to discuss the possible processes governing more complex and less well-characterized systems (and to propose a new set of testable hypotheses about them). To that end, we begin by examining the case of platinum and other noble metals on zirconia, which perhaps enjoys the longest and richest history of research available today.

3. Platinum Electrodes—Interplay of Chemical and Electrochemical Steps

Oxygen reduction on yttria-doped zirconia (YSZ) was first accomplished over 100 years ago (for the purpose of generating light) using a porous platinum electrode.[4] Since then, oxygen reduction on Pt has been one of the most well-studied electrode reaction

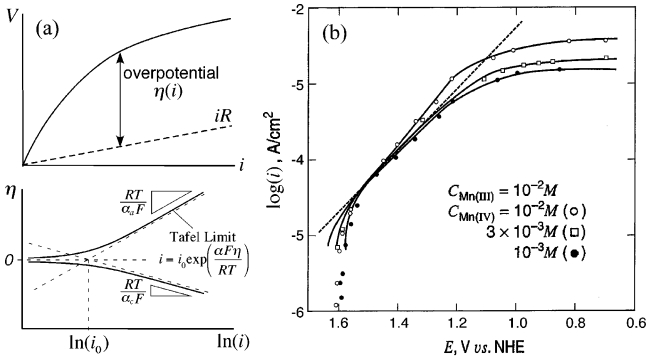

Figure 5. Measurement and analysis of steady-state $i-V$ characteristics. (a) Following subtraction of ohmic losses (determined from impedance or current-interrupt measurements), the electrode overpotential η is plotted vs ln(i). For systems governed by classic electrochemical kinetics, the slope at high overpotential yields anodic and cathodic transfer coefficients (α_a and α_c) while the intercept yields the exchange current density (i_0). These parameters can be used in an empirical rate expression for the kinetics (Butler−Volmer equation) or related to more specific parameters associated with individual reaction steps.[42] (b) Example of Mn(IV) reduction to Mn(III) at a Pt electrode in 7.5 M H_2SO_4 solution at 25 °C.[362] Below limiting current the system obeys Tafel kinetics with $\alpha_a \approx 1/4$. Data are from ref 363. (Reprinted with permission from ref 362. Copyright 2001 John Wiley & Sons.)

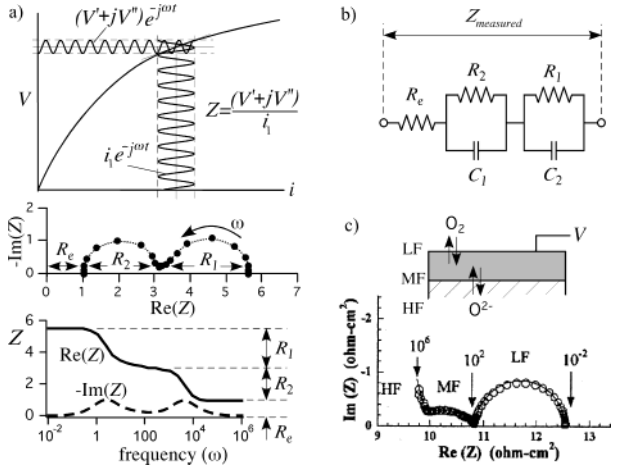

Figure 6. Electrochemical impedance spectroscopy (EIS). (a) The steady-periodic linear response of a cell to a sinusoidal current or voltage perturbation is measured and analyzed in terms of gain and phase shift as a function of frequency (ω). Results are usually expressed in terms of the impedance (Z), the complex ratio of voltage displacement to current displacement (often reported on a Nyquist or Bode plot). Ideally, each charge-transfer-limiting process (electrolyte, electrode process #1, electrode process #2, etc.) is only manifest below a distinct characteristic frequency, resulting in separate features or "arcs" in the impedance diagram of magnitude R_e, R_1, R_2, etc. (b) Since EIS is a linear response technique, the time-response of individual processes is often modeled in terms of equivalent circuit elements, with resistance representing charge transfer and capacitance (C_1, C_2, etc.) representing charge polarization. This description is often extended to noninterfacial processes by introduction of additional empirically or theoretically derived circuit elements. (c) Example of a dense $La_{0.5}Sr_{0.5}CoO_{3-\delta}$ film on single-crystal YSZ at 750 °C in oxygen.[162] The total impedance in this case is a sum of the electrolyte impedance (high frequency), an interfacial impedance at medium frequency (MF), and a low-frequency (LF) impedance associated with O_2 oxidation/reduction at the surface of the film (see section 4.3). Data are from ref 165. (Adapted with permission ref 165. Copyright 2001 American Institute of Physics.)

in the history of solid-state ionics. Yet the Pt/solid electrolyte interface is still actively studied today, with many open questions remaining. Many of these questions are relevant to more complex but technologically advanced cathode materials with relevance to today's SOFCs. Thus, platinum constitutes a useful foundation on which to build our understanding of all SOFC cathodes.

3.1. Two Schools of Thought

The field of electrochemical kinetics has traditionally focused on charge-transfer reactions occurring at the surface of a metal electrode in contact with a liquid electrolyte.[42] As shown in Figure 5, the steady-state $i-V$ characteristics for this type of reaction often obey Tafel kinetics (linear dependence of ln(i) vs V), which can be analyzed in terms of specific rate-limiting steps occurring at the interface.[47] As such, measurement and analysis of Tafel parameters have proven to be one of the most useful techniques for understanding electrode reactions, both as a means of isolating the nonlinear electrode response from the linear electrolyte losses as well as providing a theoretical framework for relating these parameters to specific mechanisms.

However, as mentioned previously, gas-diffusion electrodes usually deviate substantially from traditional electrochemical−kinetic behavior, often being limited by multiple rate-determining factors and/or changes in those factors with overpotential or other conditions. In attempting to analyze this type of electrode, one of the most influential experimental techniques to take hold in the solid-state electrochemical literature in the last 35 years is electrochemical impedance spectroscopy (EIS)—also know as a.c. impedance. As illustrated in Figure 6, by measuring the sinusoidal $i-V$ response as a function of frequency, EIS seeks to separate and identify reaction steps via time scale.[48,49] Along with current interruption experiments, early measurements of this type on Pt/YSZ or Pt/ceria allowed workers to more specifically isolate the electrode polarization from the electrolyte and begin analyzing this polarization in terms of time-dependent phenomena.

On the basis of the two classes of measurements shown in Figures 5 and 6, workers split into two fundamentally different schools of thought. The first, rooted in the well-established tradition of classical electrochemical kinetics, focused on the observation that these electrodes tend to obey Tafel kinetics at moderate to high overpotential. For example, Figure 7 shows Tafel plots for Pt electrodes on calcia-doped ceria, measured by Wang and Nowick using current interruption techniques over a wide range of T and P_{O_2}.[50,51] Except for limiting current behavior at high cathodic overpotential, these results fit a Butler−Volmer expression, yielding (at least empirically) an exchange current density and anodic and cathodic transfer coefficients. On the basis of this result, the authors concluded that the electrode reaction must be limited by electrochemical kinetics at the interface.

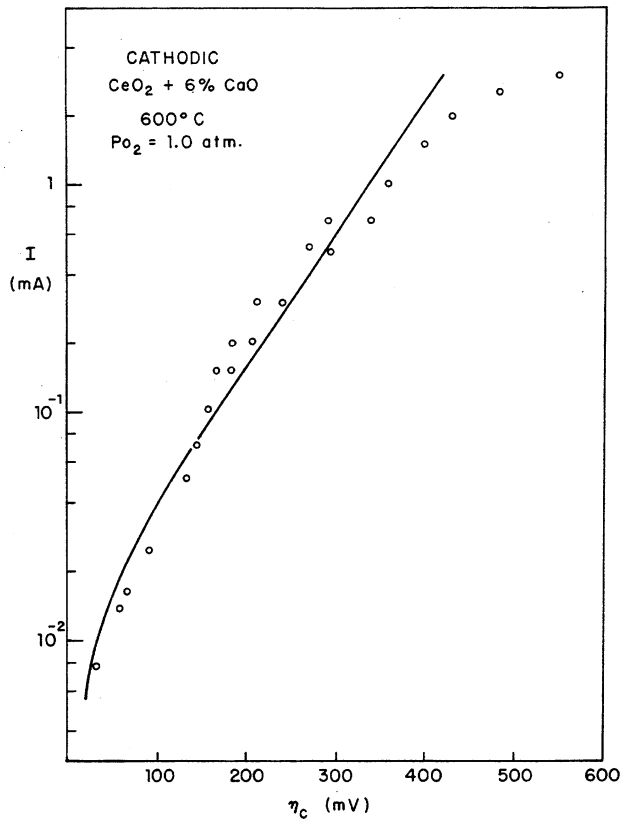

Figure 7. Steady-state cathodic current−overpotential characteristics of porous Pt electrodes on Ca-doped ceria, measured at 600 °C in air using current-interruption. (Reprinted with permission from ref 51. Copyright 1979 Electrochemical Society, Inc.)

The authors modeled the P_{O_2} dependence of the exchange current density in terms of the dissociative adsorption of oxygen on the Pt surface, which influences the exchange current through the equilibrium concentration of adsorbed atomic oxygen. These measurements also showed that the kinetics are independent of electrolyte dopant concentration, leading the authors to suggest that the limiting electrochemical step must occur on the Pt surface. Subsequent publications (as recent as the late 1990s) have continued to reinforce a default viewpoint that SOFC gas-diffusion electrodes are fundamentally limited by electrochemical kinetics.[17,52,53]

In contrast, the second school of thought focused on the impedance of these electrodes and the fact that when modeled as an equivalent RC circuit, they exhibit a very large capacitance—too large to be explained in terms of traditional double-layer polarization at an interface.[48] One of the earliest groups to apply impedance for this purpose was Kleitz and co-workers, who studied porous Pt and other noble-metal catalysts on YSZ.[54] As shown in Figure 8, they generally found that cells respond at frequencies well below 1000 Hz, several orders of magnitude too low to explain in terms of traditional interfacial polarization. Rather, the authors interpreted these low-frequency capacitive effects as changes in concentration of "neutral-O" in the vicinity of the three-phase boundary, concluding that the overpotential must be (at least in part) a concentration overpotential rather than a simple electrochemical−kinetic resistance.

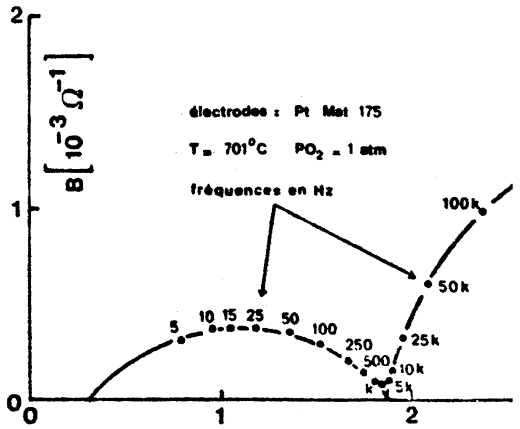

Figure 8. Complex admittance (reciprocal of impedance) or porous Pt on YSZ in air at 700 °C. The largest portion of the impedance (appearing at lowest admittance) exhibits a response frequency of ∼20 Hz (response time of ∼0.01 s). (Reprinted with permission from ref 54. Copyright 1973 Laboratoire d'Electrochimie et de Physicochimie des Materiaux et des Interfaces (INPG and CNRS), Saint Martin d'Heres, France.)

As discussed below, the hindsight of the last 30 years suggests that the truth falls in a gray area between these two schools of thought, with chemical adsorption, surface transport, and interfacial electrochemical kinetics all playing a significant role (as well as other factors which are still not fully understood). For this reason, platinum serves as a good starting point since it helps to illustrate how these various factors come into play and how they influence the overall electrode performance and characteristics.

3.2. Chemical Contributions to the Overpotential

To better understand the "diffusion-limited" school of thought mentioned above, it is worth digressing momentarily on another "noble"-metal electrode system: silver on YSZ. Kleitz and co-workers conducted a series of studies of silver point-contact microelectrodes, made by solidifying small (200−2000 μm) silver droplets onto polished YSZ surfaces.[55] Following in-situ fabrication, the impedance of these silver microelectrodes was measured as a function of T (600−800 °C), P_{O_2} (0.01−1.0 atm), and droplet radius. As an example, Figure 9a shows a Nyquist plot of the impedance under one set of conditions, which the authors resolve into two primary components, the largest (most resistive) occurring at very low frequency (0.01−0.1 Hz) and the second smaller component at moderately low frequency (∼10 Hz).

Restricting our attention to the more significant, lower-frequency impedance, the authors argue (based on time scale as well as other factors) that a majority of the observed overpotential is associated with absorption and diffusion of atomic oxygen inside the silver droplet. Their proposed mechanism is illustrated in Figure 9b. According to this model, cathodic polarization provides a driving force for atomic oxygen dissolved in the silver to be reduced to oxygen ions and pulled into the electrolyte at the silver/YSZ interface. The resulting depletion of oxygen in the metal near the silver/YSZ interface creates a chemical potential driving force for dissolved oxygen to

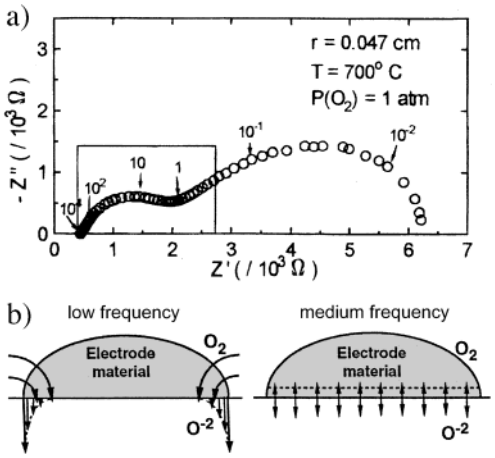

Figure 9. (a) Impedance of a single silver droplet solidified on YSZ, measured at 700 °C in oxygen. (b) Interpretation of the impedance in terms of bulk absorption and transport of oxygen in silver. Explanation for the bifurcation in response frequency: At low frequency, transport occurs everywhere in the droplet, with a higher flux near the droplet edge. At medium frequency transport is confined to a small but uniform region near the silver/YSZ interface, involving little reduction/oxidation of gaseous O_2. (Adapted with permission from ref 364. Copyright 1997 Electrochemical Society, Inc.)

diffuse to the interface from the bulk of the silver, leading ultimately to depletion of dissolved oxygen near the silver/gas interface. Depletion of oxygen in the silver relative to equilibrium with the gas then provides a driving force for dissociative absorption of gaseous O_2 into the silver. Thus, at steady state, a continuous gradient in oxygen concentration is established that partly limits the overall reaction rate. The authors argue that only this mechanism can explain the very large effective capacitance of the electrode (~1 F/cm^2). Further evidence for this interpretation includes both the T and P_{O_2} dependence of the resistance and capacitance, which are found to be quantitatively consistent with independently measured oxygen absorption and diffusion properties of silver. Van Herle and McEvoy subsequently confirmed these findings,[56] concluding further that the kinetics are partially limited by both absorption of gaseous O_2 into the silver as well as diffusion of atomic oxygen through the silver.

Although there are a number of other unresolved issues in interpreting these data (not discussed here), what is clear from their analysis is that a significant portion of the resistance to oxygen reduction in this system is not determined by how fast oxygen is reduced at the Ag/YSZ interface but rather how fast oxygen can get to that interface. On this basis and other examples, Kleitz argued in 1993 that all cathode reactions involve the equivalent of dissolved oxygen in silver—some sort of "electroactive" oxygen species, which must be replenished somehow from the gas phase. This principle, which he titled the "reaction pathway model", is illustrated in Figure 10. In this model, any charge-transfer (current) pathway A−E−B can be intermediately limited at point E by the availability of a neutral species (or neutral combination of species), whose flow rate (C−E) is not driven directly by electrical-state driving forces.

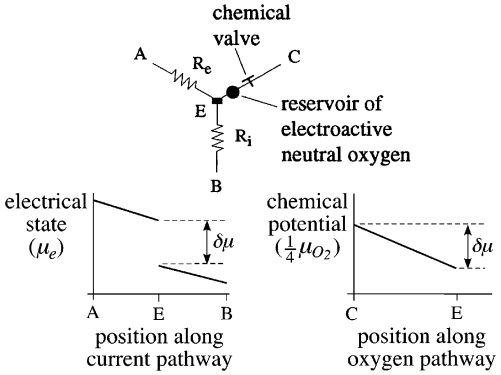

Figure 10. Kleitz's reaction pathway model for solid-state gas-diffusion electrodes. Traditionally, losses in reversible work at an electrochemical interface can be described as a series of contiguous drops in electrical state along a current pathway, for example, A−E−B. However, if charge transfer at point E is limited by the availability of a neutral electroactive intermediate (in this case ad(b)sorbed oxygen at the interface), a thermodynamic (Nernstian) step in electrical state ($\delta\mu$) develops, related to the displacement in concentration of that intermediate from equilibrium. In this way it is possible for irreversibilities along a current-independent pathway (in this case formation and transport of electroactive oxygen) to manifest themselves as electrical "resistance." This type of "chemical valve", as Kleitz calls it, may also involve a significant reservoir of intermediates that appears as a "capacitance" in transient measurements such as impedance. Portions of this image are adapted from ref 46. (Adapted with permission from ref 46. Copyright 1993 Risø National Laboratory, Denmark.)

For the purposes of clarity throughout the rest of this review, we hereby define such a neutral flow as a chemical process, since it is driven by chemical potential driving forces and may occur at a rate independent of the faradaic current (except in the limit of steady state).[366] Applying this definition, examples of chemical processes include ad(b)sorption and/or dissociation of molecular species, gas-phase diffusion, diffusion of dissolved neutral species, ambipolar (chemical) diffusion of neutral combinations of ions/electrons, or surface diffusion of adsorbed species associated with a mobile mirror charge in the solid phase. Since such species or combinations thereof are net neutral, they can accumulate in large quantity in bulk or on surfaces without violating electroneutrality, acting as a reservoir and leading to slow response times. As we will see for Pt, as well as ensuing examples involving mixed conductors, all electrode reactions are now believed to involve some sort of "chemical valve" of this type which may contribute none, some, or all of the macroscopically observed polarization resistance.

3.3. Evidence for Diffusion and Adsorption Limitations on Platinum

A significant step forward in our understanding of Pt was taken by Verkerk and Burgraff, who in 1983 analyzed the impedance of porous sputtered Pt (and Pt gauze) electrodes on YSZ and gadolinia-doped ceria (GDC).[57] As shown in Figure 11, they used a Randles circuit to model the interfacial contributions to the impedance, allowing them to subtract from the data the contributions of uncompensated iR and

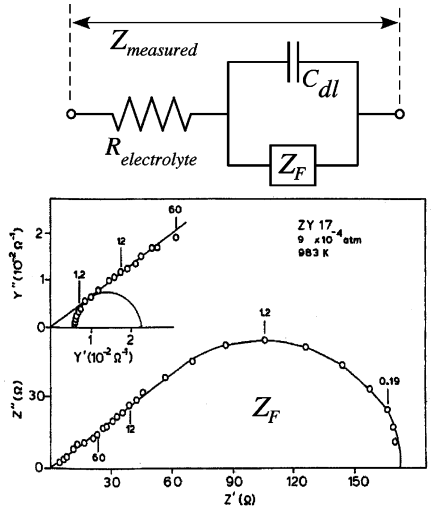

Figure 11. Electrochemical impedance of porous Pt on YSZ at 710 °C and $P_{O_2} = 10^{-3}$ atm. Data has been corrected for double-layer capacitance as described in ref 79. (Reprinted with permission from ref 79. Copyright 1983 The Electrochemical Society, Inc.)

double-layer capacitance at the metal/electrolyte interface. The remaining "faradaic" impedance (Z_F) was found, in the limit of high frequency, to have similar real and imaginary contributions (∼45° line on a Nyquist plot), which is a strong indicator that diffusion is an important step in the reaction.[49] They also showed that the P_{O_2} dependence of the impedance is independent of the electrolyte, suggesting that the diffusion process occurs on the Pt surface (or in the gas phase at lower frequencies and low P_{O_2}). On the basis of independent measurements of oxygen diffusion rates on Pt,[58] the authors estimated the diffusion distance to be about 50 nm, which supports a commonly held understanding that electrode kinetics should scale with total TPB length (at least for Pt particles larger than $\sim 10^{-5}$ cm). However, an important element left out of this analysis is why the diffusion distance is ∼50 nm. What establishes this distance? Also, if diffusion is rate limiting, how can one explain the Tafel behavior observed for these electrodes at moderate to high overpotential?

In 1987, Mizusaki and co-workers published two papers that addressed some of these questions.[59,60] By applying traditional electrochemical kinetics, they argued that the Langmuir isotherm for oxygen adsorption on platinum yields the incorrect P_{O_2} dependence for the exchange current density extracted from the data by fitting to a Butler−Volmer rate expression. They therefore concluded that electrochemical kinetics at the three-phase boundary cannot be the rate-limiting step. Instead, they proposed that the reaction is limited by either (1) dissociative adsorption of oxygen molecules on the Pt surface or (2) surface diffusion of adsorbed oxygen atoms to the three-phase interface. On the basis of the P_{O_2} dependence found in their measurements, they conclude that both situations are possible and that above 600 °C the electrode is diffusion limited while below 500 °C it becomes limited by the rate of dissociative adsorption of O_2. In either case, however, they derive a logarithmic dependence of current on overpotential, which mimics Tafel kinetics. In this way they showed that chemical steps (embodying Kleitz's reaction pathway concept) can still obey "classical" Butler−Volmer kinetics.

How can diffusion or other chemical steps give rise to Tafel behavior? An examination of Mizusaki's derivation[59] shows that even when interfacial electrochemical kinetic steps are equilibrated, there remains a Nernstian relationship between the applied potential and the activity of electroactive oxygen on the Pt surface. Thus, as the steady-state potential is varied, the surface concentration at the TPB changes approximately logarithmically. If the rate of adsorption and/or diffusion has a linear or power-law dependence on the surface concentration, it will also depend logarithmically on the potential, leading to a logarithmic dependence of current on potential. Thus, the mere existence of a Tafel slope means very little in terms of proving electrochemical kinetics is limiting or in identifying electrochemical kinetic steps. Rather, the important issue is how the Tafel parameters (empirical though they may be) depend on P_{O_2} and temperature and whether these can be rationalized in terms of specific chemical or electrochemical steps.

During the late 1980s some disagreement appeared in the literature concerning where oxygen concentration gradients exist on the Pt surface. In contrast to Mizusaki, Wang proposed a model in which electroactive oxygen is reduced along the entire interface between Pt and YSZ, with the rate-limiting diffusion process being the diffusion of adsorbed oxygen along the Pt/YSZ interface from the TPB.[61] A similar model was considered by van Hassel for Au on YSZ.[62] In 1990, however, Robertson and Michaels addressed this question for Pt by modeling steady-state polarization and potential-step chronoamperometry measurements on Pt/YSZ.[63] As illustrated in Figure 12a, they considered two cases. Model I: Adsorbed oxygen is reduced along the entire Pt/YSZ interface but must diffuse along this interface from the TPB (where surface coverage is considered to be in equilibrium with the gas). Model II: Adsorbed oxygen is reduced at the three-phase boundary but due to lack of equilibrium with the gas must diffuse along the gas-exposed surface from some other point further away. They found that the qualitative and quantitative features of their data could only be explained using this second model. In particular, as shown in Figure 12b, only diffusion on the gas-exposed Pt surface could explain the $t^{1/2}$ semi-infinite diffusion (Cottrell) behavior of the current at short times. In contrast, the first model predicts constant current until oxygen is depleted at the interface, followed by exponential decay, which was not observed. Subsequent studies of the P_{O_2} dependence of the impedance have reinforced the view that the dominant rate-determining transport step occurs on the gas-exposed Pt surface.[56,64,65]

Some debate has also appeared concerning the "charge state" of adsorbed oxygen on the Pt surface, whether it is O^{2-}, O^-, uncharged O, etc. This question arises, for example, when one tries to interpret Tafel parameters in terms of a cascade of surface-mediated electrochemical−kinetic steps.[66] However, as already

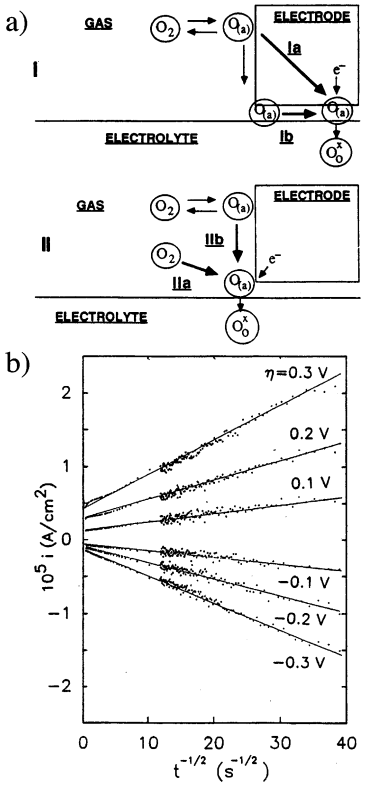

Figure 12. Modeling and measurement of oxygen surface diffusion on Pt. (a) Model I: adsorbed oxygen remains in equilibrium with the gas along the gas-exposed Pt surface but must diffuse along the Pt/YSZ interface to reach an active site for reduction. Model II: adsorbed oxygen is reduced at the TPB but must diffuse there from the gas-exposed Pt surface, which becomes depleted of oxygen near the TPB due to a finite rate of adsorption. (b) Cotrell plot of current at a porous Pt electrode at 600 °C and $P_{O_2} = 10^{-4}$ atm vs time. The linear dependence of current with $t^{-1/2}$ at short times implies semi-infinite diffusion, which is shown by the authors to be consistent only with Model II. (Reprinted with permission from ref 63. Copyright 1990 Electrochemical Society, Inc.)

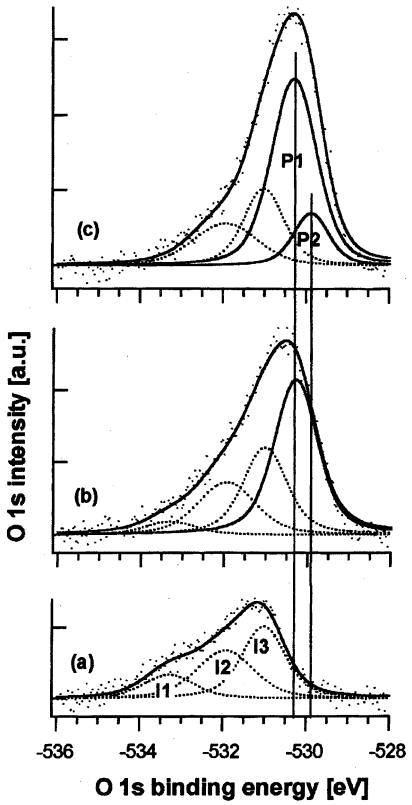

Figure 13. XPS spectra of adsorbed oxygen on a thin-film Pt electrode on single-crystal YSZ: (a) residual O^{1s} spectrum following several "cleaning" cycles at elevated temperature and vacuum ($<10^{-9}$ mbar); (b) O^{1s} spectrum at 350−400 °C under constant $P_{O_2} = 10^{-6}$ mbar; (c) O^{1s} spectrum at 350−400 °C in a vacuum during anodic polarization. The peak "P1", corresponding to the known spectrum for chemisorbed oxygen at 530.4 eV, appears upon both adsorption of oxygen from the gas (b) and electrochemical pumping of oxygen from YSZ (c). A secondary peak "P2" at lower binding energy also appears upon electrochemical pumping but is too close in energy to P1 to explain in terms of differences in charge state. The authors propose that P2 represents a different adsorption site populated only at high coverage. (Reprinted with permission from ref 67. Copyright 2001 Elsevier.)

demonstrated by the work reviewed above, a significant fraction of the overpotential can arise from chemical steps (adsorption and/or diffusion). In analyzing the rates of these chemical processes, one must question whether such partial charge assignments really have any physical meaning from the viewpoint of continuum mechanics. As recently shown by Luerssen et al. (Figure 13),[67] XPS reveals no difference in electronic structure between oxygen dissociatively adsorbed onto Pt from the gas vs "ionic oxygen species" pumped electrochemically from YSZ onto the Pt surface. Both oxygen sources result in the same change in measurable work function (through the surface dipole concentration). In other words, the "charge" associated with adsorbed oxygen appears to be a unique feature of the surface chemistry of adsorption (e.g., ionic vs covalent) rather than a variable formal valance state subject to electrochemical reduction/oxidation. In this sense, it is somewhat irrelevant what the charge on oxygen is, since (as recently demonstrated by Janek[68]) the driving force for adsorption and transport of absorbed oxygen is a change or gradient in surface *coverage* (related to oxygen activity). The rate expressions for these processes are independent of electrical state since they involve neutral combinations of adsorbed oxygen and mirror charges in Pt.

3.4. Important Refinement: Co-limited Reaction Kinetics

As shown by Mizusaki,[59,60] the faradaic processes occurring on platinum are quite complex, with the possibility that more than one rate-limiting step can dominate under various conditions. A primary piece of evidence that diffusion on Pt plays a role is a 45° straight-line relationship in the Nyquist plot at high frequency, which has led to the widespread use of Warburg elements in equivalent circuit modeling. However, Pt electrodes generally exhibit an impedance considerably different from than predicted by a Warburg element, even when corrected for double-layer capacitance.[57] Indeed, as recently pointed out by Boukamp, the 45° relationship is not unique to finite-length diffusion, but it is the case for *any* system that reduces to semi-infinite diffusion in the

limit of high frequency, including systems limited partially (or entirely) by kinetic processes at steady state.[69]

To that end, an important idea contributed by Robertson and Michaels[63] was that oxygen reduction on Pt could potentially be *co-limited* by adsorption and diffusion rather than by just one or the other. In modeling the system, they noted that it is not possible for adsorbed oxygen to be in chemical equilibrium with the gas at the gas-exposed Pt surface while at the same time being in electrochemical equilibrium with the applied potential at the three-phase boundary. To resolve this singularity, prior (and several subsequent) models for diffusion introduce an artificial fixed "diffusion length" governing transport from the gas-equilibrated surface to the TPB.[56,57,59,64,65,70] In contrast, Robertson and Michaels proposed that surface coverage is not in equilibrium with the gas but instead is governed simultaneously by finite rates of adsorption onto and diffusion along the Pt surface. They show that in the limit of short times, this scenario yields semi-infinite diffusion-limited behavior (consistent with potential step and impedance measurements) but at long times enters a co-limited regime, where the rate of both adsorption and diffusion govern the overall kinetics. Since adsorption kinetics are likely to be governed by the same mass-action relationships governing adsorption equilibrium, the co-limited case is similarly supported by the P_{O_2} dependence of the overall kinetics as the case of pure diffusion.

To better understand how a co-limited system can exist, consider the generalized adsorption/diffusion model shown in Figure 14a. A semi-infinite surface, defining a one-dimensional coordinate system (x), is exposed to a gaseous adsorbate (A) at uniform partial pressure. The rate of adsorption of A onto the surface per unit area is given by $r_A = k(c_{A0} - c_A)$, where $c_A(x,t)$ is the local surface concentration of A, c_{A0} is the surface concentration at equilibrium with the gas, and k is a surface exchange coefficient.[367] Once adsorbed, A can also diffuse along the surface, with 1-dimensional flux per unit width of $N_A = -D(\partial c_A/\partial x)$, where D is the surface diffusion coefficient. Initially, the entire surface is allowed to equilibrate with the gas at surface concentration c_{A0}. Then at $t \geq 0$, the concentration of species A at $x = 0$ is regulated externally with time-dependent value $c_{A1}(t)$ (established, for example, by equilibrium of an electrochemical reaction such as $A + e^- \leftrightarrow A^-$). This local displacement of the surface concentration provides a driving force for a finite flux of A at $x = 0$ (N_{A1}), which (if electrochemically driven) is related proportionately to current. Conservation of species A leads to

$$\frac{\partial c_A}{\partial t} = D\frac{\partial^2 c_A}{\partial x^2} + k(c_{A0} - c_A)$$

$$c_A(x, t < 0) = c_{A0}$$

$$c_A(x = 0, t) = c_{A1}(t) \qquad (2)$$

Figure 14b,c shows the time-dependent solution

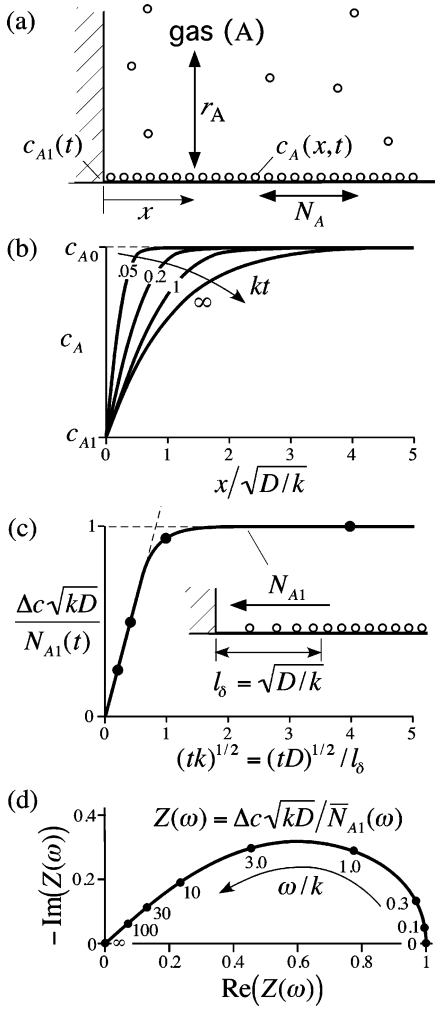

Figure 14. Simple model demonstrating how adsorption and surface diffusion can *co-limit* overall reaction kinetics, as explained in the text. (a) A semi-infinite surface establishes a uniform surface coverage C_{A0} of adsorbate "A" via equilibrium of surface diffusion and adsorption/desorption of A from/to the surrounding gas. (b) Concentration profile of adsorbed species following a step (drop) in surface coverage at the origin. (c) Surface flux of species at the origin ($N_{A1}(t)$) as a function of time. Points marked with a solid circle (●) correspond to the concentration profiles in b. (d) Surface flux of species at the origin ($\bar{N}_{A1}(\omega)$) resulting from a steady periodic sinusoidal oscillation at frequency ω of the concentration at the origin.

to this system following a step in concentration $c_{A1}(t) = c_{A0} - \Delta c$ at $x = 0$. At short times the diffusion profile expands as $t^{1/2}$, yielding Cottrell behavior for the flux of A at $x = 0$ ($N_{A1}(t)$). This expansion continues until, at steady state, the increasing rate of adsorption (due to increased active area) balances the decreasing rate of diffusion (due to a longer transport path). A utilization length l_δ is established, proportional to $\sqrt{D/k}$, that represents a "compromise" between faster kinetics and slower diffusion. The steady-state flux at $x = 0$ (N_{A1}) is proportional to $\sqrt{kD}$ and thus is governed by both kinetics and diffusion. Similarly, Figure 14d shows the stationary periodic solution to eq 2 for a sinusoidal perturbation $c_{A1}(t) = c_{A0} + \Delta c \cos(\omega t)$ as a function of frequency. The resulting half-tear-drop-shaped impedance (defined here as $\Delta c/\bar{N}_{A1}(\omega)$ at $x = 0$) is somewhat

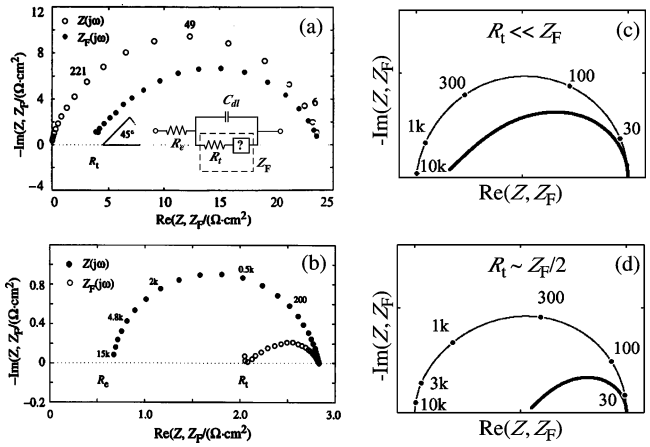

Figure 15. Faradaic impedance (Z_F) of porous Pt electrodes on single-crystal zirconia in oxygen at zero bias, as determined from the total impedance (Z) using the methods of Berthier et al.:[75] (a) T = 800 and (b) 900 °C. (c) Model assuming the interfacial electrochemical kinetic resistance (R_t) is small compared to chemical resistances. (d) Model assuming R_t is similar to chemical resistances. (Adapted with permission from refs 74 and 84. Copyright 1999 and 1997 Elsevier and Swiss Federal Institute of Technology.)

smoother and more suppressed than a Warburg impedance, with a 45° limit at high frequency and RC-like behavior at low frequency, with a characteristic time constant proportional to $1/k$ and characteristic resistance proportional to $1/\sqrt{kD}$. This response has often been called the "Gerischer impedance" because it was first derived by Gerischer in 1951 for the case of an electrode co-limited by homogeneous reaction and diffusion in the electrolyte.[69,71]

The co-limited situation illustrated above is quite different than a membrane, for example, where the relative importance of diffusion vs surface kinetics is determined by a geometric length scale (membrane thickness). Rather, by "co-limited" we mean that both k and D are important in establishing the overall rate, regardless of their values, as long as l_δ is small compared to the electrode thickness. If the ratio of D/k changes, it does not change the relative importance of diffusion vs kinetics, merely the size of the active region. This concept of a co-limited reaction rate is not unique to solids; electrochemical engineering is rich with examples of co-limited systems, including examples from classical porous electrode theory[47] as well as more closely related cases involving gas-diffusion electrodes in polymer-based fuel cells.[43,44]

Perhaps the strongest recent evidence to date that Pt/YSZ is, in fact, co-limited by adsorption and surface diffusion has been provided by Mitterdorfer and Gauckler.[72−74] These authors prepared Pt paste electrodes on single-crystal YSZ and measured impedance at T = 700−800 °C and $P_{O_2} = 10^{-4}$−1 atm in O_2/N_2 mixtures. As shown in Figure 15a,b, the authors used the method of Berthier et al.[75] to subtract the effect of double-layer capacitance and electrolyte resistance, yielding a true "faradaic impedance" Z_F, which is composed of an interfacial charge-transfer resistance (R_t) plus a chemical impedance not unlike the Gerischer impedance shown in Figure 14d. The authors constructed a numerical model for oxygen reduction on Pt/YSZ (based on a finite-difference model for the surface) that includes adsorption, diffusion, and electrochemical−kinetics at the TPB. As shown in Figure 15c,d, their model shows similar behavior and when compared to the data allows estimation of physical parameters governing adsorption, surface diffusion, and electrochemical kinetics at the TPB.

Among other things, the authors show that when Langmuir adsorption kinetics are assumed, they find the adsorption and diffusion parameters extracted from their data to depend strongly on surface coverage θ. To explain this, they propose an alternative precursor-mediated adsorption mechanism. With this modification to the model, the kinetic and transport parameters extracted from the data reveal more constant values that are argued to be in reasonable agreement with available independent measurements or calculated estimates.[73,76−79] The authors conclude that above 800 °C and high P_{O_2}, charge transfer at the TPB competes with adsorption/diffusion, constituting approximately one-half of the total impedance. With decreased temperature or lower P_{O_2} (or increased overpotential), the electrode appears to become limited primarily by chemical processes, with less than 10% attributed to the TPB interface. These results suggest that the system is quite complex and that multiple factors can be important, depending on the specific conditions. Indeed, this may help explain why there has been so much difficulty reaching a consensus on what "the" rate-limiting step really is, i.e., there is no "one" rate-limiting step.

3.5. Unresolved Issues Surrounding Oxygen Reduction on Pt/YSZ

The models proposed by Robertson and Michaels, and later by Mitterdorfer and Gauckler, imply that adsorption and diffusion of oxygen will occur over a finite utilization region, as illustrated in Figure 14b,c, establishing the electrode's functional zone. Oddly, neither set of authors reported numerical estimates of this size, based on the parameters they extracted from their data. In the case of Mitterdorfer and Gauckler, it is possible to make an estimate using eq 2 and the parameters from their model. This exercise yields values between 50 and 500 nm, depending on T and P_{O_2} (~100 nm at 700 °C in air).[368] While this range represents a significant extension of the active region beyond the TPB, it is small enough relative to microstructural features to remain consistent with studies of Pt and Pt/YSZ composite electrodes, showing that the active area scales with the geometric length of the three-phase boundary.[80,81] A more quantitative analysis of the size of the active region has yet to be conducted for Pt on YSZ.

Luerssen and co-workers recently attempted to image the concentration gradients of oxygen on a Pt film electrode near the TPB using PEEM[67](see section 3.6). They were able to show that the work function (and thus the surface oxygen coverage) changes following polarization. However, they observed no visible diffusion front emanating (on Pt)

from the TPB. As discussed by the authors, this failure may be a result of the porosity in the Pt film (resulting in changes being seen everywhere). It is also possible that at the very low P_{O_2}'s studied ($<10^{-9}$ mbar) the system becomes entirely adsorption/desorption limited, and thus the oxygen surface coverage changes uniformly over the entire Pt surface. Indeed, an estimate of l_δ at this low P_{O_2} based on Mitterdorfer's model (see above) is $\sim$80 μm at 700 °C, which is on the same order of the size of the Pt surface studied by Luerssen et al. Further studies of this type, if able to be conducted at higher P_{O_2}, may be able to reveal more about the actual size of the utilization region for Pt.

Another open question is the mechanism and electrochemical kinetics governing incorporation of adsorbed oxygen as O^{2-} at the Pt/electrolyte interface (Figure 4f). Mitterdorfer estimated (based on analysis of impedance) that this process can constitute anywhere from 10% to 50% of the electrode overpotential.[73] Of particular interest would be to better understand what role the *electrolyte* (or its constituents) plays in this process. For example, Widmer et al.[82] measured the zero-bias impedance of low-fired (750 °C) porous Pt electrodes on various electrolytes including YSZ, gadolinia-doped ceria (GDC), and Ce-implanted YSZ (made by ion implantation of cerium into the surface of YSZ). Their results show that the impedance of Pt on GDC and Ce-implanted YSZ are much lower than for Pt/YSZ. Since electrodes fired at this temperature are likely to be limited by interfacial ionic charge transfer, this result would seem to indicate that the presence of Ce aids the electrochemical kinetics at the TPB, as discussed more fully by McEvoy.[83] Unfortunately, isolation and study of this portion of the overpotential is nontrivial. As discussed previously, traditional electrochemical methods (such as steady-state Tafel analysis) are heavily obscured by chemical effects.[84] Meanwhile, impedance (which we saw can potentially isolate the resistance of the interface via frequency) is limited to linearized response and thus is unable to provide nonlinear information such as the interface-specific exchange current density and anodic/cathodic transfer coefficients. Thus, despite many years of earnest investigation, the electrochemical kinetics governing the actual Pt/YSZ interface (as distinct from adsorption and transport to the TPB) remains largely a mystery.

A related mystery is the wide variability in estimates reported for the true double-layer capacitance of Pt/YSZ interface and how sensitive one's analysis is to this value. The recent work of Mitterorfer and Gauckler[74] shown in Figure 15 illustrates the extreme degree to which the double-layer capacitance can obscure the faradaic processes occurring on the electrode at high frequency. In 1991, Robertson and Michaels attempted to measure the double-layer capacitance based on chronoamperometry, showing that the shortest relaxation time scale yields a capacitance of $\sim10^{-6}$ F/cm^2 at 700 °C, based on the superficial area.[85] More recently, Kenjo reports a value of $\sim10^{-5}$ F/cm^2 using similar measurements.[86] These values (which are 2−3 orders of magnitude smaller than the total pseudocapacitance typically ascribed to Pt) compare reasonably with estimates of the charge separation at the Pt/YSZ interface[85] as well as the capacitance of solution interfaces of similar charge concentration and mobility.[47] In contrast, the use of equivalent circuit models to extract double-layer capacitance from impedance data typically yields values on the order of $>10^{-4}$ F/cm^2.[73,85] While in some cases these values may simply be obscured by faradaic capacitive effects (as originally proposed by Robertson), it remains unclear why the apparent interfacial capacitance appearing in the impedance is so large even *after* faradaic effects have supposedly been accounted for. A likely explanation is that additional transients are occurring at the Pt/YSZ interface at the highest frequencies probed by the impedance, which are neither true interfacial polarization nor faradaic accumulation of reactive intermediates on the gas-exposed Pt surface.

3.6. Nonstationary Effects

Another unresolved issue in our understanding of Pt cathodes is that of nonstationary behavior such as hysteresis or inductive effects, reported under moderate to high polarization. In this context, the term *stationary* refers to behavior exhibiting a well-defined steady state, which is a repeatable function of the materials, processing, and testing conditions. Inherently transient measurements, such as impedance or current-interrupt response, can still be classified as stationary as long as the applied transients involve repeatable deviations from, or relaxations to, a well-defined steady state. In contrast, many workers have observed that electrode characteristics, such as $i-V$ response or the impedance itself, can depend on time and/or operating history. Such dependencies are defined here to be nonstationary since they either are irreversible, involve significant hysteresis, or relax on a time scale so long as to constitute changes in mechanism with respect to processes probed on ordinary time scales.

One of the first specific studies of these effects was reported by Schouler and Kleitz,[87] who noticed hysteresis in cyclic voltammograms at anodic potentials above about 200 mV. Subsequently a variety of other authors have reported similar findings for Pt at both anodic and cathodic overpotentials.[88−92] One recent example is provided by Jacobsen and co-workers,[90] who used linear sweep voltammetry and EIS to quantify the degree and dependence of this hysteresis for Pt ball/YSZ and point YSZ/Pt electrodes. Figure 16 shows some of their results. Unlike a system with a reactive intermediate (in which the return sweep occurs at reduced current due to unfavorable depletion or excess of the reactive intermediate), these voltammograms clearly show that current on the return sweep is enhanced following polarization at a higher potential. The hysteresis loop gets larger with *decreasing* sweep rate until extremely slow sweeps, where a steady state is finally achieved ($\leq$1 μV/s). This is actually an example of an "apparent" hysteresis (brought on by a large separation in time scales) rather than a true hysteresis in which a

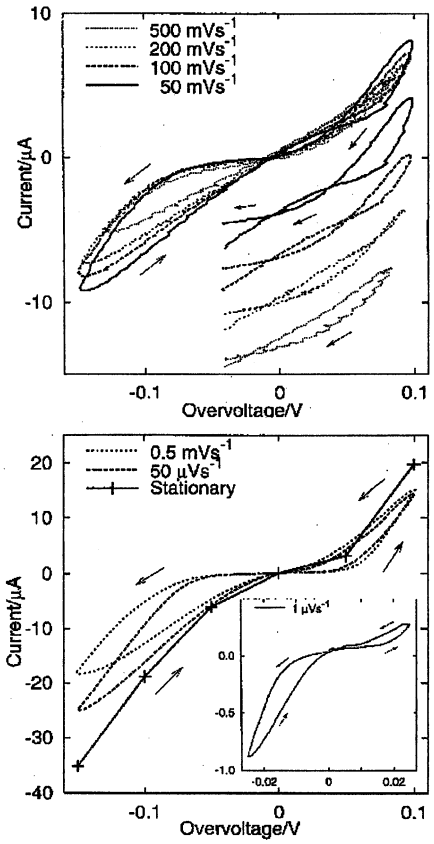

Figure 16. Linear-sweep voltammagrams of a YSZ needle electrode in contact with bulk Pt in air at 1000 °C as a function of sweep rate. (Reprinted with permission from ref 90. Copyright 2001 Elsevier.)

history-dependent stable state can be achieved (e.g., magnetic induction of a ferromagnet). As one might expect from this behavior, inductive effects are seen in the impedance, and this effect can also be observed in chronoamperometric measurements, which show a slow rise (∼30%) in current over a period of about 3 h following initial polarization. Jacobsen et al. consider, and reject, a number of explanations for this behavior including (1) reactive intermediates on the Pt surface, (2) passivation of the Pt surface by macroscopic layers of platinum oxide, (3) expansion of the reaction zone along the YSZ surface due to reduction and subsequent conduction of YSZ, and (4) Joule heating of the sample. None of these mechanisms, the authors argue, appear to consistently explain the observed transients.

A prominent explanation has been that by cathodically polarizing the cell for a significant period of time, long-lived Pt−O moieties on the surface (or at the TPB) are reduced, opening up catalytic sites for dissociative adsorption, transport, and electrochemical reduction. Perhaps relevant to this idea is a study by von Oertzen and co-workers that challenges the traditional view of Pt as a homogeneous metal surface.[93] They used PEEM to show that chemisorbed oxygen on Pt (110) can be incorporated into platinum as a subsurface oxygen "phase" at temperatures as low as 200 °C, provided CO is present to initiate reconstruction of the surface. Perhaps similar alterations of certain portions of a polycrystalline Pt surface (or Pt/YSZ interface), driven by electrochemical reduction/oxidation, might account for unexplained inductive (as well as capacitive) effects. Recent measurements of work function transients following polarization[94] seem to support the idea that Pt undergoes changes in surface structure after establishing a steady-state surface coverage. Similarly, a recent AFM study by Bay and Jacobsen shows that cathodic and anodic polarization can create submicrometer morphological changes at the Pt/YSZ interface, as revealed in postmortem analysis of point-electrode samples.[95] These observations, which imply a nonstationary Pt/YSZ interface, appear to be consistent with a model by Svensson and Nisancioglu,[96] which suggests that mobility of oxygen species along the YSZ/Pt interface is an important part (at the atomic level) in determining the interfacial electrochemical kinetics.

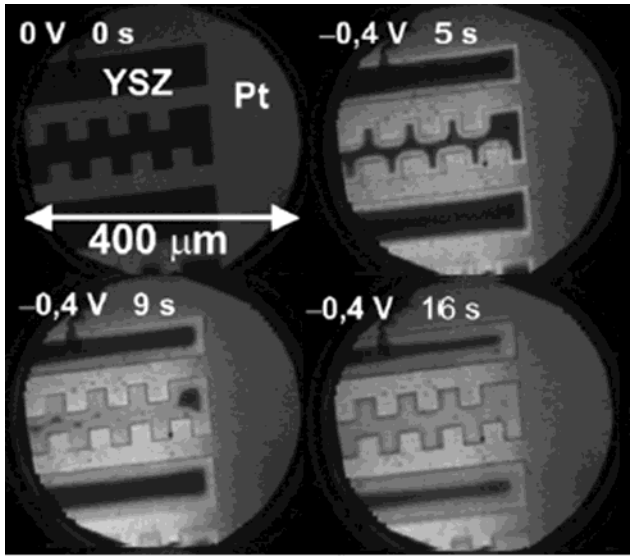

Figure 17. In-situ PEEM images of a cathodically polarized Pt/YSZ/Pt cell as a function of time following cathodic polarization. Dark area in the initial ($t = 0$) image corresponds to the gas-exposed YSZ surface, while the slightly lighter area is Pt. The bright area on Pt following initial polarization corresponds to low work function due to decreased oxygen coverage. In contrast, the bright area that grows slowly outward from the TPB along the YSZ surface corresponds to increased electron concentration. About 1 min is required for the YSZ surface to reach steady state following polarization. (Reprinted with permission from ref 97. Copyright 2002 PCCP Owner Societies.)

Finally, it is worth mentioning recent studies by Luerssen et al.,[97] who imaged the slow growth of a reduction front along single-crystal YSZ following large cathodic polarization of a Pt film electrode. As shown in Figure 17, this reduction expands the region of reduced oxygen activity well beyond the TPB and appears to alter the work-function distribution on Pt that had been established initially after polarization. Although these measurements were conducted under very low P_{O_2}, they may provide some insight about how hysteretic effects could involve the electrolyte at higher P_{O_2}. Indeed, these images recall earlier suggestions by Kleitz[55,98] and others[99] that the electrolyte can play a chemical catalytic role in the absorption and dissociation of oxygen given the right conditions and set of materials.

3.7. Summary: Platinum as a Framework for Understanding Other SOFC Cathodes

The literature reviewed in sections 2−3.6 has shown that oxygen reduction on Pt is quite complex, involving several possible rate-limiting (or co-limiting) steps. As we will see in sections 4 and 5, this complexity is a universal feature of all SOFC cathodes, with many of the same themes and issues reappearing for other materials. We therefore highlight below several general observations about the mechanism of Pt that frame the discussion for other solid-state gas-diffusion electrodes involving O_2. These observations are as follows.

(1) *Chemical reaction steps:* Even if the overall electrochemical reaction involves a molecular species (O_2), it must first be converted to some "electroactive" intermediate form via one or more processes. Although these processes are ultimately driven by depletion or surplus of intermediates relative to equilibrium, the rate at which these processes occur is independent of the current except in the limit of steady state. We therefore label these processes as *chemical processes* in the sense that they are driven by chemical potential driving forces. In the case of Pt, these steps include dissociative adsorption of O_2 onto the gas-exposed Pt surface and surface diffusion of the resulting adsorbates to the Pt/YSZ interface (where formal reduction occurs via electrochemical−kinetic processes occurring at a rate proportional to the current).

(2) *Co-limitation by kinetics and mass transfer:* If an electrode is porous, there is generally no fixed geometric length that defines the importance of diffusion relative to kinetic steps. Rather, reaction and diffusion will occur cooperatively over an active area and at an overall rate that depends on both kinetic and diffusion parameters simultaneously over a wide range of values. We label this situation as a co-limited reaction. In the case of Pt at high P_{O_2}, it would appear that the rates of adsorption and surface diffusion are balanced over a relatively small active region close to the TPB (50−500 nm). This appears to explain why the activity of a Pt electrode generally scales with the length of the geometric three-phase boundary.

(3) *Electrochemical kinetics confined to TPB:* For platinum, the important chemical processes of catalytic reduction and transport occur on the Pt surface, and thus the electroactive species formed are most readily available near the Pt-surface/YSZ interface (TPB). Although it is not entirely clear how these electroactive species are subsequently incorporated into the electrolyte bulk or what role the electrolyte itself plays in this process, there is strong circumstantial evidence that the electrochemical−kinetic step is restricted to an area close to the TPB. Unfortunately very little is known about the nature of this reaction since the details are often obscured by chemical effects involving the Pt surface.

(4) *Nonstationary behavior:* Platinum on YSZ exhibits pronounced hysteretic effects, suggesting that passage of current can alter either the kinetics of the reaction or the dominant reaction pathway itself. As we saw in section 3.6 (and will again in section 5.4), this type of nonstationary behavior (behavior for which a well-defined steady state does not exist or is subject to relatively long relaxations) remains largely an unsolved mystery for Pt as well as other types of electrodes.

4. Perovskite Mixed Conductors and the Role of Bulk Material Properties

The observations summarized in section 3.7 suggest that if one could extend the transport process of electroactive species from the surface to the *bulk* of the electrode material (as we saw with silver, for example), one could enlarge the active area over which chemical processes occur as well as extend the electrochemical interface to include the entire electrode/electrolyte contact area (not just the TPB). Although silver appears to exhibit sufficient bulk oxygen transport to accomplish these goals, it has not proven to be suitable as an SOFC cathode due to poor catalytic activity toward O_2 as well as mechanical and thermodynamic instability. In contrast, some transition-metal oxides, in addition to being good O_2 catalysts and electronic conductors, exhibit significant ionic conduction while remaining relatively stable at operating conditions. For these mixed conductors (materials which conduct both ions and electrons) the bulk appears to play a significant if not dominant role in determining the electrode kinetics. As such, these materials provide another useful asymptote to consider when extrapolating to more complex materials such as LSM.

4.1. Perovskite Oxides—Low-Cost Alternative to Platinum

Transition-metal oxides were originally investigated as SOFC cathodes due to their good electrical conductivity (most oxides are insulators) and as a relatively low-cost alternative to Pt, which prior to about 1965 was the only SOFC cathode material being considered extensively. One of the first such materials studied was $La_{1-x}Sr_xCoO_{3-\delta}$ (LSC) (now one of the most well-studied mixed conductors), reported by Button and Archer in 1966.[4] This was followed quickly thereafter by a number of other materials having perovskite crystal structure, including $La_{1-x}Sr_xMnO_{3\pm\delta}$ (LSM), which as of ∼1973 became the favored material for SOFC cathodes. Since LSM has been so well studied and is also a poor ion conductor (at least at ambient P_{O_2}), we discuss this somewhat more complex material system in its own section (section 5). In the present section we focus on perovskites materials which exhibit significant bulk oxygen ion transport at typical cathodic P_{O_2} and the role this transport plays in the oxygen reduction mechanism.

One of the first such kinetic studies of a perovskite mixed conducting electrode was reported by Ohno and co-workers in 1981, who found $La_{1-x}Ca_xCoO_{3-\delta}$ to have better kinetic properties than Pt as an SOFC cathode at 1000−1100 °C.[100] A number of other *περοωσκιτεσ* of general formula $La_{1-x}Sr_xMO_{3-\delta}$ (M = Cr, Mn, Fe, Co) were later studied by Takeda et al.[101] To avoid reaction of the perovskites with the YSZ

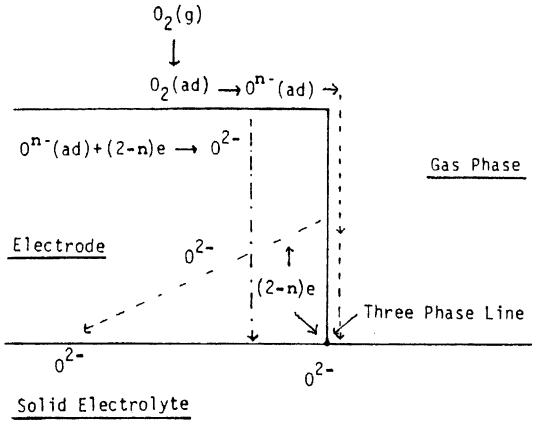

Figure 18. Possible pathways by which oxygen is reduced in a porous mixed conducting electrode. Following dissociative adsorption (which forms a surface-polarizing species O^{n-}, where n represents the unknown partial charge state of adsorbed oxygen), O^{n-} either travels by surface diffusion to the TPB (where it is fully reduced) or is incorporated directly into the mixed conductor as O^{2-}, where it then diffuses to the solid/solid interface. (Adapted with permission from ref 203. Copyright 1987 The Electrochemical Society, Inc.)

electrolyte, these electrodes were fabricated by sputtering porous films of thickness varying from 1 to 3 μm at modest temperatures. They found the best performance with LSC, which initially exhibits significantly lower overpotential than either $La_{0.7}Sr_{0.3}FeO_{3\pm\delta}$ (LSF) or LSM under the conditions studied. The $i-V$ characteristics of LSC were found to be linear at low current density and obey Tafel kinetics at higher current density. The exchange current density obtained by fitting the data to a Butler–Volmer rate expression scales approximately as $P_{O_2}^{1/4}$ and has an activation energy of ~220 kJ/mol. The authors generally found that the overall kinetics improves with increasing Sr content (x), except for $LaCoO_3$ (which was the best composition they studied). They also noted a thickness dependence—the overall performance improved with thickness until about 2–3 μm, at which point a plateau or slight decline in performance with thickness was observed.

In interpreting their results, Tekada et al. provided the now often-duplicated picture shown in Figure 18, which illustrates the possible paths by which oxygen may become reduced. Citing the high chemical diffusion coefficient for oxygen in LSC, the authors claimed that bulk transport in LSC allows a much larger region of the electrode to be active for oxygen reduction and that this effect is largely responsible the improved performance over platinum. On the other hand, citing the Tafel behavior, weak P_{O_2} dependence, and high activation energy, the authors argue that the electrode must be limited by interfacial electrochemical kinetics with absorption and transport of oxygen in/on LSC being so fast as to be equilibrated. Although the subsequent 20 years of research have shown that these electrodes are not generally limited by interfacial electrochemical kinetics, this work was foundational in redirecting the SOFC cathode materials effort and in framing the debate for two decades as to what actually limits the rate of oxygen reduction with these materials. Of particular interest is the suggestion that the *bulk* of the material plays an important role in determining the overall kinetics. As we will see below, this has been proven to be largely correct.

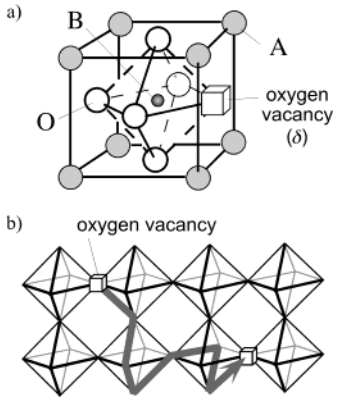

Figure 19. Atomic structure and oxygen transport in mixed conducting perovskites $ABO_{3-\delta}$. (a) Basic structural element, consisting of a corner-sharing BO_6 octahedron surrounded by charge-compensating A-site cations. (b) Bulk oxygen transport mechanism, involving random hopping of oxygen ion vacancies on the oxygen sublattice.

4.2. Thermodynamic, Kinetic, and Transport Properties of Perovskite Mixed Conductors

Figure 19 illustrates the general perovskite crystal structure $ABO_{3-\delta}$ as it relates to the electronic and ionic transport properties of some transition-metal oxides. In this case, the B-site cation is a reducible transition metal such as Co or Fe (or mixture thereof) and the A-site cation is a mixture of rare and alkaline earths (such as La and Sr). The octahedral symmetry around the transition metal often promotes a metallic or semiconducting band structure at high temperature, leading to high electronic conduction. This structure is also quite stable relative to other crystalline phases, and thus with a judicious choice of A- and B-site cations, it can stably support a large number of oxygen ion vacancies (δ) at SOFC operating conditions, thus facilitating significant bulk ionic oxygen transport. The literature surrounding the properties of transition-metal perovskites extends back more than 50 years and is well beyond the scope of this review; however, the following few paragraphs attempt to summarize some of the salient features.

All materials in the $La_{1-x}Sr_xCo_{1-y}Fe_yO_{3-\delta}$ (LSCF) family of materials have electronic transference numbers approaching unity. The electronic structure LSC and LSF has often been described in terms of partially delocalized $O^{2p}-Co^{3d}$ band states based on the t_g^2 and e_g levels of crystal-field theory.[102–104] In the case of LSC (Figure 20a), at high temperature and with 10 mol % Sr or higher, the Fermi energy appears to fall within a half-filled band, comprising a mixture of somewhat localized t^2 states with more delocalized e (σ^*) states.[105–111] Consistent with this picture, LSC exhibits metallic or semimetallic conduction with a conductivity that decreases with temperature above ca. 500 °C and a Seebeck coefficient approaching zero as the temperature is increased.[112,113] In contrast, LSF appears to exhibit a weak Hubbard or Hubbard-like band gap arising

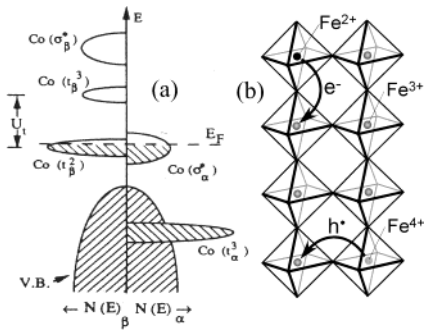

Figure 20. Electronic structure and transport in mixed conducting perovskites. (a) Band picture of electronic structure in the high-temperature metallic phase of $La_{1-x}Sr_xCoO_{3-\delta}$. (Reprinted with permission from ref 109. Copyright 1995 Elsevier.) (b) Localized picture of electron/hole transport in semimetallic $La_{1-x}Sr_xFeO_{3-\delta}$, involving hopping of electrons and/or electron holes (depending on the oxidation state of iron).

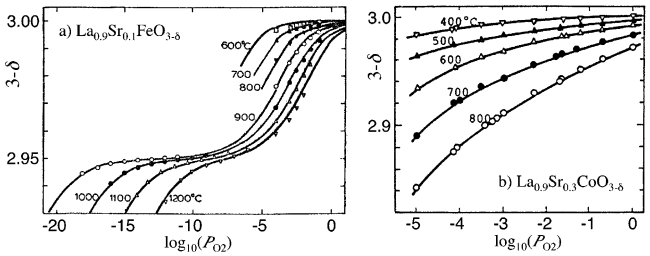

Figure 21. Oxygen stoichiometry in (a) LSF ($x = 0.1$) and (b) LSC ($x = 0.3$) as a function of P_{O_2} and temperature. (Adapted with permission from refs 119 and 121. Copyright 1985 and 1989 Elsevier.)

from electron−electron repulsion on the iron site.[114,115] This gap results in more localized electronic states, which can be thought of as a spatially localized disproportionation of Fe^{3+} to Fe^{2+} and Fe^{4+}(Figure 20b). As such, LSF has semiconducting or semimetallic properties at high temperature, exhibiting p-type conductivity and Seebeck coefficient at high P_{O_2} (where iron is intermediate between Fe^{3+} and Fe^{4+}) and n-type conductivity and Seebeck coefficient at low P_{O_2} (where iron is intermediate between Fe^{2+} and Fe^{3+}).[116] For solid solutions of LSC and LSF having a mixture of iron and cobalt on the B-site, the electronic structure is more complex but generally exhibits more semiconductor-like behavior with high iron content ($y = 0.8$) while being more metallic with high Co content ($y = 0.1$).[117,118]

Consistent with these differences in electronic structure, LSC and LSF also exhibit very different defect thermodynamics in terms of the dependence of oxygen vacancy concentration (nonstoichiometry δ) as a function of Sr content (x), T, and P_{O_2}. As shown in Figure 21a,[119] LSF exhibits a plateau in oxygen nonstoichiometry with P_{O_2} where $\delta = x/2$, corresponding to an average iron oxidation state of Fe^{3+}. At higher P_{O_2} iron becomes oxidized, leading to lower δ, while at lower P_{O_2} more vacancies are formed. As shown by Mizusaki,[119] this behavior can be explained quantitatively in terms of point-defect theory,[120] assuming equilibria among O_2 gas, oxygen vacancies, and localized electrons and holes. In contrast, Figure 21b[121] shows that the oxygen nonstoichiometry in LSC exhibits no such plateau but rather a continuous

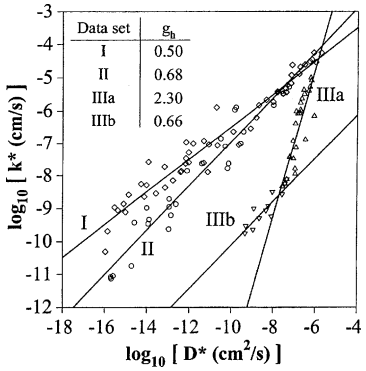

Figure 22. Correlation of the isotope tracer surface exchange coefficient (k^*) vs the oxygen tracer diffusion coefficient (D^*). Data represent a variety of materials under various temperature and P_{O_2} conditions but are classified according to groups. Group I: $La_{1-x}Sr_xMn_{1-y}Co_yO_{3\pm\delta}$, $Sm_{1-x}CoO_{3-\delta}$, and $La_{1-x}Sr_xFe_{1-y}Co_yO_{3-\delta}$. Group II: $CaZr_{0.9}In_{0.1}O_{2.95}$, $SrCe_{0.95}Yb_{0.05}O_{2.975}$, and $La_{1-x}Sr_xYO_{3-x/2}$. Group IIIa: oxide fluorites at high temperature plus $La_{0.9}Sr_{0.1}Ga_{0.8}Mn_{0.2}O_{2.85}$. Group IIIb: oxide fluorites at low temperature. (Reprinted with permission from ref 141. Copyright 1999 Elsevier.)

increase in vacancy concentration with decreasing P_{O_2}.[121−124] Mizusaki noted that that this behavior implies that the partial entropy of oxygen incorporation is dominated by the configuration entropy of the vacancies while electron/hole entropy is constant.[121] More recently, Lankhorst et al. modeled this behavior using a point-defect view for oxygen vacancies but treating electrons as delocalized according to a rigid-band model.[125−127] Nonstoichiometry for mixed iron and cobalt materials has also been investigated[117,118,128,129] and can be explained to a certain degree by hybrid models invoking both localized and itinerant electronic states.[130]

Although these materials are primarily electronic conductors ($t_{n,p} \approx 1$), the very large concentrations of oxygen vacancies generated in these materials (as shown in Figure 19) has been found to lead to rapid bulk oxygen ionic transport as well as increased rates of exchange of oxygen with the gas. The rates of these processes have been measured by a variety of techniques including electronic blocking methods,[131−133] $^{18}O_2$ tracer techniques based on postmortem SIMS analysis,[134−142] relaxation methods involving the measurement of mass, conductivity, or other properties following a sudden change in P_{O_2},[135,143−148] or direct measurement of permeation through a dense membrane.[149−153] Although we do not review this literature in detail, some of the highlights relevant to the present discussion are included.

(1) *Higher vacancy concentration leads to faster ion transport and surface exchange.* In general, the more vacancies there are, the faster oxygen can be absorbed by, and move through, the lattice for a given chemical potential driving force. In fact, as shown in Figure 22, many workers have noticed a strong correlation between the equilibrium surface isotope exchange rate (k^*) and the bulk tracer diffusion rate (D^*) that spans 10 orders of magnitude in property values across several classes of materials.[141]

(2) *Higher electronic conduction is correlated with faster oxygen exchange.* As shown in Figure 22,

materials with high concentrations and/or more mobile electronic carriers tend to have much better surface catalytic properties (k^*) than more purely ionically conductive materials with similar rates of bulk ion transport (D^*). The existence of this universal correlation suggests that there may be a fundamental limit to how active the surface of these materials can be without some type of additional enhancement.

(3) *Available kinetic and transport data are limited to linearized driving force.* The measurement techniques listed above (particularly tracer and relaxation techniques) only probe the rate of oxygen diffusion and surface exchange at or near equilibrium conditions. While transport data can normally be extrapolated to higher driving force (through consideration of the defect structure and appropriate thermodynamic factors), extrapolation of equilibrium surface exchange data to high driving force is impossible without a priori knowledge of the exchange mechanism, which is still an open question. Thus, the nonlinear rate expressions governing absorption or evolution of oxygen at the mixed-conductor surface remain largely unknown today.

4.3. Defining the Role of the Bulk—Dense Thin-Film Mixed-Conducting Electrodes

To better understand the role of bulk oxygen transport in determining the characteristics of mixed-conducting oxide electrodes, workers have focused considerable attention in the last 10−12 years on dense thin-film electrodes having little or no three-phase boundary contact area.[27,124,154−166] Early attempts struggled with sample preparation, it being difficult to make and verify the existence of uncracked and dense films. Perhaps the first success in this direction was that of Mizusaki and co-workers,[157] who used a pulsed KrF excimer laser to flash evaporate and deposit 1−2 μm thick films of $La_{0.5}Sr_{0.5}MnO_3$ on YSZ. Prior to polarization, these electrodes exhibited a zero-bias impedance much higher than porous LSM electrodes and a performance that *decreased* with increasing P_{O_2}, which is contrary to the normal situation with porous electrodes. They also noticed that the performance scaled inversely with electrode thickness. On the basis of these results, they modeled the electrode as being limited by ambipolar diffusion of oxygen through the bulk of the film and showed that the majority of their observations were consistent with this model, based on the known defect structure of LSM. More recent results appear to confirm this conclusion.[159,167] It was thus shown that even with a poor ionic conductor such as LSM, a bulk path exists for oxygen reduction and a TPB interface is not strictly necessary for the reaction to occur.

However, as discussed more fully in section 5, it is not entirely clear how significant the bulk path is in the case of LSM, which is almost a pure electronic conductor under typical cathode conditions. In the Mizusaki study cited above, the authors went on to show that following anodic polarization (or strong cathodic polarization), the LSM film becomes severely damaged and cracked and reverts to behavior more consistent with a porous LSM electrode. The authors conclude that this damage results in a creation of TPB contact area and thus changes the relative importance of bulk vs surface transport in allowing electroactive oxygen to reach the electrode/electrolyte interface. In other words, by constraining transport to the bulk artificially using a thin film, one can only prove that bulk transport occurs not that it is the dominant path for transport under all conditions.

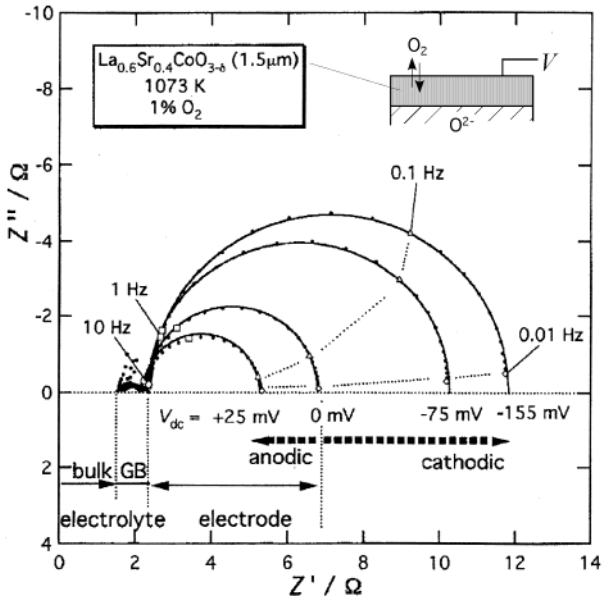

Figure 23. Impedance response of a thin film of LSC ($x = 0.4$) on GDC at 800 °C and $P_{O_2} = 10^{-2}$ atm as a function of polarization. (Reprinted with permission from ref 124. Copyright 2002 Electrochemical Society Inc.)

In contrast, in a series of collaborative studies, Kawada, Masuda, and co-workers reported excellent success making thin-film electrodes of LSC ($La_{0.6}Sr_{0.4}CoO_{3-\delta}$) on Ca-doped ceria (CDC) using laser ablation.[124,158,161] These homogeneous and very-well characterized films were studied by impedance over a range of T, P_{O_2}, and thickness as well as isotope exchange methods to help determine where the resistance to oxygen reduction occurs. As shown in Figure 23, these films exhibit nearly perfect low-frequency semicircular impedances having a resistance and capacitance that can be analyzed quantitatively assuming that absorption/desorption of oxygen at the gas/film interface is rate limiting. The author's isotope-exchange measurements on the same system confirm that the film contributes virtually no resistance to bulk oxygen transport and that there is no resistance for $^{18}O^{2-}/^{16}O^{2-}$ exchange across the LSC/CDC interface. Subsequently published studies have consistently confirmed these findings for other perovskite phases having high ionic conductivities.[27,124,162−166] Both Kawada et al.[161] and Yang et al.[165] compared the oxygen surface exchange coefficient for the gas/mixed conductor interface obtained from isotope measurements to that predicted from the impedance and found quantitative agreement over a range of temperatures and P_{O_2}. These results suggest that over length scales of a few micrometers, the bulk will provide little opposition to oxygen transport and thus will be a dominant transport path.

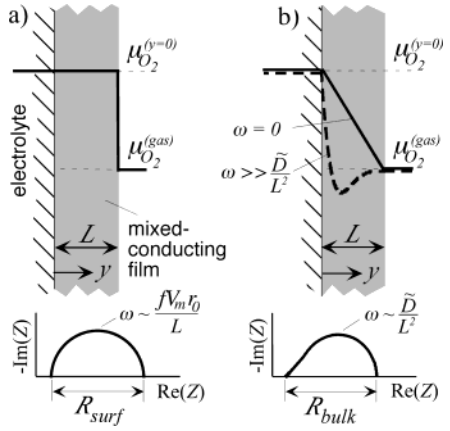

Figure 24. Models illustrating the source of "chemical capacitance" for thin film mixed conducting electrodes. (a) Oxygen reduction/oxidation is limited by absorption/desorption at the gas-exposed surface. (b) Oxygen reduction/oxidation is limited by ambipolar diffusion of O^{2-} through the mixed conducting film. The characteristic time constant for these two physical situations is different (as shown) but involves the same chemical capacitance C_L, as explained in the text.

Results are similar for films deposited on YSZ; however, there appears to be a difference between films deposited on ceria vs YSZ in terms of interfacial electrochemical resistance. As shown previously in Figure 6c, LSC films on YSZ often exhibit a second high-frequency impedance associated with oxygen-ion exchange across the electrode/electrolyte interface.[27,164−166] That this difference is associated with the solid−solid interface has been confirmed by Mims and co-workers using isotope-exchange methods.[164] As discussed in greater detail in sections 6.1−6.3, this interfacial resistance appears to result from a reaction between the electrode and electrolyte, sometimes detected as a secondary phase at the interface.

As with platinum, these studies reillustrate that oxygen reduction can be separated into chemical steps (in this case absorption of oxygen into and ambipolar transport through the bulk of the mixed conductor film) and electrochemical−kinetic steps (exchange of oxygen ions across the mixed-conductor/electrolyte interface). Besides highlighting the important role of these chemical steps in determining the overall *resistance* of mixed-conducting electrodes, another important consequence of this separation is the concept of chemical capacitance (also known as faradaic or pseudocapacitance) associated with the bulk oxidation/reduction of the material. As discussed below, this chemical capacitance is normally much larger than surface or interfacial capacitances and thus is a useful measure of how much of the bulk is involved, even when we step away from thin films to more complex microstructures.

4.4. Chemical Capacitance

Figure 24 illustrates what gives rise to the measured resistance and capacitance of a mixed-conducting film (as determined by impedance) when the reaction is limited by either (a) chemical reduction of O_2 to O^{2-} at the gas/film interface or (b) transport of oxygen ions in the bulk of the film (where electronic conduction is facile).

If O_2 exchange at the gas-exposed surface is rate limiting (Figure 24a), the relatively fast transport of oxygen ions in the film will cause the film to act as a uniformly concentrated and electrically neutral reservoir for oxygen vacancies and associated electrons/holes. Conservation of vacancies in the film in this case is therefore given by

$$L\frac{\partial[V_O^{\cdot\cdot}]}{\partial t} = N_{V_O^{\cdot\cdot}}|_{y=0} - N_{V_O^{\cdot\cdot}}|_{y=L} \tag{3}$$

where $[V_O^{\cdot\cdot}] = \delta/V_m$ is the vacancy concentration, δ is the oxygen nonstoichiometry in $ABO_{3-\delta}$, V_m is the molar volume of the oxide, and $N_{V_O^{\cdot\cdot}}$ is the vacancy flux in the y direction. In the absence of impedance at the solid−solid interface, a sinusoidal modulation of the current density (i) will cause a proportional faradaic modulation of vacancy flux across the solid−solid interface at $y = 0$

$$N_{V_O^{\cdot\cdot}}|_{y=0} = \frac{-i}{2F} = \frac{-i_1 e^{j\omega t}}{2F} \tag{4}$$

where i_1 is the current modulation amplitude and ω is the frequency in s^{-1}. At the gas/solid interface the absorption/desorption of oxygen results in a vacancy flux related to the displacement of the solid oxygen chemical potential from equilibrium with the gas. Upon linearization, any rate expression for this process can be written in terms of the displacement of δ from equilibrium

$$N_{V_O^{\cdot\cdot}}|_{y=L}\Big|_{N_{V_O^{\cdot\cdot}}\to 0} = \lim_{N_{V_O^{\cdot\cdot}}\to 0}\{r_0(1 - e^{(\mu_{O2}^{solid} - \mu_{O2}^{gas})/2RT})\} = r_0 f(\delta - \delta_0) \tag{5}$$

where r_0 is the equilibrium oxygen exchange rate, δ_0 is the value of δ at equilibrium with the gas, and $f = (-\partial\mu_{O2}/\partial\delta)/RT$ is a thermodynamic factor expressing the ease with which the material changes stoichiometry for a given change in P_{O_2} ($f \approx 1$ means stoichiometry changes easily, $f \gg 1$ means it is hard to change stoichiometry). For a good electronic conductor in the limit of small vacancy concentration, configurational entropy tends to dominate the vacancy free energy such that f scales approximately inversely with vacancy concentration.

Since the solid−solid interface and bulk of the mixed conductor remain in chemical and electrical equilibrium, the measured overpotential η is related directly to the spatially uniform oxidation state of the film through the Nernst equation: $4F\eta = RTf(\delta - \delta_0)$. Solving for $\delta(t)$ and recognizing that the impedance $Z = \eta/i$, one obtains

$$Z = \frac{R_{surf}}{1 + j\omega R_{surf} C_L}$$

$$R_{surf} = \frac{RT}{4F^2}\frac{1}{2r_0}$$

$$C_L = \frac{4F^2}{RT}\frac{2L}{fV_m} \tag{6}$$

where R_{surf} is the area-specific resistance associated with oxygen reduction at the gas-exposed surface and C_L is the effective *chemical* (noninterfacial) capacitance associated with changes in oxygen stoichiometry in the film of thickness L. As shown by the Nyquist plot in Figure 24a, this impedance has a semicircular shape with width R_{surf} and characteristic frequency $1/R_{surf}C_L$. A similar expression for the chemical capacitance of a surface-limited film was recently derived by Kawada et al. using a transmission line approach.[124]

In the second case (limit of fast kinetics at the gas−solid interface), the film becomes entirely bulk transport limited, corresponding to the limit of Hebb−Wagner polarization. Since electronic conduction is fast, this situation yields a Warburg impedance for finite length diffusion[49]

$$Z = R_{bulk}\frac{\tanh(\sqrt{j\omega R_{bulk}C_L})}{\sqrt{j\omega R_{bulk}C_L}}$$

$$R_{bulk} = \frac{RT}{4F^2}\frac{fV_mL}{2\tilde{D}} = \frac{L}{\sigma_i} \qquad (7)$$

where R_{bulk} is the area-specific resistance associated with ambipolar oxygen diffusion trough the bulk of the film (assuming facile electron transport) and $\tilde{D}$ is the chemical diffusion coefficient for oxygen ions. One can also express R_{bulk} in terms of the oxygen ionic conductivity of the film, σ_i, as shown in eq 7. Since oxygen stoichiometry changes occur over the entire thickness of the film, this situation yields the same chemical capacitance (C_L) as the surface-limited case.[168]

Thus, in the case of a thin film, when chemical steps (absorption and/or bulk diffusion) are rate limiting, accumulation of electroactive intermediates in the bulk results in a large effective capacitance proportional to the thickness of the film and the ease by which it changes nonstoichiometry. As recently shown by Kawada et al.,[124] this capacitance is very large (0.1−1 F/cm^2) even for relatively thin (1.5 μm) mixed-conducting films. This value is significantly larger than the pseudocapacitance of Pt ($\sim 10^{-3}$ F/cm^2), which is dominated by adsorption and transport of oxygen on the Pt surface. If we compare this value to the apparent true interfacial polarization capacitance of the Pt/YSZ interface (10^{-6}−10^{-5} F/cm^2), we see an even larger difference. Thus, capacitance is a strong indicator (independent of resistance) as to what degree the interface, surface, and/or bulk are playing in the reaction kinetics for a given material and set of conditions.

Some authors have expressed concerns that bulk accumulation of reactive intermediates (and thus chemical capacitance) violates electroneutrality.[169,170] However, it should be recalled that reduction (or oxidation) of a material not only involves depletion (or accumulation) of oxygen ions in the bulk but neutral combinations of oxygen ions and compensating electrons/holes which together may accumulate without violating electroneutrality.[47] Indeed, no other mechanisms have yet been proposed which satisfactorily explain such a large capacitance without invoking a bulk reaction pathway. As we will see below, workers have used this concept to understand what is happening in more complex porous systems where the relative roles of kinetics, transport, bulk, and surface are not nearly as clear.

4.5. Porous Mixed Conductors—A More Complex Case

Returning briefly to Figure 4, we see a summary of some of the physical mechanisms postulated in the literature to limit the rate of oxygen reduction in a porous mixed-conducting electrode (some of which we have discussed previously in the context of porous Pt and dense mixed conducting electrodes). These include (a) kinetics of O_2 incorporation into the bulk mixed conductor, (b) kinetics of adsorption and/or partial reduction of oxygen on the mixed-conductor surface, (c) rate of bulk or (d) surface transport of O^{2-} or O^{n-}, respectively, to the mixed-conductor/electrolyte interface, (e) electrochemical−kinetics of charge transfer for O^{2-} or (f) combinations of O^{n-} and e^-, respectively, across the mixed-conductor/electrolyte interface, and (g) rates of one or more of these mechanisms wherein the electrolyte itself acts as a mixed conductor due to doping by reaction with the electrode materials.

In the case of a LSM thin film, we noted above that introduction of TPB contact area (via damage of the film) resulted in a fundamental change in the rate-determining step from bulk oxygen transport to some other step (or combination of steps) likely involving the surface. The same fundamental question arises when considering a porous mixed conductor with high ionic conductivity. For a thin film we saw that the mechanism is dominated by the bulk path, a−c−e, with the surface exchange process (a) being rate determining (plus a small contribution from charge transfer (e) when YSZ is the electrolyte). If porosity, and therefore direct TPB contact area, is introduced, does the relative importance of these steps change and/or does a surface path (b−d−f) begin to play a role as it does in the case of Pt?

As discussed in section 4.2, strong interest in mixed-conducting perovskites as gas-separation membranes stimulated a large volume of work in the late 1980s and early 1990s to better understand the properties of mixed-conducting perovskites, including defect thermodynamics, ionic and electronic transport properties, and surface kinetics for absorption/desorption of oxygen. Prompted by the availability of these data, a number of workers in the mid-1990s began a modeling effort to better understand the performance of porous mixed-conducting electrodes[171,172] and membrane coatings[173,174] based on these properties. Although these models only consider a limited set of the physics shown in Figure 4, they successfully confirmed the important role of the bulk and (where valid) provided design guidelines relating performance to microstructure and bulk materials properties. Spending some time to understand these models is therefore worth a few pages, both because they help understand the reaction in some limiting cases as well as being a launching platform for

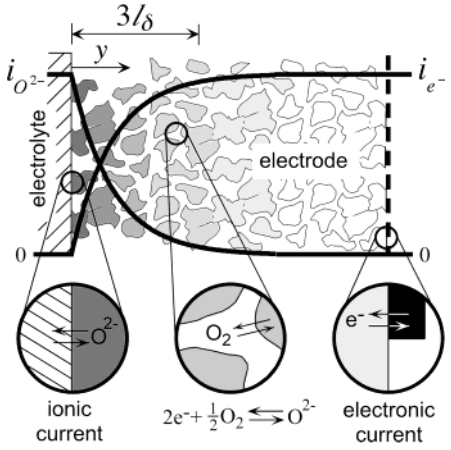

Figure 25. Adler's 1D macrohomogeneous model for the impedance response of a porous mixed conducting electrode. Oxygen reduction is viewed as a homogeneous conversion of electronic to ionic current within the porous electrode matrix, occurring primarily within a distance l_δ from the electrode/electrolyte interface (utilization region). (Adapted with permission from ref 28. Copyright 1998 Elsevier.)

understanding more complex cases where the models break down. Where and how these models break down is interesting because it sheds light on what other physical processes may be active.

4.6. One Asymptotic Limit—The Bulk Reaction Path

One limit of behavior considered in the models cited above is an entirely bulk path consisting of steps a−c−e in Figure 4. This asymptote corresponds to a situation where bulk oxygen absorption and solid-state diffusion is so facile that the bulk path dominates the overall electrode performance even when the surface path (b−d−f) is available due to existence of a TPB. Most of these models focus on steady-state behavior at moderate to high driving forces; however, one exception is a model by Adler et al.[171] which examines the consequences of the bulk-path assumption for the impedance and chemical capacitance of mixed-conducting electrodes. Because capacitance is such a strong measure of bulk involvement (see above), the results of this model are of particular interest to the present discussion.

As shown schematically in Figure 25, the Adler model takes as its testable hypothesis that mixed conductors with high ionic conductivity function by the same underlying mechanism as a dense film, i.e., path a−c−e in Figure 4. In addition, because ionic transport is relatively fast, the model also assumes that variations in composition within the electrode will occur over distances larger than the size of individual microstructural features (particles) making up the porous electrode. Thus, as is often done in porous electrode theory, transport and reaction in and between the solid and gaseous phases are treated using average structural parameters: surface area (a), porosity (ϵ), and tortuosity (τ). With this assumption, the overall electrode reaction, $2e^- + {}^1/_2O_2 \rightarrow O^{2-}$, can be viewed as a 1D macrohomogeneous conversion of electronic current to ionic current over the thickness of the electrode, where in this case oxygen absorption and diffusion act as Kleitz's "chemical valve" (Figure 10), limiting overall charge flow (current) at steady state. This model also considers the effects of gas-phase diffusion and charge-transfer resistance at the electrode/current collector contact.

Because the Adler model is time dependent, it allows prediction of the impedance as well as the corresponding gaseous and solid-state concentration profiles within the electrode as a function of time. Under zero-bias conditions, the model predicts that the measured impedance can be expressed as a sum of electrolyte resistance ($R_{\text{electrolyte}}$), electrochemical kinetic impedances at the current collector and electrolyte interfaces ($Z_{\text{interfaces}}$), and a "chemical" impedance (Z_{chem}) which is a convolution of contributions from chemical processes including oxygen absorption, solid-state diffusion, and gas-phase diffusion inside and outside the electrode.

In the limit of a semi-infinite (thick) porous electrode with no gas-phase diffusion limitations, the chemical term Z_{chem} reduces to an impedance reflecting co-limitation by oxygen absorption and transport.[369]

$$Z_{\text{chem}} = R_{\text{chem}}\sqrt{\frac{1}{1 + j\omega(R_{\text{chem}}C_{l_\delta})}} \tag{8}$$

where R_{chem} and $C_{l\delta}$ are a characteristic resistance and capacitance, respectively, reflecting co-limitation by surface kinetic and transport properties of the mixed conductor

$$R_{\text{chem}} = \frac{RT}{4F^2}\sqrt{\frac{fV_{\text{m}}}{\tilde{D}_{\text{eff}}ar_0}} = \sqrt{\frac{4R_{\text{surf}}}{\sigma_{i,\text{eff}}a}}$$

$$C_{l_\delta} = \frac{4F^2}{RT}\frac{(1-\epsilon)l_\delta}{fV_{\text{m}}} \tag{9}$$

where Vm is the molar volume, $\tilde{D}_{\text{eff}} = (1-\epsilon)\tilde{D}/\tau$ is the effective oxygen-ion chemical diffusion coefficient in the solid (corrected for porosity and path tortuosity), and r_0 and f (as defined previously in eq 5) are the linearized rate of oxygen absorption/desorption and a thermodynamic factor, respectively. As shown in eq 9, one can also express R_{chem} in terms of surface and bulk resistances defined previously in eqs 6 and 7 for a thin film: R_{surf} and $\sigma_{\text{i,eff}} = (1-\epsilon)\sigma_i/\tau$.

Equation 9 shows that the chemical capacitance in this case is similar to that derived previously in eq 6 for a thin film (C_L); however, in the co-limited situation the important length parameter is not L but rather a characteristic "utilization" length given by

$$l_\delta = \sqrt{\frac{\tilde{D}_{\text{eff}}}{fV_{\text{m}}ar_0}} = \sqrt{\frac{\sigma_{i,\text{eff}}R_{\text{surf}}}{a}} \tag{10}$$

The significance of this length parameter l_δ can be understood by examining the predicted steady-state vacancy concentration profile in the porous electrode as shown in Figure 26a. At steady state, the model predicts that the mixed conductor will be reduced by an amount that decays exponentially with distance

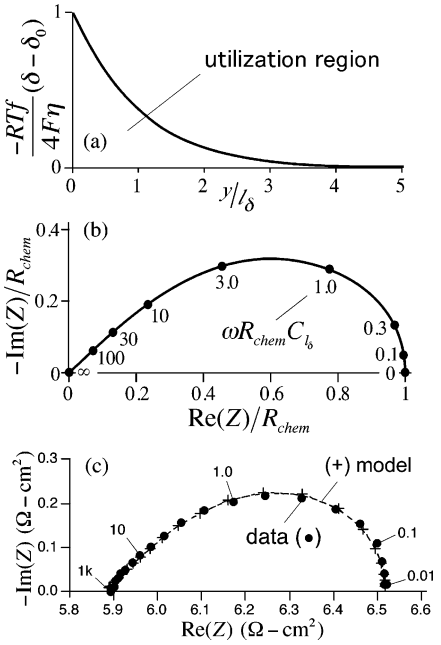

Figure 26. Predictions of the Adler model shown in Figure 25 assuming interfacial electrochemical kinetics are fast. (a) Predicted steady-state profile of the oxygen vacancy concentration (δ) in the mixed conductor as a function of distance from the electrode/electrolyte interface. (b) Predicted impedance. (c) Measured impedance of $La_{0.6}Ca_{0.4}Fe_{0.8}Co_{0.2}O_{3-\delta}$ electrodes on SDC at 700 °C in air, fit to the model shown in b using nonlinear complex least squares. Data are from ref 171.

from the electrolyte interface with a characteristic length l_δ describing the size of the active region. Equation 9 shows that the chemical capacitance will be proportional to the size of this region, just as the chemical capacitance of a dense film is proportional to its thickness (eq 6). The difference here is that the amount of material contributing to the capacitance is determined by the kinetic and diffusion parameters rather than a geometric length scale.

Figure 26b shows the impedance predicted by eqs 8 and 9. As previously discussed, this function is known as the Gerischer impedance, derived earlier in section 3.4 for a situation involving co-limited adsorption and surface diffusion (in the context of Pt). As with the surface-mediated case, the present result corresponds to a co-limited reaction regime where both kinetics and transport determine the electrode characteristics (as reflected in the dependency of R_{chem} and $C_{l\delta}$ on both r_0 and D_{eff}). The essential difference between this and the Pt case is that here the kinetics and diffusion parameters refer to a bulk-mediated rather than surface-mediated process.

As shown in Figure 26c and as discussed more fully elsewhere,[171] initial comparisons of this model to impedance data for $La_{0.6}Sr_{0.4}Co_{0.2}Fe_{0.8}O_{3-\delta}$ (LSCF) on gadolinia-doped ceria were favorable. A fit of the impedance to eq 8 yielded values of R_{chem} and $C_{l\delta}$ that were reasonably consistent with those calculated based on the known bulk properties of LSCF. The large chemical capacitance observed (and calculated) in this case corresponds to a significant reduction/oxidation of the bulk, while the Gerischer shape of the impedance (and absence of other impedance features) suggests that the reaction is co-limited by absorption and transport to the interface.

This result prompted a more complete experimental study by Adler of the impedance of porous $La_{1-x}Sr_xCoO_{3-\delta}$ electrodes on SDC.[28] Symmetric LSC/SDC/LSC cells with 2.0 cm^2 active area were fabricated at three values of strontium content, $x = 0.2$, 0.3, and 0.4, and characterized in terms of surface area (a) and porosity (ϵ) (tortuosity (τ) of the bulk path was also estimated). The impedances of these cells were then studied over a range T and P_{O_2}. Although the resulting impedance data did not match eq 8 as well as shown in Figure 26c, the data did exhibit a single arc with a Gerischer shape and were fit to obtain values of R_{chem} and $t_{chem} = R_{chem}C_{l\delta}$. On the basis of these values (and without other adjustable parameters), the oxygen vacancy diffusion and surface-exchange coefficients were back calculated and compared to independent measurements based on isotope exchange or membrane permeation (see section 4.2). The results suggest the following.

(1) *Preference for the bulk path*. With notable exceptions (see the following section), quantitative comparison of the vacancy diffusion coefficient and surface-exchange coefficient back calculated from the resistance and capacitance are in reasonable agreement with independent measurement both in value as well as dependencies on P_{O_2} and temperature (activation energy). This result suggests that for materials with high ionic conductivity, it is the bulk path (a−c−e in Figure 4) rather than the surface path (b−d−f) that dominates at open circuit. This appears to be the only explanation consistent with the large observed chemical capacitance. Not surprisingly, agreement is best for materials with the highest oxygen vacancy concentration. Application of the model to LSM (which is a poor ionic conductor in air) grossly underpredicts performance, suggesting that porous LSM functions primarily by a surface-mediated mechanism at least near open circuit (see section 5).

(2) *Co-limited kinetics with a significant utilization region*. As with platinum, the model predicts that the chemical portion of the reaction will be co-limited by molecular dissociation and transport. Values of l_δ calculated from the model for the analyzed conditions vary from 0.4 to 20 μm depending on P_{O_2}, temperature, and electrode surface area, with typical values in the 3−5 μm range. This result indicates that a significant portion of the electrode surface is active for oxygen reduction, which explains Takeda's (and other's) observation that the performance of LSC electrodes on YSZ improves with thickness up to a limit of a few micrometers.[101,175] At around the same time as the Adler model, Zhou and co-workers modeled the effect of porous perfusion layers on mixed-conducting membranes, drawing similar conclusions regarding the co-limited nature of the reaction and estimates of the utilization length.[176] These models further predict that for small surface areas (a) l_δ will exceed the thickness of the porous layer/electrode such that the entire layer becomes active with surface-absorption-limited behavior (semicircular impedance) rather than co-limited. Adler confirmed this

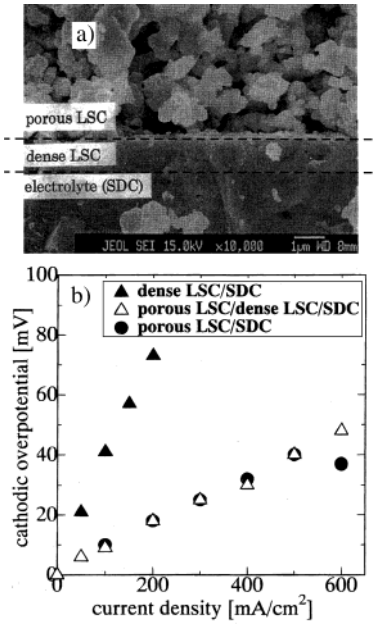

Figure 27. Measured overpotential of a porous LSC electrode on SDC with and without a dense LSC layer in between. (Reprinted with permission from ref 179. Copyright 1998 Electrochemical Society, Inc.)

prediction by oversintering the electrode and showing that the electrode exhibits a surface-limited impedance similar to that predicted by eq 6.[28]

(3) *Absence of electrochemical−kinetic resistances*. For LSC on SDC at 550 °C and above, additional high-frequency impedance features indicating the presence of an interfacial resistance/capacitance were not observed. This result suggests that the majority of the overpotential is associated with absorption and bulk transport of oxygen, while ion exchange at the LSC/SDC interface remains in electrochemical equilibrium. As we will see in section 6, this conclusion is not universally true of all materials; additional impedance arcs have been observed for perovskites on YSZ and with ceria at lower temperatures or with certain electrolyte dopants. Nonetheless, this result did strongly challenge prior thinking, which had assumed interfacial electrochemical kinetics would be limiting if transport is facile.[101]

Subsequent studies of porous mixed-conducting electrodes under a variety of conditions have since reinforced the view that the bulk pathway plays an important (if not dominant) role in the electrode kinetics for these materials.[19,177−184] Of particular note is a study (published the same year as the Adler studies) by Endo and co-workers who used pulsed laser deposition to cast a dense thin (∼1 μm) film of LSC (40% Sr) onto SDC prior to screen printing and firing a porous LSC electrode of the same composition[179] (Figure 27a). As shown in Figure 27b, they found that the overpotential of the porous electrode is independent of the presence of the film. This result appears to confirm the dominance of the bulk path, since elimination of any possible surface path (including TPB contact area) does nothing to alter the electrode performance. This result also appears to confirm that the active region of the porous LSC layer is large compared to the superficial electrode area, since replacement of the gas-exposed electrolyte with additional (presumably active) LSC does not significantly enhance performance. Also consistent with a large utilization region is a study by Koyama et al. of porous $Sm_{0.5}Sr_{0.5}CoO_{3-\delta}$ (SSC) on SDC as a function of electrode thickness;[184] they found that the electrode performance improves with thickness up to about 10−15 μm, after which performance saturates.

During the time period that the results described above were published (mid-1990s), workers studying porous mixed conducting electrodes fell into multiple schools of thought regarding the mechanism (not unlike those discussed previously for Pt/YSZ). A number of papers appeared which expressed conflicting (or dissenting) views vis-a-vis the role of the bulk and interface in governing the mechanism and the extent of the utilization region. One of these was work by Gödickemeier et al., who used current-interruption techniques to study the steady-state current−overpotential relationships for LSM and LSC on samaria- and gadolinia-doped ceria.[14,17] They found that their results fit well to a Butler−Volmer rate expression and thus concluded the electrodes are limited by interfacial electrochemical kinetics rather being than transport limited. In this case, by "transport limited" the authors meant simply that a limiting current was not observed at high overpotentials.

However, as we saw in section 3.3 for platinum on YSZ, the fact that $i-\eta$ data fits a Butler−Volmer expression does not necessarily indicate that the electrode is limited by interfacial electrochemical kinetics. Supporting this point is a series of papers published by Svensson et al.,[172,185,186] who modeled the current−overpotential ($i-\eta$) characteristics of porous mixed-conducting electrodes. As shown in Figure 28a, these models take a similar mechanistic approach as the Adler model but consider additional physics (surface adsorption and transport) and forego time dependence (required to predict impedance) in order to solve for the full nonlinear $i-\eta$ characteristics at steady state.

One significant prediction of the Svensson models is that regardless of whether the reaction path is surface or bulk dominated, the $i-\eta$ characteristics appear Tafelian, even if interfacial electrochemical kinetic steps are equilibrated. As an example, Figure 28b shows the predicted $i-V$ characteristics of a mixed conducting electrode assuming a bulk path as a function of the oxygen vacancy diffusion coefficient. As evidenced by the linear dependence of ln(i) on V at high currents, the model obeys Tafel kinetics, yet the Tafel parameters ("exchange current density") depend on a transport parameter. In other words, just as we saw for platinum on YSZ (section 3.3), the mere fact that $i-\eta$ data fits a Butler−Volmer expression does not prove that the electrode is limited by interfacial electrochemical kinetics. The Svensson models show that chemical steps of ad(b)sorption and transport can dominate the observed kinetics well below limiting current, and thus the absence of a measured limiting current does not indicate an absence of transport limitations. On the contrary, diffusion in this case is predicted to produce a variety of finite, Tafel-like, characteristics.

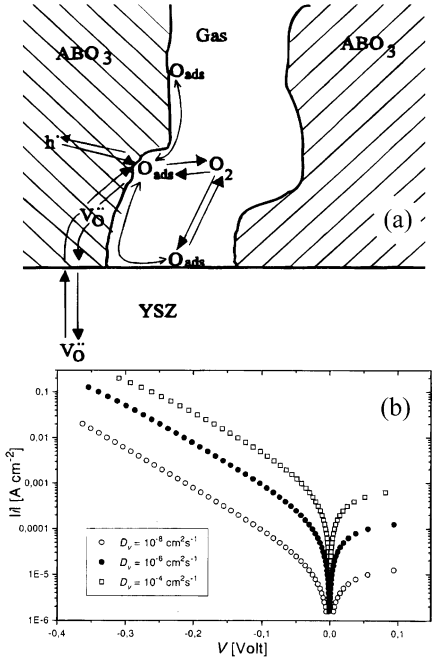

Figure 28. Svensson's macrohomogeneous model for the $i-V$ characteristics of a porous mixed-conducting electrode. (a) The reduction mechanism assuming that both surface and bulk diffusion are active and that direct exchange of oxygen vacancies between the mixed conductor and the electrolyte may occur. (b) Tafel plot of the predicted steady-state $i-V$ characteristics as a function of the bulk oxygen vacancy diffusion coefficient. (Reprinted with permission from ref 186. Copyright 1998 Electrochemical Society, Inc.)

Another set of papers countering the conclusions of the Adler studies (as well as implicitly the Svensson studies) were published by Liu and co-workers, who questioned the validity of the Adler model on several levels.[169,170,187,188] As discussed elsewhere,[189] many of these questions appear to have arisen primarily from a misunderstanding about the assumptions and terminology of the model (so we will not belabor the points raised again here). However, Liu also raised the more general concern that the model does not consider the "direct" reduction of O_2 at the TPB (traditionally considered the route by which the cathode reaction occurs). While this is certainly true, perhaps the more relevant question is what we mean by the "three-phase boundary"? Certainly from the phenomenological standpoint (Figure 3), one must have thee phases involved in the reaction for oxygen reduction to occur. However, when one begins to consider the specific chemical, electrochemical, and transport steps involved, one must abandon the idea of an ideal 1D geometric surface and consider the specific phases, surfaces, and interfaces involved in these steps. A separate consideration of the "direct" TPB reaction is not necessary since it is exactly this reaction that the various models discussed in this review attempt to embody. While a mechanistic approach almost certainly involves oversimplification of the physics, it also allows workers to pose specific hypotheses about the mechanism, predict the consequences of those hypotheses, and test these predictions against measurement. As we will see in the following section, the failure of existing models to predict certain features

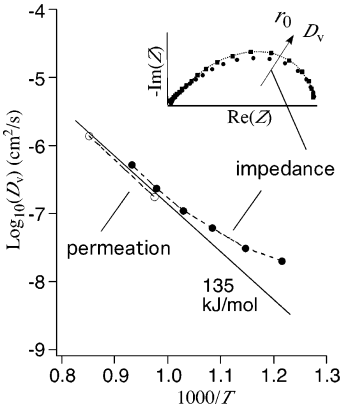

Figure 29. Comparison of the oxygen vacancy diffusion coefficient (D_v) in LSC ($x = 0.2$) determined from permeation measurements vs that extracted from impedance measurements using the model in Figure 26. Data are from refs 190 and 28. (Adapted with permission from ref 28. Copyright 1998 Elsevier.)

of the data and their inconsistency with measurements under certain conditions is actually useful information for understanding how other factors and mechanisms (besides the bulk path) come into play.

4.7. Limitations of Bulk, 1D Transport Models for Porous Mixed Conductors

While subsequent work[19,177−184] has continued to reinforce the importance of the bulk for porous mixed-conducting electrodes, authors generally debate the degree to which the bulk vs surface paths dominate and under what conditions. In the asymptotic limit of high ionic conductivity, the 1D models discussed above appear to explain $i-V$ characteristics and impedance data well under conditions of facile bulk transport and a reversible interface. However, what happens when the ionic conductivity is not so high and/or the utilization length becomes competitive with microstructural features? Also, what happens when the interface is not reversible?

One clue to this question is provided by where and how the Adler model breaks down in explaining the impedance characteristics of LSC on SDC. For example, Figure 29 compares the apparent vacancy diffusion coefficient of $La_{0.8}Sr_{0.2}CoO_{3-\delta}$ (extracted from the chemical resistance and capacitance[28]) to the measured value for a bulk membrane (determined from permeation measurements[190,191]) as a function of temperature in air. At the highest temperatures, agreement is reasonable in both value and activation energy. However, at lower temperatures there is a systematic deviation from activated behavior, with the apparent diffusion coefficient being perhaps 10 times larger than predicted by extrapolation of the permeation data. This deviation also corresponds to a change in the shape of the impedance to being less "Gerischer-like".[28] In addition, for $La_{0.8}Sr_{0.2}CoO_{3-\delta}$, the Adler model predicts a utilization length of $l_\delta = 0.3-0.6\ \mu$m, which is competitive with the microstructural features of the electrode and thus a violation of the formal assumptions of the model.

There are several possible explanations for this behavior, all of which speak to various deficiencies of current models. First, even if the bulk path

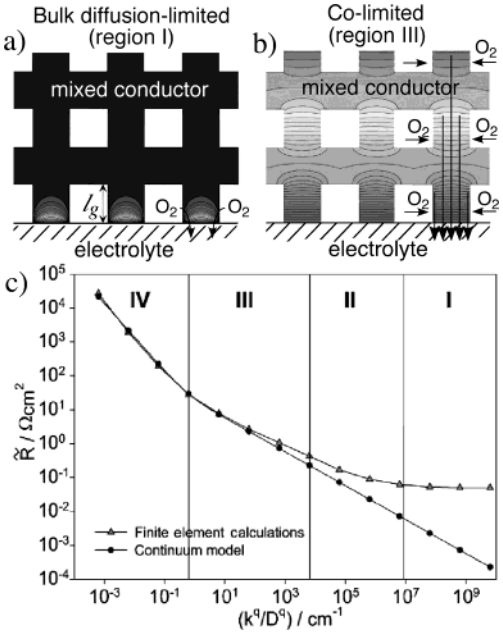

Figure 30. Finite-element calculation of the oxygen vacancy concentration profiles in a porous mixed conducting electrode, assuming a cylinder−block microstructure having a single characteristic dimension l_g. (a) Oxygen reduction is entirely bulk-transport limited. (b) Oxygen is co-limited by absorption and bulk transport as in Figures 25 and 26. (c) Comparison of the predicted resistance to that of a macrohomogeneous model (Figure 26) as a function of absorption kinetics, assuming $l_g = 1.6$ μm. (Adapted with permission from ref 194. Copyright 2003 Annual Reviews.)

dominates, we expect that as the utilization length becomes small, the assumption that reaction/transport can be treated using a 1D macrohomogeneous representation of the microstructure will break down. The most complete studies of this effect has been published by Fleig,[192−194] who used finite-element analysis (FEA) to compare the predictions of a 1D macrohomogeneous model to that of a full 3D microstructural model. As shown in Figure 30, the 3D model considers bulk absorption and diffusion of oxygen in a hypothetical "cylinder−block" microstructure having characteristic length $l_g = 1.6$ μm. Fleig compared the linearized electrode resistivity predicted by this 3D model to that of a 1D macrohomogeneous representation of the same system as a function of k^q at fixed D^q, where k^q and D^q are linearized constants for surface absorption and bulk diffusion.[195−197] This comparison shows that as k^q/D^q increases beyond a value of about 0.1−1 μm^{-1}, the macrohomogeneous assumption breaks down. Indeed, based on the analysis presented in section 4.6, we expect this breakdown to occur when the utilization length $l_\delta \approx \sqrt{l_g D^q/k^q}$ (approximate translation of eq 10 for Fleig's variables k^q and D^q) becomes on the same order or smaller than the particle dimensions l_g. This occurs when $k^q/D^q \approx l_g^{-1}$, which in this case is 0.6 μm^{-1}, in good agreement with Fleig's results. Furthermore, Fleig shows that when surface absorption becomes fast, the electrode becomes entirely transport limited (with a plateau in performance) vs the macrohomogeneous model (which predicts continued improvement as kinetics get faster). Such purely transport-limited behavior is not possible with a surface mechanism—this is a unique feature of bulk transport in two or three dimensions.

What Fleig's results suggest is that even without invoking other mechanisms besides the bulk path, one would have difficulty fitting the characteristics of a porous mixed-conducting electrode accurately using a 1D model (such as the Adler or Svensson models) when l_δ is less than a few micrometers. The degree to which these effects are responsible for any lack of agreement with data are unknown. To date, a quantitative modeling of the impedance of LSC or LSF electrodes considering 3D effects has not yet been conducted. This is an ambitious task for several reasons. First, it is not clear that a geometric idealization of the microstructure (such as that used by Fleig) would be sufficient—at the length scale of an individual particle, the details of the actual microstructure (particle size distribution, particle connectivity, contact angle, etc.) might become important. Second, Fleig's model predicts that under increasingly 3D transport-limited conditions, the ionic oxygen flux will not be uniform across the electrode/electrolyte interface but rather increasingly constricted through an area close to the TPB. This constriction raises the question of whether electrochemical kinetics at the interface might become increasingly important due to reduced area available for charge transfer. Such considerations add considerable complexity to the problem, in terms of both nonlinearity and inhomogeneity at this interface as well as the effect of interfacial resistance on the concentration profiles in the bulk.

However, even if one took 3D effects into consideration, it is unlikely that one could explain all the discrepancies between the Adler model and the measured impedance. For example, Figure 29 shows that the assumption of 1D bulk transport appears to *underpredict* the measured performance. In contrast, Fleig's modeling studies suggest that ignoring 3D transport effects will generally *overpredict* performance (Figure 30). This forces us to consider a second reason the Adler model may break down: As bulk transport becomes less facile, a parallel mechanism involving the surface path may become increasingly important. Although this widely held belief has not yet been proven definitely, it is nonetheless circumstantially consistent with a variety of observations.

(1) *Inconsistency of performance with a bulk path at low vacancy concentration*. A quantitative comparison between predictions of the Adler model and impedance data for LSC shows the poorest agreement (underprediction of performance) at low temperatures, high P_{O_2}, and/or low Sr content.[28] These are the conditions under which the bulk vacancy concentration (and thus also the ionic conductivity and surface exchange rate of oxygen with the bulk) are the lowest. These are exactly the conditions under which we would expect a parallel surface path (if it existed) to manifest itself, raising performance above that predicted for the bulk path alone. Indeed, as discussed more fully in section 5, the Adler model breaks down completely for LSM (a poor ionic conductor at open-circuit conditions), predicting an

electrode impedance many orders of magnitude higher than observed experimentally.[171]

(2) *Inconsistencies in the chemical capacitance.* As the bulk vacancy concentration is reduced, and hence the predicted chemical capacitance of the bulk (per unit volume) becomes smaller, the portion of chemical capacitance associated with surface species may become increasingly significant. Kuznecov et al. showed that a surface-dominated mechanism should exhibit a similar Gersischer shape as a bulk-dominated mechanism,[198] only with a smaller chemical capacitance. One possible piece of evidence that this occurs is the observation that the apparent utilization length l_δ (as extracted from impedance data assuming the Adler model[28]) generally *decreases* with conditions promoting lower vacancy concentration (lower Sr content, higher P_{O_2}). This observation is somewhat inconsistent with eq 10, which for most mixed conductors predicts that the utilization length will stay approximately *constant* with changes in stoichiometry (as shown previously in Figure 22, the bulk oxygen vacancy concentration tends to influence oxygen exchange and bulk diffusion rates of perovskites similarly,[141] leading to a constant ratio of $\tilde{D}_{\text{eff}}/fr_0$ in eq 10). One resolution to this apparent inconsistency might be a parallel surface path, which could alternatively explain the measured decrease in chemical capacitance as a confinement of stoichiometry variations to the surface rather than a shrinkage of the bulk utilization region.

(3) *Nonlinear electrode kinetics.* Another possible indicator of a parallel surface path is nonlinearity of the current−overpotential characteristics. In particular, one conclusion of the model by Zhou and coworkers mentioned previously[176] was that the permeation resistance of a porous membrane overlayer is fairly constant with driving force (i.e., linear force−flux relationship) for mixed conductors having high vacancy concentration. This result appears to be consistent with recent measurements of Horita et al.,[181] who conducted a study of the impedance of porous LSC electrodes on $La_{0.8}Sr_{0.2}Ga_{0.8}Mg_{0.2}O_{2.8}$ (LSGM) electrolyte as a function of cathode overpotential. Among other things, these results show that the electrode kinetics are fairly linear with overpotential for materials with high vacancy concentration but become increasingly nonlinear for materials and conditions promoting the lowest vacancy concentrations. For example, $La_{0.8}Sr_{0.2}CoO_{3-\delta}$ is more nonlinear than $La_{0.6}Sr_{0.4}CoO_{3-\delta}$, and both materials are increasingly nonlinear at lower temperatures. Although the linearity of the bulk path itself has not been well investigated, an increase in nonlinearity with decreasing vacancy concentration might indicate a shift toward a surface-mediated reaction mechanism involving more nonlinear behavior (e.g., increased charge-transfer resistance at the interface due to confinement of the flux near the TPB).

Since the mid-1990's, several models which consider both a bulk *and* surface path have been proposed, including the Svensson models as well as a more recent model by Coffey and co-workers.[199] However, these models have not been definitive in addressing the bulk vs surface question for at least two fundamental reasons. First, a common feature of these models is that they are limited to nonlinear steady-state behavior and therefore cannot be used to analyze impedance or other measurements with time resolution for various physical processes. As mentioned previously, it is hard to tell what is going on from Tafel parameters since so many things mimic Tafel kinetics. Second and perhaps more fundamentally, there is simply a dearth of independent data for model parameters. Although the mobility of oxygen on the surface of a perovskite is generally thought to be "fast", its rate relative to bulk transport (as a function of defect concentration) has never been quantitatively determined. Coffey et al. summarize the situation nicely in the concluding paragraph of their paper.[199]

"Unfortunately many of these parameters are at best rough approximations if not outright guesses. Consequently our results are not at this time useful in interpreting available electrochemical data; however they are useful in defining what additional experimental measurements need to be made."

Indeed, in the spirit of this latter comment, the purpose of this review is to consolidate our understanding of SOFC cathodes so that it becomes easier to identify and propose new avenues of research.

4.8. Summary: Importance of the Bulk for Mixed-Conducting SOFC Cathodes

In this section we saw that the active region of a SOFC cathode can be significantly enhanced by incorporating a mixed conductor (a material which conducts both ions and electrons). While electrodes of this type have proven challenging to implement in a SOFC operating environment (see section 6), they nonetheless have taught us a lot about what factors can limit electrode performance and opened the realm of possibilities for future materials development. To summarize, some of the salient points of our current understanding are listed.

(1) *Role of the bulk transport path.* In section 3 we saw that for Pt the dissociation of oxygen and transport of reactive intermediates to the electrode/electrolyte interface is confined to the material surface. With mixed conductors, it is possible for oxygen reduced at the surface to be transported through the bulk of the material to the electrode/electrolyte interface. If bulk transport is facile, this path may dominate, extending both the accessible surface for O_2 reduction as well as broadening the active charge-transfer area from the TPB to include the entire solid−solid contact area.

(2) *Chemical capacitance.* When the mechanism involves significant involvement of the bulk, accumulation of reactive intermediates not only involves surface species but oxidation and reduction of the bulk. This can be detected as an anomalously high effective capacitance, often referred to as a *chemical* (or *pseudo*) *capacitance.* This capacitance can be as large as 0.1−1 F/cm^2 and thus easily detected by current-interruption or impedance techniques. Thus, capacitance is a strong indicator (independent of resistance) as to what degree the interface, surface, and/or bulk are playing in the

reaction kinetics for a given material and set of conditions.

(3) *Co-limited kinetics*. As with platinum, porous mixed-conducting electrodes are co-limited by molecular dissociation and transport. For mixed conductors with high rates of bulk ionic transport, values of l_δ vary from 0.4 to 20 μm depending on P_{O_2}, temperature, and electrode surface area with typical values in the 3−5 μm range. This result indicates that a significant portion of the electrode surface is active for oxygen reduction, not just material in the immediate vicinity of the TPB.

(4) *Sensitivity of interfacial resistance to various factors*. For perovskite mixed conductors on some ceria-based electrolytes, workers have reported virtually zero interfacial resistance such that the electrode overpotential is dominated entirely by dissociation of O_2 and transport of intermediates to the electrode/electrolyte interface. As we will see in section 6, this conclusion is not universally true of all materials; additional impedance arcs have been observed for perovskites on YSZ and with ceria at lower temperatures or with certain electrolyte dopants.

(5) *Relative role of surface vs bulk path not yet known quantitatively*. While it has been clearly established that the bulk transport path plays a role (and may dominate) in the mechanism of mixed-conducting electrodes, our quantitative understanding is currently limited to asymptotic cases (such as thin films or materials with unusually high bulk transport rates). We currently lack general techniques to measure or predict the relative role of the surface vs bulk paths in electrodes of arbitrary composition and processing. Development of such techniques will be an important step in understanding more complex materials and microstructures and in making intelligent materials design choices.

5. Lanthanum Strontium Manganese Oxide (LSM): Where Surface and Bulk Converge

In sections 3 and 4 we examined two asymptotic cases for the mechanism of oxygen reduction. With porous Pt, oxygen reduction appears to occur by a surface-mediated mechanism, where dissociative adsorption and diffusion of oxygen on the gas-exposed Pt surface play a significant (if not dominant) role in determining the overall electrode kinetics. Likewise, for porous mixed conductors with high ionic conductivity, molecular dissociation and transport are equally important; however, with these materials the mechanism appears to proceed by a primarily bulk-mediated path. In both cases it was shown that due to porosity, oxygen dissociation and transport tend to co-limit the reaction (rather than contribute independently). Interfacial electrochemical kinetics can also play a significant role, depending on the exact materials and conditions. Finally, we saw that these two asymptotic limits of behavior begin to merge for materials having some bulk ionic conductivity but not as facile as the best mixed conductors.

Consideration of these asymptotic limits is useful because it potentially helps us to identify, discuss, and study the various physical processes underlying electrode kinetics, even outside those limits. However, the performances of "real" SOFC cathodes of technological interest generally fall outside these limits for two fundamental reasons. First, SOFC cathodes must satisfy a number of other constraints besides performance, including mechanical and chemical stability, cost, manufacturability, etc.—it is therefore nearly impossible to optimize electrode materials according to only one or two physical properties. Second, as people optimize any system, they will tend to mitigate (knowingly or unknowingly) the most rate-limiting factor until other factors naturally come into play. In other words, if a material's behavior is asymptotic, it is not likely to be optimized or satisfy more than one design constraint.

One such "more complex" case is $La_{1-x}Sr_xMnO_{3\pm\delta}$ (LSM), which starting in the mid-1970s became (and has remained) one of the most heavily pursued electrode materials for SOFC cathodes. As mentioned earlier, LSM was originally investigated as an SOFC cathode (along with a variety of other transition-metal perovskites) due to its good electrical conductivity and relatively low cost.[4] However, LSM quickly distinguished itself for a variety of reasons. First, with the right choice of Sr content (x), a nearly exact thermal expansion match between LSM and YSZ can be achieved. This allowed workers to fabricate and explore a wide variety of electrode microstructures and cell geometries with reduced thermal stress generated by thermal cycling. Likewise, Mn is generally less reducible than other transition metals (Co, Fe) in a perovskite matrix, and thus LSM exhibits little or no chemical expansivity,[200,201] another source of thermal−mechanical stress potentially threatening the integrity of the electrode microstructure. Another advantage of LSM is that it is generally more thermodynamically stable than mixed conductors containing cobalt or iron.[202] It is nonetheless reasonably catalytic for O_2 dissociation, unlike materials having similar or higher stability, such as $La_{1-x}Sr_xCrO_3$ for example.[203]

As with other SOFC cathode materials (including Pt), early kinetic studies of LSM in the mid-1980s gave rise to multiple schools of thought regarding the reaction mechanism. At that time, LSM was often studied alongside Pt or other perovskites and thus lumped together with these materials in the same debates regarding the rate-limiting step, the role of bulk transport, etc. However, beginning in the early 1990s it became clear that LSM is somewhat different than both Pt or other (more reducible) perovskites in terms of the reaction mechanism, falling somewhat in a gray area among the asymptotic limits described previously. Although the last 10−15 years of work have added significantly to our *qualitative* understanding of LSM, this material has so far continued to elude quantitative descriptions of its performance in terms of underlying mechanisms. For this reason and because LSM is so important technologically, we devote this section to it.

5.1. Three-Phase Boundary: Not the Whole Picture

In the case of Pt, mechanistic considerations suggest that the active region of the electrode is confined

to a region close to the three-phase boundary (TPB), and thus performance has often been reported to scale with the available TPB area. Thus, in addressing the question of how localized the O_2 reduction is in LSM, one approach workers have used is to examine the relationship of performance to microstructure. For example, Mizusaki and co-workers carefully characterized and measured the impedance of $La_{1-x}Ca_xMnO_3$ (LCM) electrodes on YSZ (a very similar material system to LSM/YSZ) as a function of morphology, controlled using various preparation methods and firing conditions.[204] They used SEM to estimate the contact area of LCM and YSZ as well as the geometric length of the TPB. While their results showed that the electrode *capacitance* scales with the electrode/electrolyte contact area (as one would expect for interfacial polarization), the resistance and overpotential were found to scale inversely with the length of the TPB, at least at low polarization. A number of other studies of single-phase and composite electrodes have since reinforced the view that the electrode kinetics scale with TPB contact area.[205−207]

However, there are several equally valid interpretations to this commonly observed result. One possibility is that the reaction is co-limited by adsorption and surface diffusion, where the utilization length is small compared to the average particle size. An alternative (but not mutually exclusive) possibility is that the reaction is limited by electrochemical kinetics at the TPB itself. As with Pt, both situations or a combination thereof would result in the resistance scaling with the reciprocal of the TPB length. A third possibility is that reaction is limited by mechanisms acting farther from the TPB but which scale with electrode geometric factors (such as the electrode surface area) that are strongly *correlated* to the length of the TPB (through the process of sintering, for example). Without the ability to separately control the TPB length while leaving other geometric parameters constant, it is difficult to distinguish these various possibilities. Also, the conditions under which the electrode performance scales with the TPB may not be universal—the electrode may have multiple regimes of operation depending on overpotential and other factors.

One study that tried to address this question was conducted by van Heuveln and co-workers, who attempted to separate the effects of electrode surface area from TPB contact area.[208,209] Variations in surface area were obtained by using different sintering temperatures, while changes in TPB contact area were accomplished through the use of two powders having different morphologies. Surface area and TPB contact area were determined by image analysis of SEM cross sections; for the surface area the electrode bulk was examined, while for the TPB contact area the electrodes were etched off and the underlying "stain" on YSZ was analyzed. Electrode performance was measured in terms of the overpotential at a fixed current density of 100 mA/cm^2.

Within the statistical certainty of the data, no general correlation was found between overpotential and TPB length. This could mean that no such general correlation exists and thus prior studies have been interpreted too narrowly. On the other hand, it is not clear that the comparisons in performance drawn by the authors in this case are fully meaningful. The authors point out that the electrode kinetics are (1) highly nonlinear and (2) very dependent on the polarization history. Thus, it is difficult to say whether two cells operating at the same current density (but different overpotentials) are really at the same operating point vis-à-vis comparison of TPB contact area. Rather, a more significant observation we might draw from such a study is how *difficult* it is to meaningfully correlate the complex (often nonstationary) electrochemical characteristics of LSM to the highly complex microstructure of a porous electrode, at least with today's tools and techniques. As we will see in the sections below, workers have had more success over the last 10−15 years examining electrodes with defined and/or microfabricated geometries, where TPB area and material composition can be more carefully controlled and analyzed.

5.2. Complex Stationary Electrochemical Characteristics and Properties

Like all cathodes, early electrochemical kinetic studies of LSM focused heavily on steady-state d.c. characteristics, attempting to extract mechanistic information from the T and P_{O_2} dependence of linear and Tafel parameters.[13,203] As recently as 1997, some workers have continued to support a view that LSM is limited entirely by electrochemical kinetics at the LSM/electrolyte interface based on this type of analysis.[14,17] However, as we have seen for other materials (including Pt), the fact that an electrode obeys Butler−Volmer kinetics means little in terms of identifying rate-limiting phenomena or in determining how close the reaction occurs to the TPB. To understand LSM at a nonempirical level, we must examine other techniques and results.

As we saw with Pt and other perovskites, one such approach is electrochemical impedance spectroscopy (EIS), which attempts to separate various mechanistic steps via time scale. Although quantitative analysis of impedance data in a complex material system like porous LSM involves many uncertainties (see sections 3.1 and 6.7 as well as ref 49), it is usually reliable in terms of separating rough time scales on which various physical processes occur. An example of this approach for understanding LSM is a study by Østergård and Mogensen,[210] which examined the impedance of single-phase porous LSM on YSZ as a function of T, P_{O_2}, and polarization. The observed impedance was found to contain at least three distinct features. The highest frequency feature was attributed to interfacial electrochemical kinetic processes at the LSM/YSZ interface. The two lower frequency features were assigned to dissociation and transport, respectively, of oxygen species on the LSM surface.

While such one-to-one assignments of impedance features to specific reaction steps are appealing, it is not clear how definitive they are without further analysis. In particular, based on what we know about

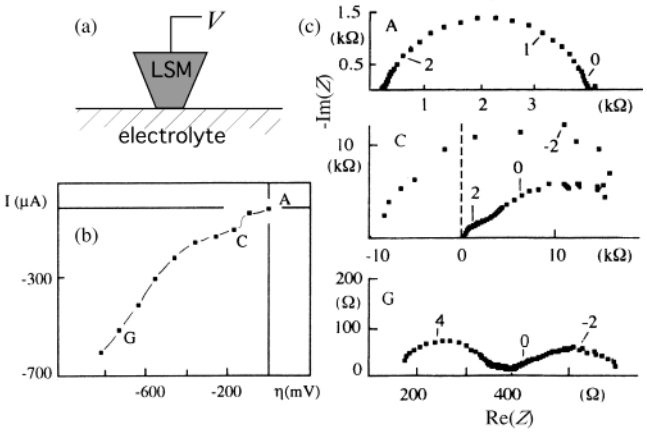

Figure 31. Measurements of polarization and impedance of LSM point-contact electrodes on YSZ. (a) Schematic showing the geometry of the electrode. (b) Steady-state cathodic polarization at 960 °C and $P_{O_2} = 10^{-3}$ atm. (c) Impedance measured under polarization at the conditions marked in b. (Adapted with permission from ref 211. Copyright 1995 Elsevier.)

Pt and perovskite mixed conductors, we might expect oxygen dissociation and transport on LSM to be co-limiting, resulting in a single "Gerischer-like" impedance feature (as shown in Figures 14 and 15) rather than two independent low-frequency features (as proposed by Østergård and Mogensen). Also, these particular authors did not attempt to quantitatively analyze the chemical capacitance in terms of a utilization length or bulk vs surface contributions. Without this it is hard to conclude what these various features actually correspond to except perhaps broadly in terms of "chemical" vs "interfacial" time scales.

An important contribution in this regard was a series of studies published by the Laboratoire d'Ionique et d'Electrochemie du Solide (Grenoble), which looked in detail at the $i-V$ characteristics and impedance of LSM point-contact electrodes on YSZ.[211,212] As shown in Figure 31a, these measurements involved making a single-point contact between a pin-shaped LSM sample and YSZ with known contact area. The $i-V$ characteristics (Figure 31b) show a distinct change in the characteristics of the electrode at cathodic overpotentials greater than a particular critical value, where a relatively discontinuous jump in current is observed. They found this transition occurs anywhere from −150 to −500 mV vs air and is only present in the cathodic direction. The impedance measured at points well below, near, and well above this transition are shown in Figure 31c (A,C,G). Well below the transition (A) the impedance is high with a single arc having resistance ∼4000 Ω and capacitance $\sim 10^{-6}$ F. Near the transition (C) the impedance becomes small enough to notice the presence of both a low- and high-frequency feature, but these features are too obscured by inductive effects to resolve completely. Well above the transition (G) both features become well resolved: one at high frequency having resistance ∼200 Ω and capacitance 10^{-7} F and the other at low frequency with resistance ∼300 Ω and capacitance 10^{-1} F. This low-frequency feature, seen only at high overpotential, is highly reminiscent of the chemical contributions to the impedance for mixed conductors having high ionic conductivity, as discussed in section 4.

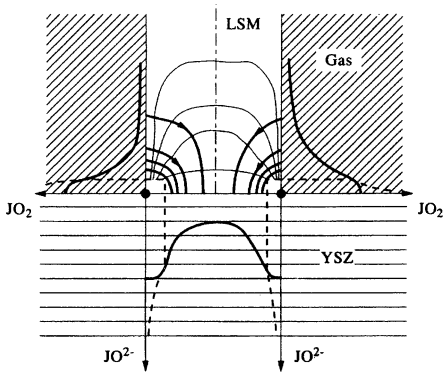

Figure 32. Schematic illustrating the possible location and distribution of bulk oxygen flow in LSM under high polarization conditions. (Reprinted with permission from ref 211. Copyright 1995 Elsevier.)

To explain these results, the workers at Grenoble theorized the existence of two different operating regimes. As shown in Figure 32, the authors proposed that at high overpotential the LSM becomes substantially reduced, creating a large concentration of oxygen ion vacancies near the interface. This non-equilibrium population of vacancies thereby creates a facile transport path through the bulk of the material, leading to a large chemical capacitance (>1 F/cm^2 when compared on an area-normalized basis). The presence of an equally sized high-frequency feature likewise suggests a significant contribution to the impedance from oxygen ionic exchange at the solid−solid interface, associated with a much smaller capacitance related to interfacial polarization. The existence of such a "bulk" operating regime at high overpotential appears to be consistent with in-situ X-ray photoelectron spectroscopy (XPS) measurements of porous LSM, which show significant reduction of Mn far beyond the electrode/electrolyte interface upon polarization.[213] More recently, as shown in Figure 33, Kuznecov and co-workers showed using field-emission SEM that sustained high cathodic polarization results in the apparent formation of Kirkendall porosity in the bulk of LSM within one particle diameter of the solid−solid interface—a strong indicator of oxygen chemical potential gradients in the bulk.[214]

In contrast, at low overpotential the workers at Grenoble theorized that LSM is primarily an electronic conductor and thus the bulk path is closed off. The observation of finite impedance near open circuit (despite the fact that LSM is a poor bulk ion conductor under these conditions) suggests the existence of a parallel "surface" path that allows transport even when the bulk is not available. Since this surface path involves a much smaller inventory of electroactive species, it is associated with a much smaller chemical capacitance than the bulk path and thus a much higher frequency (Figure 31c (A)). As the overpotential is reduced and the mechanism shifts from bulk to surface, chemical and electrochemical time scales begin to merge, making them difficult to distinguish as separate features in the impedance.

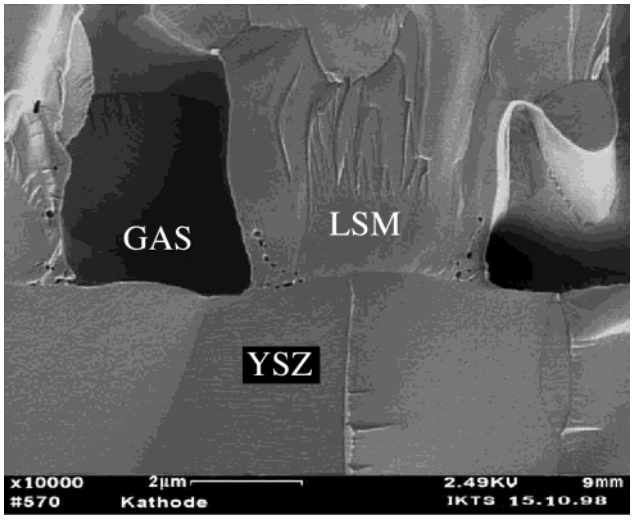

Figure 33. High-resolution field emission SEM of a porous LSM/YSZ interface following polarization for 3 h at −0.8 V at 950 °C in air. The porosity evident at the TPB is not seen in images taken prior to polarization. (Reprinted with permission from ref 214. Copyright 2003 Elsevier.)

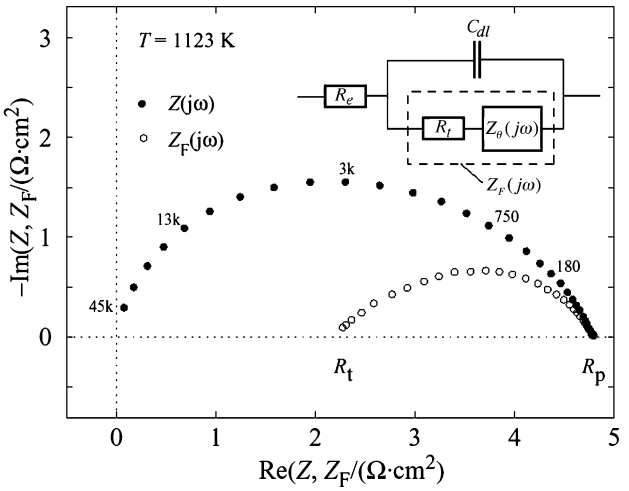

Figure 34. Total impedance (Z) and faradaic impedance (Z_F) of unsintered porous LSM on YSZ measured in air at 850 °C. Electrolyte resistance (R_e) has been subtracted from the total impedance, while both R_e and the double-layer capacitance (C_{dl}) have been subtracted from Z_F. (Reprinted with permission from ref 215. Copyright 1998 Elsevier.)

Hence, a single arc is observed with relatively high characteristic frequency.

More recent impedance studies by Mitterdorfer and Gauckler[215] of porous LSM on YSZ at low overpotential have shown that this single arc can be separated into electrochemical and chemical contributions by correcting the data for double-layer capacitance using the method of Berthier et al.[75] As shown in Figure 34, these studies suggest that the electrochemical resistance at the LSM/YSZ interface is generally not zero, even when the LSM/YSZ interface is left unfired. The remaining "faradic" (chemical) impedance has a Gerischer-like shape, consistent with co-limitation by dissociative adsorption and surface diffusion of oxygen. An estimate of the chemical capacitance based on this arc is on the order of 10^{-4} F/cm^2, which when compared to asymptotic values of LSC and Pt is more consistent with a surface process than a bulk process.

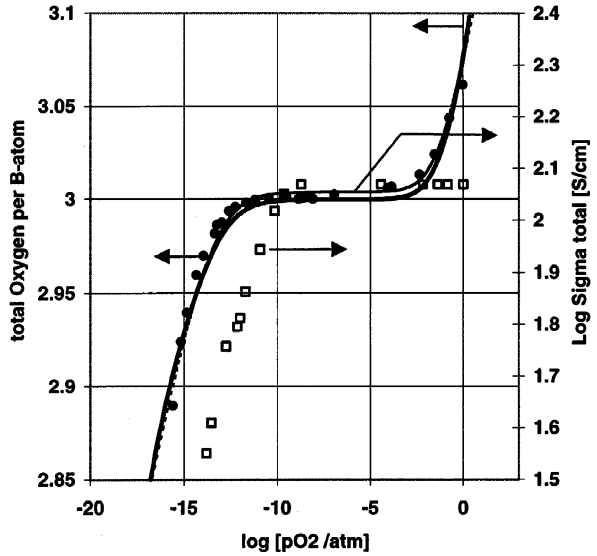

Figure 35. Total conductivity, σ, and oxygen stoichiometry, $3-\delta$, at 1000 °C of $La_{0.9}Sr_{0.1}MnO_{3-\delta}$, from measurements by Kuo et al.[365] The model calculations are based on a large polaron model with equilibrium constants as given in ref 216. Thick line: calculated stoichiometry. thin line: calculated conductivity. (Reprinted with permission from ref 216. Copyright 2000 Elsevier.)

A natural question to ask is whether this "two-regime" theory is consistent with the known properties of LSM. As recently reviewed by Poulsen,[216] the defect structure of LSM has some similarities with other more reducible perovskites such as LSC and LSF. Like these other perovskites, LSM has electrical properties on the border between that of a p-type semiconductor and a metal[217−219] and becomes oxygen substoichiometric at high temperature and low P_{O_2},[202,220] as shown in Figure 35. However, unlike its more reducible cousins (which may have significant vacancy concentration at atmospheric P_{O_2}), LSM maintains a nearly full perovskite stoichiometry above $\sim 10^{-10}$ atm and in fact becomes superstoichiometric at high P_{O_2} ($>10^{-3}$ atm), containing more oxygen than is consistent with the formal ABO_3 unit cell. Neutron diffraction studies[221] as well as numerous defect thermodynamic models[216,222,223] show that this "superstoichiometric" behavior actually results from the formation of cation vacancies on the A and B sites while the oxygen sublattice remains fully occupied.

One expected consequence of these properties is that LSM will not be a mixed conductor at low polarization under normal cathode conditions. Likewise, at cathode polarizations thermodynamically corresponding to $P_{O_2} < \sim 10^{-10}$ atm (~ -500 mV) we expect LSM to become reduced, exhibiting ionic transport properties similar to that of LSC or LSF. This transition from a nearly pure electronic conductor at low overpotential to a good mixed conductor at high overpotential is consistent with the Grenoble "two-regime" theory, at least qualitatively. Furthermore, since a transition from superstoichiometric to substoichiometric LSM involves a change in concentration and thus transport of cation vacancies (generally much slower than anions at these temperatures), we might expect significant hysteresis, irreversibility, and/or other nonstationary behavior near the transi-

tion between these two operating regimes. Indeed, as discussed in more detail in section 5.4, work by a variety of authors has shown nonstationary behavior consistent with slow or irreversible transitions under cathodic polarization[40,213,224−226]. While it is not clear if Mn reduction is the only cause of this behavior, it has certainly been identified as one likely factor.

5.3. Dense and Patterned Thin Films: Confirming Two Regimes of Operation

The previous two sections illustrate the difficulty of understanding the mechanisms governing oxygen reduction on LSM without exact control of the electrode geometry, materials, fabrication, and operating conditions/history. To that end, workers have made significant progress in the last 5−10 years microfabricating dense, patterned electrodes in which geometric lengths such as thickness and TPB length can be specifically controlled. In this way it has been possible to examine various asymptotes of behavior (such as the surface and bulk paths) and probe electrode mechanisms using a variety of techniques including impedance and isotope tracer experiments. These studies have significantly clarified our understanding of LSM and provided a variety of tools that will no doubt be built on extensively in the future.

One asymptote of interest has been the low-overpotential regime, which has been investigated extensively by impedance techniques using thin films. As mentioned previously in section 4.3, one of the first successful attempts to fabricate thin-film perovskites was published by Mizusaki and co-workers,[157] who used a pulsed KrF excimer laser to flash evaporate and deposit 1−2 μm thick films of $La_{0.5}Sr_{0.5}MnO_3$ on YSZ. Near open circuit the initial impedance of these electrodes was found to be controlled by bulk transport of oxygen though the film with a resistance that scales with electrode thickness and performance that *decreases* with increasing P_{O_2}. Indeed, this result appears consistent with what we know of LSM, since in the absence of a parallel surface path the bulk path will be controlled by the very low anionic conductivity of LSM at open-circuit conditions. Following significant anode polarization, the authors found that the LSM film becomes severely damaged and cracked and reverts to impedance behavior more consistent (in shape, time scale, and P_{O_2} dependence) with a porous LSM electrode at low polarization. The authors conclude that this damage results in creation of TPB contact area and thus changes the relative importance of bulk vs surface transport in allowing electroactive oxygen to reach the electrode/electrolyte interface.

More recent studies of dense LSM films appear to confirm these original conclusions as well as fill in some of the details.[27,159,160,167,227] In particular, Ioroi and co-workers[159,160] were able to produce very high quality films with clean, well-resolved impedances at 800−1000 °C in air, as shown in Figure 36. Consistent with bulk transport limitations, the impedance of these films was Warburg-like in shape and scaled properly with electrode area and electrode thickness, assuming an entirely bulk path. By extrapolating their results to zero film thickness, the authors also found evidence of a small finite resistance associated with the gas−solid and/or solid−solid interface(s). This appears to be consistent with the distortion of the impedance from a 45° limit at high frequency, a strong indicator of an electrochemical kinetic contribution and double-layer capacitance associated with the solid−solid interface.[215]

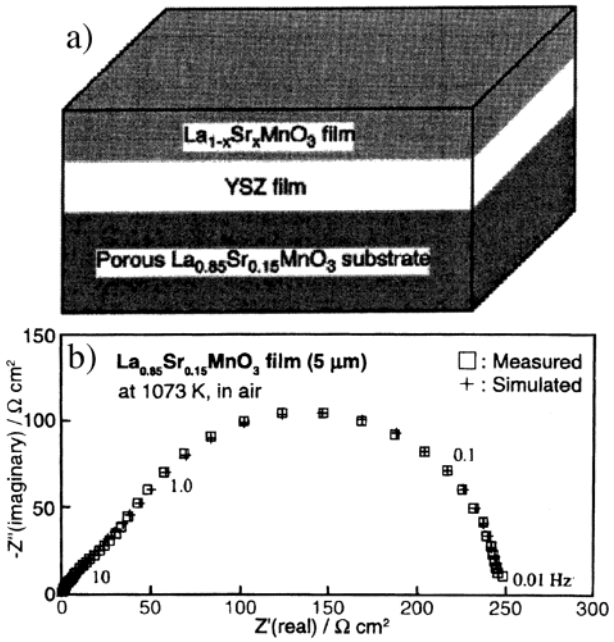

Figure 36. Measured (□) and simulated (+) impedance of a thin (5 μm) dense LSM film on YSZ at 800 °C in air. Simulation is based on a Warburg model for finite length diffusion. (Reprinted with permission from ref 160. Copyright 1998 Electrochemical Society, Inc.)

An interesting exercise is to extrapolate Ioroi's values for the bulk transport resistance of a thin film to predict the minimum performance of a porous electrode, assuming bulk transport is rate limiting. In this scenario the interfaces are equilibrated, yielding a 3D bulk transport situation as modeled by Fleig.[183] By appropriately scaling Fleig's results (Figure 30, region I), one can predict the area-specific resistance of a porous body of block microstructure as a function of σ_i and surface area a. Using the value of L/R_{bulk} from Ioroi's data at 800 °C,[159] eq 7 yields a value of σ_i of ca. 10^{-6} Ω^{-1} cm^{-1}. Applying this value to Figure 30 for a typical electrode area (20 000 cm^2/cm^3), one obtains a minimum resistance of ∼0.003 Ω cm^2. By comparison, the actual impedance of a porous LSM electrode of the same composition (made by the same laboratory) at 1000 °C (a much higher temperature) is ∼1 (Ω cm^2).[159]

What this calculation shows is that the rate of bulk transport observed in a thin film of LSM is at least 3 orders of magnitude too low to explain the performance of porous LSM at low overpotential, assuming an entirely bulk transport path. This calculation echoes prior estimates of Adler and co-workers, who showed that the zero-bias impedance of porous LSM cannot be explained in terms of a bulk path.[171] In addition, estimates of the chemical capacitance based on Ioroi's impedance for porous LSM yield values of 10^{-4}−10^{-3} F/cm^2, which as mentioned previously in section 5.2 are more consistent with a surface process

than a bulk process. Comparing this capacitance to that of Pt, we might expect a utilization region (l_δ) on the LSM surface of perhaps 100−1000 nm; however, no estimates have yet been offered in the literature for this distance.

Stepping beyond the low-overpotential regime, Horita and co-workers examined the degree to which a dense film LSM electrode becomes reduced under moderate to high cathodic polarization using ^{18}O tracer techniques.[227] In these experiments an $^{18}O_2$ tracer was introduced to the gas atmosphere during steady-state cathodic operation, and then at some later time the tracer was frozen in place via quenching of the sample. The resulting ^{18}O depth profile through the film was then analyzed using secondary-ion mass spectrometry (SIMS). These profiles were found to be consistent with increased vacancy concentration (and thus tracer diffusivity) near the YSZ interface caused by reduction of the film. This result provides perhaps the most direct evidence to date that bulk oxygen transport in LSM is enhanced near the YSZ interface under moderate to high polarization. However, because this film is dense (and thus precludes a parallel surface path), it is difficult to assess the importance of this enhancement vis-à-vis other reaction steps. In particular, the authors observed no difference in tracer ratio across the gas/LSM or LSM/YSZ interfaces, suggesting that the enhancement is not so great in this case as to be faster than interfacial processes.

A more recent study by Brichzin and co-workers[228] examined the impact of enhanced bulk transport at high overpotential on the kinetics when a TPB is present. To accomplish this, the authors took the thin-film technique one step further by examining small circular microelectrode films of varying diameters, contacted individually using a micromanipulator. By varying diameter and thickness and introduction of an alumina-blocking layer at the solid−solid interface, these workers were able to control the ratio of areas available for the surface and bulk paths. Reported were mostly steady-state polarization measurements as a function of geometry factors and anodic or cathodic polarization (±300 mV). The resolution of the data appears to be quite good, and distinct trends were observed in how the polarization resistance scales with the various geometric factors. The authors analyzed these trends in terms of a qualitative model which estimates the relative importance of the "surface" and "bulk" paths in contributing to the current in the anodic and cathodic regimes.

The results of this analysis are summarized in Figure 37. Like prior workers studying thin films, the authors conclude that dense films without a TPB under small or cathodic polarizations operate primarily by a bulk path since the surface path is blocked. (Interestingly, they found that dense films under *anodic* polarization appear to operate under a mixed regime, although it is not clear how much nucleation and transport of O_2 along the solid−solid interface contributes to the apparent surface path current.) In contrast, as the "porosity" is increased (microelectrode diameter is decreased), the surface path becomes increasingly important until at high surface areas the surface path dominates at small (and anodic) overpotentials. This appears to be consistent with the calculation discussed above, which shows that the bulk path is insufficient to explain observed current densities at low polarization. Meanwhile, at high cathodic polarization the bulk path appears to remain an important factor even with high TPB area, consistent with the Grenoble and other results (described previously) showing substantial reduction of Mn and an increase in chemical capacitance.

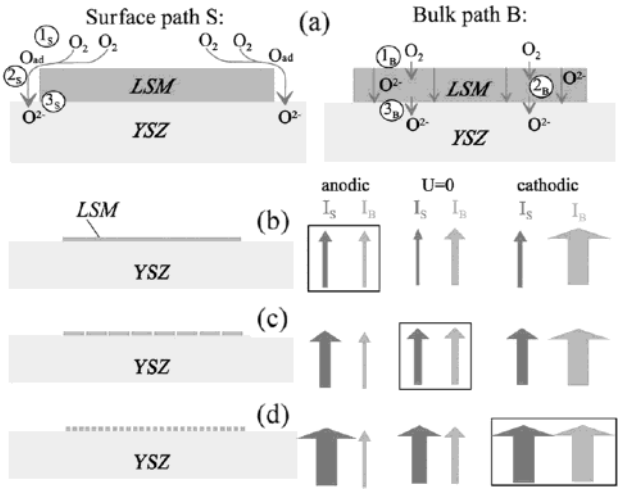

Figure 37. Qualitative summary of current contributions from the surface path (I_S) and the bulk path (I_B) for LSM disk microelectrodes on YSZ based on $i-V$ measurements in air at 800 °C. (Reprinted with permission from ref 228. Copyright 2002 Elsevier.)

While Brichzin et al.'s results provide further support for a "two-regime" view (at least from a macroscopic viewpoint), it remains unclear exactly where and how the surface-to-bulk transition occurs and to what degree these regimes overlap under a given set of conditions. In particular, Figures 30, 32, and 33 suggest that when surface adsorption/desorption on LSM is fast relative to bulk diffusion, the bulk transport path will be confined primarily to a small region near the TPB interface. In other words, even when a bulk transport path is active, its macroscopic scaling may still obey that of the surface path, making it impossible to separate from true surface processes via geometric scaling alone. Further work of this type involving impedance and other quantitative measurements would undoubtedly help clarify some of these questions.

Also contributing significantly to this "surface vs bulk" debate has been a series of studies by Horita and co-workers employing isotope tracers to track the relative importance of the surface and bulk paths.[227,229−231] As shown in Figure 38, these authors used *rf* sputtering to deposit a thin-film grid of LSM having thickness 0.5 μm and width 2 μm on the surface of polished polycrystalline YSZ. An $^{18}O_2$ tracer was then introduced to the atmosphere during cathodic polarization, followed by postmortem analysis of the quenched sample using SIMS (as described previously). By removing the LSM from YSZ in an acid bath, it was also possible to examine the YSZ underneath the LSM grid. The authors also examined

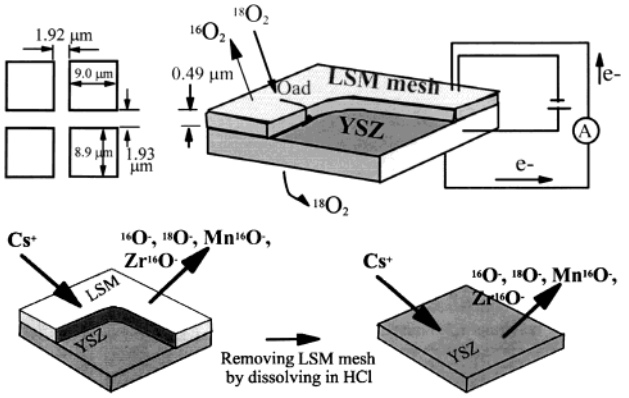

Figure 38. Schematic and geometry of patterned thin-film LSM electrode on YSZ studied by Horita and co-workers. After establishing steady-state cathodic polarization, the atmosphere surrounding the electrode is rapidly switched from $^{16}O_2$- to $^{18}O_2$-rich for 10 min at fixed total P_{O_2}. The sample is then quenched to room temperature and postmortem analyzed using secondary-ion mass spectrometry (SIMS) imaging. (Reprinted with permission from ref 230. Copyright 2000 Elsevier.)

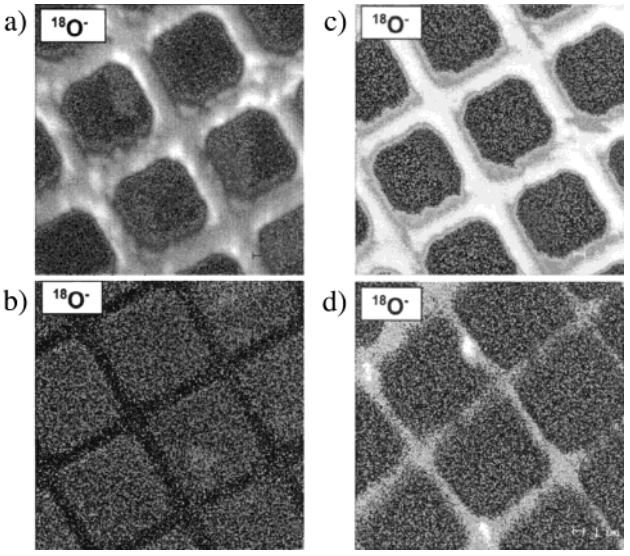

Figure 39. Secondary-ion maps of $^{18}O-$ (oxygen tracer) and $Mn^{16}O-$ (positional reference) of the patterned thin-film electrode shown in Figure 38 following polarization at −0.34 V at 700 °C. (a) Tracer map at the top surface of LSM/YSZ, showing selective incorporation into LSM. (b) Tracer map near the LSM/YSZ interface (acquired after ablation of LSM off the surface with Cs^+), showing deep penetration of tracer into LSM. (Reprinted with permission from ref 230. Copyright 2000 Elsevier.)

the position of various cations (Zr, Mn), both as a spatial reference and as a way to gauge cation interdiffusion.

Figure 39 shows isotope tracer maps for LSM both at the surface and near the interface as a function of polarization. These results indicate that under increasing polarization, isotope tracer is incorporated more deeply into the LSM bulk and that this incorporation occurs everywhere with the LSM near the interface not just at the TPB. This result would seem to corroborate the increased significance of the bulk path with increased overpotential. Consistent with this result, when the LSM is removed and the YSZ underneath is analyzed (Figure 40a), it is found that

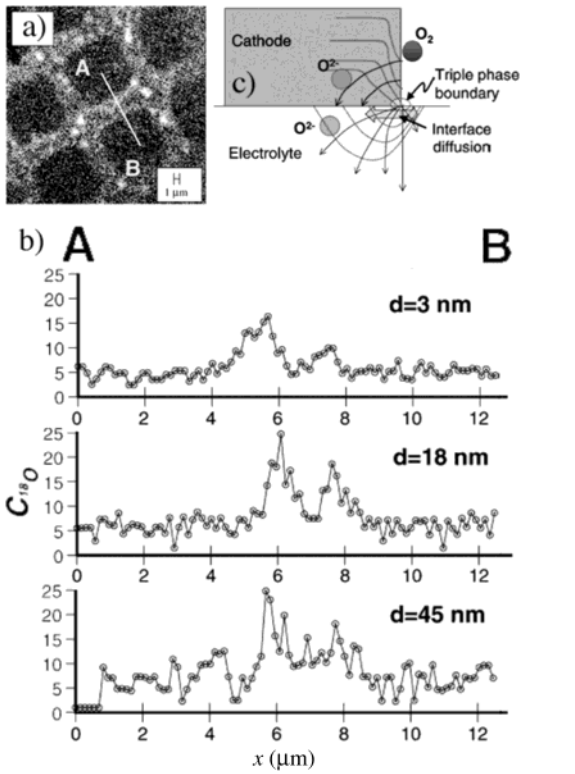

Figure 40. Secondary-ion ratio map ($^{18}O/^{16}O$) of YSZ in the cell shown in Figure 39 following removal of LSM by etching in acid. (a) Map at the exposed YSZ surface. (b) Local analysis of the tracer across the region A−B shown in a at various depths, achieved by Cs^+ ion ablation. (c) Qualitative models for oxygen incorporation used to rationalize the results in b. (Reprinted with permission from ref 231. Copyright 2002 Elsevier.)

a significant amount of the tracer is drawn into the YSZ (unlike the gas-exposed YSZ surface, which exhibits no exchange). However, when the isotope profile in the YSZ is carefully analyzed, it is found that a higher-than-average amount of tracer is absorbed in a region beneath the LSM closest to the TPB. Figure 40b shows cross sections of this profile as a function of depth into the YSZ. The region over which the isotope is found to spread is approximately independent of depth.

In interpreting their results Horita et al. considered two possible reasons for increased activity near the TPB (Figure 40c). One possibility is that a parallel surface path exists which produces a high current density and thus tracer incorporation near the TPB. However, this scenario is predicted to result in a narrow distribution of the tracer near the TPB, which increases with depth. In contrast, if the ionic current is generated by a bulk path, a higher-than-average ionic current is also predicted near the TPB (per the results of Fleig shown in Figure 30). However, the spread of the tracer in this case would be approximately independent of depth, which is what Horita et al. observed. If correct, this result suggests that increased current associated with the TPB results from a bulk as well as surface pathway.

What casts some doubt on this interpretation is that the tracer exhibits significant lateral dispersion perpendicular to the TPB, even for gold on YSZ (which the authors also studied). Indeed, the profile

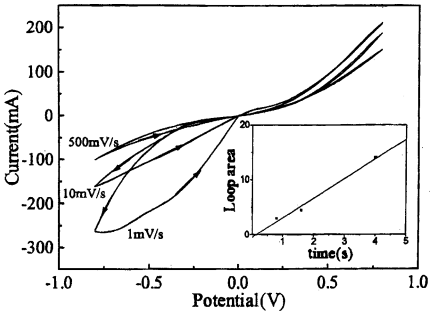

Figure 41. Linear-sweep voltammagrams of a porous LSM electrode on YSZ in air at 950 °C as a function of sweep rate. (Reprinted with permission from ref 233. Copyright 1998 The Electrochemical Society, Inc.)

images show evidence of significant defects in the grid film, including spots of enhanced or retarded isotope exchange beneath the LSM. These defects might involve microcracks or interfacial fissures having enhanced tracer mobility relative to the flow of tracer with the applied current. More work is needed (both in measurements and modeling) before this type of study yields a definitive conclusion regarding the relative importance of the surface and bulk paths under an arbitrary set of conditions as well as the size of the active region when the bulk path is engaged.

5.4. Nonstationary Behavior in LSM

In addition to the possibility of multiple transport paths, our understanding of reaction mechanisms on LSM is further complicated (as with platinum) by pronounced nonstationary behavior in the form of hysteresis of inductive effects. These effects are sometimes manifest as the often-mentioned (but little-documented) phenomenon of "burn-in", a term used in development circles to describe the initial improvement (or sometimes decline) of the cathode kinetics after a few hours or days following initial polarization (after which the performance becomes relatively stable). As recently reported by McIntosh et al., this effect can improve the measured impedance of a composite LSM/YSZ cathode by a factor of *50* relative to an unpolarized cathode at OCV.[40] Such an effect is important to understand not only because it may lead to insight about the underlying electrode kinetics (and ways to improve them), but also because it challenges the metrics often used to assess and compare relative cell performance.

For perovskite electrodes, the earliest kinetic study of hysteretic effects appears to come from Hammouche and co-workers, who showed that the $i-\eta$ characteristics of porous LSM/YSZ in air at 960 °C exhibit a potentiodynamic hysteresis when scanned slowly (1 mV/s) between 0 and −1200 mV cathodic polarization.[224] A clearer demonstration of this effect, more recently provided by Jiang and co-workers, is shown in Figure 41.[232,233] Hammouche and co-workers attributed this hysteresis to the formation of oxygen vacancies in LSM at high overpotential, which (as discussed in sections 5.2 and 5.3) appears to open a parallel bulk-transport-mediated reaction pathway. However, if this was the only explanation,

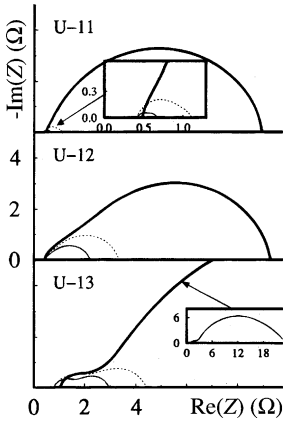

Figure 42. Impedance characteristics of porous LSM electrodes on YSZ, measured at zero bias and 945 °C in air, as a function of polarization history and processing conditions. U-11, U-12, and U-13 correspond to firing temperatures of 1100, 1200, and 1300 °C, respectively. Bold line: initial impedance. Thin line: impedance measured 2 min following cathodic polarization at 100 mA/cm^2 for 30−90 min. Dashed line: impedance measured 30 min following cathodic polarization. (Reprinted with permission from ref 209. Copyright 1997 The Electrochemical Society, Inc.)

one would expect this hysteresis to close with decreasing scan rate, not open. Indeed, the relaxation time for bulk oxygen vacancy disturbances (based on the impedance under the same conditions[211]) is about 16 s, much faster than implied by the voltammograms (20+ min).

Perhaps further insight can be gained by examining the impedance as a function of polarization history, which has been documented by a number of workers.[40,208,209,226,234,235] As shown by van Heuveln et al.,[209] reproduced in Figure 42, the zero-bias impedance of porous LSM electrodes on YSZ at 945 °C in air decreases following 30−90 min of cathodic polarization and then relaxes back toward its original characteristics over a similar period of time. This return to original behavior, consistent with the reversal of the hysteresis in the voltammograms in Figure 41, eliminates irreversible microstructural evolution as a primary cause of this effect, as proposed earlier by Tsukuda.[236] Although the authors failed to mark frequencies on their impedance diagrams, they fit the impedance to an equivalent circuit exhibiting two time scales and reported the capacitances. From this it can be determined that the higher frequency feature of the impedance (with a time scale of ∼100 kHz, capacitance ≈ 10^{-5}F/cm^2) is independent of polarization history, while the lower frequency feature (100−1000 Hz, capacitance ≈ 10^{-3}F/cm^2) shrinks following polarization by up to a factor of 50, depending on electrode firing temperature. Jiang and co-workers reported similar behavior for A-site-deficient LSM on YSZ at 800 °C (where all time scales get longer), showing that it takes ∼4 h for polarization to have its full effect. More recently, McIntosh et al.[40] witnessed similar effects for composite LSM/YSZ electrode in an operating fuel cell; both the impedance and steady-state overpotential at low polarization drop by a factor of 50 following high polarization, and these changes primarily effect

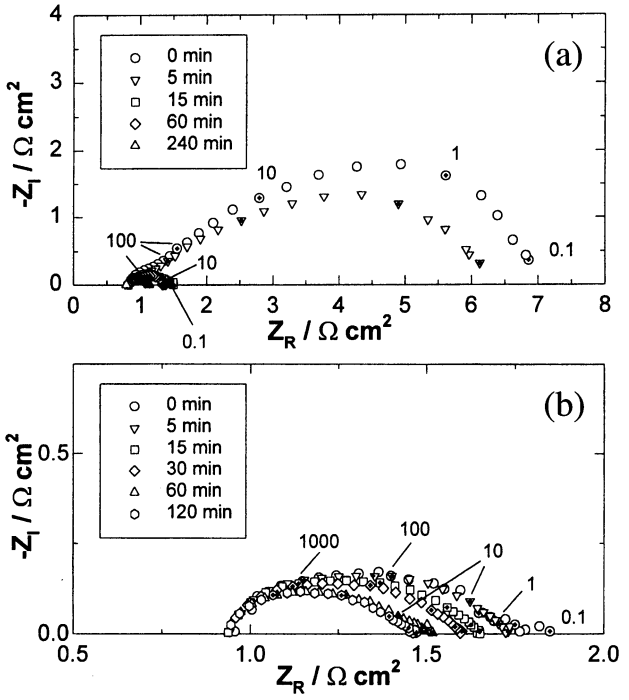

Figure 43. Impedance characteristics of porous LSM electrodes on YSZ, measured at zero bias and 900 °C in air, following various amounts of time under cathodic polarization at 200 mA/cm^2: (a) normal sample, (b) sample etched in 1 M HCl solution for ~15 min. (Reprinted with permission from ref 226. Copyright 2001 Elsevier.)

the low-frequency portion of the impedance. The initial characteristics of the cell are largely recovered after several hours sitting at zero polarization.

As discussed in sections 5.2 and 5.3 (and elaborated on more fully in section 6), the higher frequency feature is likely related to the interface while the low-frequency feature is more consistent with chemical processes on the LSM surface. Thus, van Heuveln's result above suggests it is surface diffusion (as proposed van Heuveln[209]) and/or oxygen adsorption/dissociation that temporarily improves with polarization. Hammouche's suggestion (above) that this hysteresis corresponds to the opening and closing of a parallel bulk oxygen transport path seems unlikely, since the lowest frequencies in the impedance (~0.01 Hz at 950 °C[211]) come nowhere close to the 1−10 h time scales exhibited by the hysteresis.

A result of significant interest in this discussion is that of Jiang and Love,[226] who examined the effects of acid treatment (as well as polarization) on the performance of A-site-deficient porous LSM on YSZ at 900 °C in air (Figure 43). Consistent with prior studies, they showed that cathodic polarization substantially reduces the low-frequency portion of the impedance response at zero bias. They then studied an identical electrode that had been etched in 1 M HCl for ~15 min at room temperature prior to testing. The acid-etched cell had a much smaller impedance to start with, nearly identical to that of an unetched cell that had been polarized for several hours. Cathodic polarization of the etched cell yielded little additional benefit. Again, it was only the low-frequency portion of the impedance that was reduced by acid etching.

One explanation offered by the authors is that MnOx- and/or SrO-like phases or moieties naturally exist on the LSM surface, which initially retard O_2 adsorption; upon etching (and presumably upon polarization somehow), these obstructing phases are removed, facilitating dissociative adsorption and/or surface transport. One piece of evidence that the LSM surface composition is altered significantly comes from the observation that following the etching the acid was found by ICP analysis to contain amounts of Sr, Mn, and La inconsistent with the bulk cation stoichiometry, suggesting selective etching of Sr > Mn ≫ La. Thus, either LSM started with excess Mn and Sr on the surface or ended up depleted in Mn and Sr. One appeal of this theory is that the time required for similar changes to occur to the electrode surface under polarization would be dictated by diffusion of the cations involved (La, Sr, Mn), which might reasonably require many hours even at 973 K. Such a slow change appears to be more consistent with the relaxation time of the electrode performance (hours) than other processes such as anion diffusion (minutes).

It has been noted (mostly in the context of perovskite membranes) that a large gradient in oxygen chemical potential can cause kinetic demixing of the cation constituents in a transition-metal oxide.[237−242] While we do not review this literature in any detail, a common observation is that for a binary or ternary oxide, segregation of different cations along the μ_{O2} gradient are expected, depending on their mobility and transport coupling. This is particularly true for LSM, which is cation nonstoichiometric under ambient P_{O_2};[216] thus, cation motion and crystal convection is expected under P_{O_2} gradients. We saw strong evidence in section 5 that under high polarization, LSM operates (at least in part) via a bulk oxygen transport path, which similarly corresponds to a μ_{O2} gradient across the material between the gas-exposed surface and the solid−solid interface. Thus, any sustained bulk oxygen transport might easily explain cation segregation to/from the surface. Some evidence for cation movement is apparent Kirkendall porosity formed in the corner region of LSM near the TPB under sustained cathodic polarization (Figure 33). Thus, while the hysteresis may not correspond *directly* to a change from surface to bulk path (and back), it may nonetheless be caused by this transition given sufficient time under load.

As discussed in section 6.1, a relatively exhaustive HRTEM and AFM study was conducted by Mitterdorfer and Gauckler of how secondary phases form at the LSM/YSZ boundary and how these phases effect electrode kinetics.[215] This study placed the time scale for cation-transport processes in the correct range to be consistent with the theory described above. However, while all this may be interesting and useful speculation, to date no in-depth studies of the LSM surface as a function of A/B ratio, polarization history, or other factors have been performed which would corroborate any of these hypotheses. Such a study would require combining detailed materials characterization with careful electrochemical measurements on well-defined model systems. Given the

fact that polarization has such a profound (and generally underappreciated) influence on performance, it seems likely this would be an important subject for investigation in the future.

5.5. Summary: Uncertainties in Our Understanding of Oxygen Reduction on LSM

The work reviewed in sections 5.1−5.4 represents a significant improvement over the last 10−15 years in our understanding of oxygen reduction mechanisms on LSM. However, significant uncertainties remain due in part to the complexity of the reaction mechanism itself but also the extreme sensitivity of the limiting factors to the exact structure, processing history, operating conditions, and operation history of the electrode. To summarize, some of the relevant highlights (and remaining challenges) are given below.

(1) *Surface path at low overpotential*. Qualitative and quantitative analysis of impedance data, tracer studies, as well as various studies of thin-film electrodes suggest that under low-overpotential LSM operates primarily via a surface-mediated mechanism (like Pt). This conclusion appears to be consistent with the properties of LSM, which is fully oxygen stoichiometric under ambient P_{O_2}. However, little is known about how far the active region of reduction extends beyond the solid/solid interface (via surface diffusion) or the relative importance of chemical steps (on the LSM surface) vs electrochemical kinetics at the solid/solid interface.

(2) *Bulk path at moderate to high overpotential*. Studies of impedance time scales, tracer diffusion profiles, and electrode microstructure suggest that at moderate to high cathodic overpotential, LSM becomes sufficiently reduced to open up a parallel bulk transport path near the three-phase boundary (like the perovskite mixed conductors). This effect may explain the complex dependence of electrode performance on electrode geometry and length scale. To date, no quantitative measurements or models have provided a means to determine the degree to which surface and bulk paths contribute under an arbitrary set of conditions.

(3) *Pronounced nonstationary behavior*. Numerous workers have reported significant hysteresis and/or irreversibility in the behavior of LSM. This factor is important to be aware of since it is possible for two labs studying the same types of electrodes under similar conditions to arrive at completely different conclusions, depending on the exact history of fabrication and testing. Hopefully as workers move forward, these effects will provide additional clues as to the reaction mechanism dominating under specific conditions.

(4) *Extreme sensitivity to processing and operating history*. It has proven difficult to arrive at a consensus understanding of oxygen reduction on LSM, in part because electrode performance/characteristics depend so strongly on the exact details of processing and operating history. Many of the outstanding issues are tied so strongly to the subtleties of processing that they warrant their own section (section 6). For example, as discussed in sections 6.1−6.3, the resistance of the solid/solid interface may depend significantly on the formation of insulating reaction products between LSM and the electrolyte. In addition, the composite microstructure of a commercially relevant fuel-cell electrode is significantly more complex than the ideal structures discussed so far—a significant remaining issue is the relationship of performance to microstructure in light of our understanding of the reaction mechanism itself (section 6.4).

6. Factors Complicating our Understanding of SOFC Cathode Mechanisms

The results reviewed in sections 3−5 represent significant progress over the last ∼20 years in understanding basic mechanisms governing oxygen reduction in SOFC cathodes. However, it should be emphasized that this knowledge has been built by studying a large number of materials and cases over a long period of time, often by examining model systems or asymptotic cases. This is not the same thing as being able to diagnose the mechanism of a particular electrode under a specific set of conditions or knowing all the factors that govern the rates of the various physical processes comprising that mechanism. In particular, workers have found that the rates of these processes as well as their relative importance in the mechanism depend significantly on a number of "outside" factors not determined by the mechanism itself. Some examples include secondary phases and impurities influencing electrochemical kinetics at the interface, the macroscopic geometry and microstructure of the electrode, or changes in the properties of the materials due to fabrication conditions or degradation. An enormous amount of work has been conducted in the last 15−20 years to understand these various factors; the purpose of this section is to review those factors that have been the most well studied and/or appear to have the greatest significance in determining the rate of oxygen reduction within SOFC cathodes.

6.1. Sensitivity of Interfacial Electrochemical Kinetics to Secondary Phases and Impurities

One of the most heavily studied factors thought to influence cathode performance has been the issue of *reactivity* between the electrode material and the electrolyte (usually YSZ) to form insulating secondary phases. This subject is sufficiently broad and complex to warrant its own review, and readers having a detailed interest in this topic are encouraged to read previous literature reviews in papers by Kawada[243] and Mitterdorfer.[215] Our main focus here is on how these secondary phases (or other impurities) appear to retard the reaction, particularly electrochemical kinetic processes occurring at the interface.

As early as 1969, studies of perovskites on YSZ suggested the formation of insulating reaction products at the interface during processing and/or cell operation.[244] This was confirmed in 1985 by Lau and Singhal, who showed that $La_2Zr_2O_7$ forms at the interface between dense LSM and single-crystal YSZ at typical electrode processing temperatures.[245] Soon after, Yamamoto and co-workers published a study

of sputtered $La_{1-x}Sr_xMO_{3-\delta}$ electrodes on YSZ (M = Co, Fe, Mn, Cr), annealed at various temperatures from 900 to 1100 °C and examined using SEM and X-ray diffraction (XRD). These studies identified multiple secondary phases which were identified as $La_2Zr_2O_7$ (LZ) and Sr_2ZrO_4 (SZ). The amount of these secondary phases depended on the exact composition of the materials involved but generally increased with annealing temperature and time. They likewise found that electrode resistance increases with annealing time, suggesting that these phases play a significant role in retarding electrode/electrolyte interfacial processes. A variety of other perovskite electrode materials have since been shown to react with YSZ, including $La_{1-x}Ca_xMnO_{3\pm\delta}$ (LCM),[246,247] $Gd_{1-x}Sr_xCoO_{3-\delta}$,[248] $La_{1-x}Sr_xCo_{1-y}Fe_yO_{3-\delta}$ (LSCF),[249,250] and LSC and LSF.[251] Yokokawa and co-workers examined the relative thermodynamic stability of various perovskite phases with respect to reaction products in the presence of zirconia, providing a framework for understanding the thermodynamic driving force behind the formation of these phases.[252,253]

Exactly how these secondary phases influence cathode performance remains somewhat circumstantial. Labrincha et al.[254] studied the electrical properties of LZ over a range of temperature and P_{O_2} and found it to have low conductivity under typical SOFC cathode operating conditions ($\sim 10^{-4}$ Ω cm^2 at 1000 °C). This suggests that even a small layer of this material is likely to significantly interfere with charge transfer at the perovskite/YSZ interface. Poulsen and Vanderpuil[255] have likewise shown that a variety of possible lanthanum zirconate and srontium zirconate reaction products are possible, which have electrical properties likely to interfere with interfacial charge transfer. Consistent with this hypothesis, numerous workers have reported perovskites on YSZ to exhibit a high-frequency impedance feature suggestive of interfacial resistance.[27,164−166,187,210,211,215] Workers have also made significant progress in understanding how and where these phases form, leading to a variety of logical suppositions about why they may influence interfacial electrochemical kinetics or other processes governing performance.

One of the first studies of how these secondary phases form was performed by van Roosmalen and Cordfunke.[256] These authors used SEM/EDS and XRD to study postannealed diffusion couples of LSM and YSZ as well as pressed and fired powder mixtures of LSM and YSZ. These experiments showed that reaction products in sufficient quantity to detect by XRD (1−3%) form at temperatures as low as 1170 °C. The two principle reaction products observed were $La_2Zr_2O_7$ (LZ) and $SrZrO_3$ (SZ), with the relative amount of LZ and SZ depending on the La/Sr ratio in the LSM. Calcia- and baria-doped $LaMnO_3$ were found to be similarly reactive with YSZ, and reactivity of LSM with YSZ having 3% or 8% yttria was found to be similar. In the case of the diffusion couples, the layer of reaction products formed at the interface was found (using SEM) to be on the order of 1 μm after 600 h at 1280 °C and 10−15 μm after 600 h at 1480 °C. By employing Pt diffusion markers at the diffusion couple interface, the authors concluded that the reaction proceeds by cationic diffusion of La and Sr through the interfacial LZ and/or SZ layer, resulting in the formation of cation vacancies in LSM and the continued precipitation of LZ and/or SZ on the YSZ side of the interfacial layer. Consistent with this hypothesis was the observation of Kirkendall porosity in the LSM phase near the interface, which would be expected to form upon sufficient depletion of A-site cations in the LSM phase.

Since the formation of secondary phases at the interface appears to be associated with activity and mobility of the A-site cations, a variety of workers have investigated perovskites with A/B cation ratio <1 in an attempt to mitigate the formation of reaction products. An early example is a study by Yamamoto et al.,[257] who showed using XRD that no reaction products form between $La_{0.8}MnO_3$ and YSZ after sintering at 1200 °C for 200 h. Such prevention (or at least delay/retardation) of reaction products for perovskites with A/B ratio <1 has since been reported by a variety of workers.[235,243,249,258−261] Unfortunately there are generally few results that really tie the reduction of these phases to improvements in electrode performance (let alone particular aspects of that performance such as the interfacial electrochemical kinetics). Indeed, even with materials having A/B ratios <1, reaction products often still appear at higher temperatures and/or longer annealing times. Thus, given that these phases are often detected using XRD (which has a detection limit of 1−3%), it is not entirely clear that secondary phases are not still present in undetectable quantities. Also, depending on the mechanism of secondary phase formation, the low A/B ratio may only serve to delay rather than prevent secondary phases. For example, one prominent idea has been that dissolution of relatively small and mobile B-site cations from the electrode material into YSZ leads to a local increase in A-site activity at the interface.[243] Given enough time and temperature, this may occur even when the A/B ratio is initially low enough to be thermodynamically stable with respect to reaction products. In support of this idea are thermodynamic calculations by Yokokawa et al.,[252,253,262] who showed that Mn is highly soluble in YSZ and that this solubility is P_{O_2} dependent, suggesting that the formation of these various phases may be very sensitive to how easily oxygen can transport to/from the interface during electrode processing.

Of interest to this discussion is a paper by Simner et al.,[251] which challenges whether one can always detect deleterious materials at the interface as explicit phases. Motivated by the observation that perovskites LSC and LSF exhibit better performance on ceria (see section 6.3), they did a careful examination of the reactivity of LSC and LSF with 8 mol % YSZ, fired as mixed and pressed powders up to 1400 °C. Not surprisingly, LSC was found to be very reactive, forming large amounts of LZ, SZ, and Co_3O_4. In contrast, LSF was generally less reactive, and in the case of A-site-deficient LSF, $(La_{0.8}Sr_{0.2})_{0.95}FeO_{3-\delta}$, the authors could not find evidence of secondary phases using SEM or XRD. Nonetheless, measurable

angle shifts (~2° in 2Θ) were observed for the primary LSF diffraction lines, indicating a significant change in average unit cell size. The authors interpreted this change in terms of Zr^{4+} dissolution into the perovskite, which they show to reduce substantially the electrical conductivity of LSF. While it is not clear how deeply Zr would dissolve into an LSF electrode, it is also not clear how much would be needed to degrade performance. In other words, it is entirely possible that even when secondary phases are not detected in large enough quantities to see by SEM and XRD, a thin (1−10 nm) insulating layer of a secondary phase (or simply a compositionally modified primary phase) could still exist that introduces an interfacial resistance.

We should also point out that annealing of the interface, though ultimately responsible for the formation of secondary phases, may be a very important part of establishing ionic contact. For example, Horita et al.[263] recently conducted $^{18}O_2$ tracer experiments on sputtered films of LSM on YSZ and showed that the "as-sputtered" interface (fabricated at 700 °C) has significantly higher resistance to ion exchange, which they attribute (based on SEM images) to a lack of bonding at a local level. With increased annealing time and temperature, the LSM and YSZ bond more completely, corresponding to facile ion exchange across the LSM/YSZ interface.

To better understand the structure and composition of the interface and its impact on interfacial electrochemical kinetics, a number of workers have conducted more detailed characterization studies of the perovskite/electrolyte interface using high-resolution transmission electron microscopy (HRTEM), electron diffraction, X-ray photoelectron spectroscopy (XPS), and atomic force microscopy (AFM).[215,264−268] Of particular interest is a paper by Mitterdorfer and Gauckler,[215] who studied nucleation and growth of LZ between porous $La_{0.85}Sr_{0.15}Mn_yO_{3\pm\delta}$ with (001)-oriented 9.5 mol % doped YSZ single crystals using HRTEM, AFM, and XPS, as well as the impact of these phases in terms of electrode impedance. As illustrated in Figure 44, their results suggest that when LSM is A-site rich ($y = 0.98$), nucleation of LZ occurs at the TPB, where oxygen exchange is facile and La^{3+} and Zr^{4+} are available via surface diffusion. Once an island of LZ forms, it can then grow along the LSM/YSZ interface. In contrast, when LSM is A-site deficient ($y = 1.02$), initial nucleation of LZ is retarded; epitaxial growth of a Mn-rich YSZ phase occurs first, drawing Mn out of LSM and Zr^{4+} and Y^{3+} from the surrounding YSZ surface. Once sufficient Mn has been extracted from LSM, LZ then precipitates at the TPB.

What these results show is that regardless of A-site deficiency, eventual nucleation of the undesirable phase occurs exactly where it is least desired: at the TPB, where it results in an insulating gap between the LSM and YSZ surfaces. Restricting our attention to the low-overpotential regime, we might expect this gap to interfere with two processes: (1) surface diffusion of electroactive oxygen along the LSM surface to the TPB and (2) the electrochemical formation of O^{2-} at the TPB due to limited availability of electronic charge carriers. Consistent with this hypothesis, Mitterdorfer and Gauckler observed apparent increases in both electrochemical and chemical contributions to the impedance upon annealing of the electrode.[215]

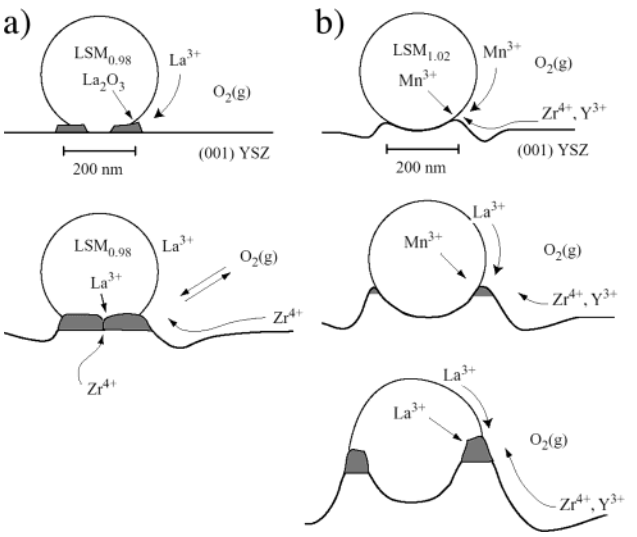

Figure 44. Qualitative description of $La_2Zr_2O_7$ (LZ) formation at the LSM/YSZ single-crystal interface based on HRTEM and AFM measurements, as explained in the text. Shaded region corresponds to LZ. (Adapted with permission from ref 215. Copyright 1998 Elsevier.)

However, beyond this, it is difficult to draw a more specific conclusion. In particular, it is now known how the electrochemical and chemical contributions to the impedance evolve through the different stages of development of these phases. Also, at higher overpotential (or with perovskite mixed conductors) we might expect the impact of these secondary phases to depend significantly on the relative roles of the surface and bulk paths as well as how far these phases spread along the LSM/YSZ interface (where they may also block ionic exchange across the solid/solid interface). Unfortunately, besides the general observation that performance gets worse with the formation of these phases, little is known. A more direct linkage of these phases to the exact changes seen in resistance and frequency response (as a function of overpotential and time) remains elusive.

Finally, it would be remiss not to mention the potential impact of *impurities* in influencing various electrode rate processes, particularly at the electrode/electrolyte interface. For example, Kuscer and coworkers[269] showed that during accelerated aging of LSM electrodes on YSZ, small amounts of silica in the electrolyte tended to migrate to the interface, forming an amorphous La−silicate phase between the electrode and electrolyte. Besides the potential impact on interfacial electrochemical kinetics, formation of this phase was implicated in the observed delamination of the electrode from the electrolyte over time (see section 6.6). Similarly, concurrent preliminary work at Imperial College has shown that small amounts of silica introduced during processing of perovskite/ceria electrodes had a deleterious influence on performance.[270,271] Given the propensity of silica to form low-melting eutectics and move along ceramic grain boundaries, one would also suspect

sensitivity to the presence of alkaline or alkaline-earth materials (common components of furnace insulation!). However, while the impact of certain impurities (particularly silica) on the properties of ion conductors is well known,[272−275] there have only been a few studies to date that really investigate the impact of these impurities on electrode performance.

6.2. Alteration of Material Properties Near the Interface

Further complicating our understanding of interfacial electrochemical kinetics (as well as electrode kinetics as a whole) is the observation that bonding of the electrode material with the electrolyte may result in changes to the electrode and/or electrolyte materials in the general vicinity of the interface. In section 6.1 we already saw some examples of this, for example, the dissolution on Mn in YSZ, altering its ionic conductivity,[243,276] or the dissolution of Zr into LSF, potentially reducing its electronic conductivity.[251] Thus, it is possible that effects that appear to be associated with the interface (due to their geometric scaling or impedance time scale) may in fact be local variations of chemical processes in the near-interfacial region.

One notable possibility is that interdiffusion of the electrode and electrolyte during bonding may result in changes in cation composition (and therefore properties) of the electrode. Recent results supporting this possibility were published by Horita et al.,[263] who examined $^{18}O_2$ tracer diffusion in a sputtered thin film of A-site-deficient LSM on YSZ. As discussed previously, this result showed enhancement of ionic exchange across the LSM/YSZ interface with annealing, due to improved bonding. What is also of interest is that the authors observed an approximately 3-fold decrease in the apparent ^{18}O tracer diffusion coefficient of the film upon annealing above ~1000 °C. This was explained by the authors in terms of changes in cation composition of the film due to diffusion of Y and Zr into LSM, which according to their SIMS depth profiles penetrate ~1 μm at 1300 °C. Although SIMS intensities are not considered a quantitative measure of concentration, the Y and Zr intensities 800 nm deep into the LSM region were on the order of 10% of that in YSZ itself. Unfortunately, since no XRD or TEM cross-sections were performed, it is difficult to entirely eliminate the possibility that secondary phases contribute to these cation intensities. However, this study does serve to illustrate that significant changes in bulk transport properties may occur simply due to interdiffusive bonding.

A related finding was reported by Kawada et al.,[124] who studied the impedance of thin laser-deposited films of LSC on SDC. As discussed in section 4.3, they analyzed the apparent chemical capacitance of the films in terms of changes in bulk oxygen stoichiometry. In so doing they discovered a very surprising result: the apparent oxygen vacancy concentration in the film in air is approximately 4 times smaller than for bulk LSC having the same cation composition (60/40 La/Sr). Further analysis suggested that the *enthalpy* of oxygen incorporation into LSC is different for the film than for the bulk material. ICP analysis of the film following dissolution in acid confirmed that it had a 60/40 La/Sr ratio, although somewhat depleted in Co (6%). This level of B-site deficiency does not seem to explain such a significant departure from bulk properties. After considering and rejecting several other possibilities, the authors proposed that *stress* in the film due to a forced match with the underlying ceria might explain the apparent additional contribution to the oxygen exchange enthalpy. This as yet unproven hypothesis is intriguing since it implies that material properties may be subject to modification at an interface even when reaction and/or interdiffusion does not occur.

Finally, another possibility often discussed in the literature is that cation "dopants" from the electrode may enhance the electronic conductivity of the gas-exposed surface of the electrolyte in the vicinity of the TPB, thereby extending the reduction zone along the electrolyte surface via mixed conduction. The surface exchange rate of oxygen on both YSZ- and rare-earth-doped ceria (as measured by isotope methods) is only about 1 order of magnitude lower than on LSM at 700 °C.[277−279] Thus, if there were sufficient electronic conduction at the surface or in the bulk of the electrolyte, it might be possible for net reduction to O^{2-} to occur on the gas-exposed electrolyte surface. There is precedence in the catalysis literature that this can happen; for example, workers studying CO or CH_4 oxidation on CeO_2/ZrO_2-supported Pt and Pd catalysts at high temperature[280,281] have generally shown that the support enhances performance via reduction and mixed conduction of oxygen in the fluorite phase. Workers have also suggested that mixed conduction in ceria can play a role in SOFC anodes.[282] Various workers have provided circumstantial evidence that this might occur under oxidizing conditions at an SOFC cathode. For example, Kleitz and co-workers[55] noted that the high-frequency (presumably interfacial) impedance of small silver droplet electrode scales as $r^{-0.6}$, where r is the droplet radius. They explained this weak geometry dependence as an outward expansion of the charge-transfer zone away from the TPB along the electrolyte surface. Another example is work by van Hassel and co-workers, who, as shown in Figure 45, found that the performance of porous gold cathodes on YSZ (normally a very poor oxygen catalyst) is significantly enhanced at all overpotentials by prior coating with Fe_2O_3 and/or implantation of iron into the electrolyte surface.[99,283] Widmar and co-workers reported similar enhancements for low-fired (750 °C) Pt electrode on YSZ implanted with Ce or Mn at low overpotential.[82]

However, to date there does not appear to be much evidence that *mixed conduction* in the electrolyte plays the dominant role in the enhancements mentioned above. First, it should be emphasized that a finite rate of oxygen exchange at the electrolyte surface (as measured at equilibrium by isotope methods) is a necessary but insufficient criterion for finite rates of oxygen reduction; for there to be a *net* production of O^{2-} at the electrolyte surface, electrons

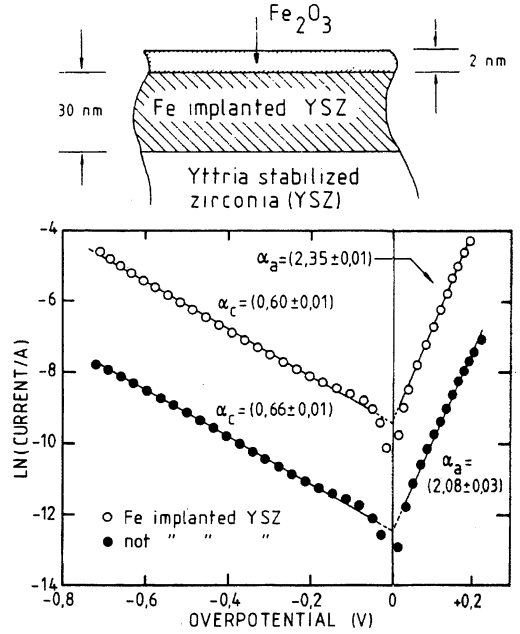

Figure 45. Current−overpotential characteristics of porous gold electrodes on YSZ at 770 °C and $P_{O_2} = 1$ atm, comparing YSZ that has, and has not, been implanted with 8×10^{16} atoms/cm^2 of ^{56}Fe at 15 kV. (Reprinted with permission from ref 99. Copyright 1992 Elsevier.)

must also be able to gain access to the surface. Workers have generally shown that when YSZ is implanted or alloyed homogeneously with Fe or Mn, its electrical conductivity is not significantly enhanced, even under moderately reducing conditions.[82,243,284−286] Second, in isotope studies of low-temperature bifunctional CO oxidation catalysts, such as Au/Fe_2O_3, workers have shown that the role of the transition metal in the support is essentially *catalytic*, i.e., stabilization of physisorbed O_2 at the Au/oxide interface, leading to enhanced oxidation rates.[287−289] It is likewise possible that enhanced performance of metal cathodes on YSZ incorporating transition metals or (other d-orbital cations) is an electrochemical−kinetic effect localized to the TPB where by "localized" we mean simply "within a distance accessible by electrons from the electrode material". Indeed, as shown in Figure 45, the enhancements observed by van Hassel and co-workers upon implantation of Fe into YSZ correspond to an increase in the apparent exchange current density while the Tafel slope remains constant over several orders of magnitude. This observation suggests that iron acts to promote the existing rate processes (either on the Au surface or at the TPB) rather than by changing the mechanism toward an alternative chemical pathway involving the electrolyte. Finally, we should point out that gold is a poor oxygen catalyst at high temperature. In the case of a highly catalytic perovskite, it is not clear that incorporation of transition metals from the electrode into the electrolyte surface is going to provide any significant catalytic benefit not already provided by the electrode itself, particularly in cases where the utilization region is large and thus the exposed electrolyte surface makes up such a small percentage of the area available for dissociative adsorption.

6.3. Ceria as an Alternative Electrolytic Interface

In attempting to develop fuel cells based on ceria-based electrolytes, workers have also examined the reactivity of various perovskite electrode materials with doped ceria. An early example is a study by Chen and co-workers,[250] who used a spin-coating technique to deposit LSCF electrodes on YSZ as well as 20 mol % samaria-doped ceria $(CeO_2)_{0.8}(SmO_{1.5})_{0.2}$ (SDC). Consistent with previous findings, LSCF was observed to react with YSZ to form LZ and SZ byproducts. In contrast, analogous Ce-based compounds resulting from a reaction between LSCF and SDC were not observed. Consistent with this observation were Chen et al.'s measurements of electrode impedance, which suggest LSCF exhibits less interfacial resistance when processed and tested under the same conditions on the same substrate. On the basis of this result, the authors suggested addition of a ceria-based "protection layer" between the perovskite electrode and YSZ, an idea which is now actively being developed for intermediate temperature fuel cells.[251]

Consistent with Chen et al.'s observations was a study by Adler and co-workers (described previously in section 4), who measured the impedance of LSCF on SDC at intermediate temperatures. Their measurements showed that above about 700 °C in air the impedance is dominated by a single Gerischer-like impedance found to be consistent with a bulk-mediated reaction pathway. Although the possible role of the surface path cannot be entirely excluded in this case, what is clear is that the impedance is dominated by chemical dissociation and transport steps while electrochemical incorporation at the interface remains largely equilibrated at least above ~650 °C. Adler et al. mention in passing that at lower temperatures (450−550 °C) a small high-frequency arc with a high activation energy appears, indicating the onset of interfacial electrochemical kinetic resistance. However, it is unclear if this additional resistance is associated with secondary phases or simply an inherent resistance to ionic exchange between two dissimilar ionic phases (as has been observed, for example, at the physical interface between two pieces of YSZ[290]). This apparent lack of an interfacial resistance (as evidenced by the absence of a distinct high-frequency impedance arc) appears to be a general feature of perovskite mixed conductors on rare-earth-doped ceria or $(La,Sr)(Ga,Mn)O_3$ electrolytes.[18,19,22,28,177,179−181,184,250,291,292]

A notable exception may be Sr-doped ceria. As reported by Liu and Wu,[187] LSCF electrodes on 10 mol % Sr-doped ceria exhibit a significant high-frequency impedance arc in air at 650−750 °C, which is comparable in frequency (but somewhat smaller) to that observed for identically processed and tested LSCF electrodes on 8 mol % YSZ. One explanation may be found in the thermodynamic data for the Sr−Ce−O system, which shows that the solubility of SrO in CeO_2 is less than 10 mol % at these temperatures.[293−295] Thus, precipitation of $SrCeO_3$ at the LSCF/ceria interface is favored, depending on the exact firing conditions and A/B ratio of the perovskite. Oddly, the authors did not consider this possibility,

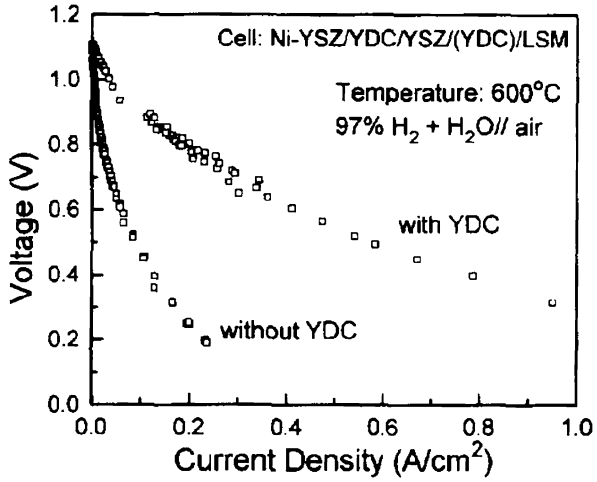

Figure 46. Performance characteristics of a cathode-supported thin film Ni−YSZ/YSZ/LSM fuel cell at 600 °C in humidified H_2 and air with and without a dense protective yttria-doped ceria (YDC) protection layer introduced between the porous LSM cathode and the thin-film electrolyte. (Reprinted with permission from ref 296. Copyright 1997 Elsevier.)

citing the variations in impedance with different electrolytes as proof that oxygen reduction is limited by electrochemical kinetics at the TPB. On the contrary, the very large apparent chemical capacitance (~1 F/cm^2) associated with the low-frequency impedance feature (which is similar in shape, size, and frequency for both YSZ- and Sr-doped ceria) suggests a bulk-mediated path involving absorption and transport in LSCF. Meanwhile, the differences seen at high frequency between YSZ- and Sr-doped ceria might easily be explained in terms of different secondary phases formed, whose likely effect is to interfere with ion-transfer across the entire solid−solid interface (not just at the TPB).

Given the apparent reversibility of the perovskite/rare-earth-doped ceria interface, Various workers have more recently investigated Chen's original suggestion of a ceria-based protection layer between YSZ and perovskite cathodes.[296−299] As shown in Figure 46, Tsai and co-workers found that by introducing a 0.4 μm thick sputtered layer of yttria-doped ceria between YSZ and porous LSM, overall current density of their cathode-supported fuel cell could be improved by a factor of approximately 5×. More recently, anode-supported YSZ fuel cells using a single-phase porous LSF cathode with a Sm-doped ceria protection layer have been reported to exceed operating voltages of 900 mV at current densities of 100 mA/cm.[2298] This performance is competitive with some of the best composite LSM/YSZ cathodes available today (see section 6.4). While these results are exciting, more work is needed to confirm/reject current hypotheses about how these layers actually work to improve performance and compare performances meaningfully among various development groups.

6.4. Composite Microstructures

Figure 2 illustrated two dominant strategies that have been used to enhance the performance of SOFC cathodes. One has been the introduction of ionic conduction into the electrode material so as to extend the active region beyond the electrode/electrolyte interface. Along with ionic conduction, however, comes potential problems including increased chemical and thermal expansion and higher apparent reactivity between electrode and electrolyte (section 6.1). An alternative strategy has been to combine a YSZ-compatible electrode material such as LSM with an ionically conducting second phase (e.g., YSZ itself) in a composite matrix. While the active region of an LSM electrode may generally be more confined to the LSM/YSZ interface than a mixed conductor, the composite matrix makes up for this deficiency by extending the LSM/YSZ interface. This strategy has proven to be very promising but adds some complexity to our diagnosis and understanding of which processes dominate the overall observed overpotential.

One of the first attempts to implement this strategy was reported by Kenjo and co-workers,[300,301] who fabricated and tested the performance of porous Pt composite electrodes containing YSZ, SDC, and erbia-stabilized bismuth oxide (ESB) as well as composites of A-site-deficient $La_{0.85}MnO_3$ (LM) and YSZ. The electrode polarization losses of these electrodes were measured using current-interruption techniques as a function of electrode thickness. For Pt/ESB and LM/YSZ, the presence of the electrolyte was found to enhance performance significantly (5−10 times) depending on processing conditions and the volume fraction of the electrolyte. As shown in Figure 47, performance was also found to increase with electrode thickness, saturating at a thickness of ~10 μm (30 or 40 μm for Pt/ESB). In the case of Pt/YSZ and Pt/SDC, no enhancement was observed; however, the authors proved using electrical conductivity measurements that with their particular preparation method any significant fraction of YSZ and SDC particles interferes with the electrical connectivity among Pt particles, making the electrode too resistive to function in these cases.

As shown in Figure 48, the authors explained their results in terms of a macrohomogeneous model similar to that used previously for aqueous gas-diffusion electrodes.[302] With this approach the electronic and ionic conductors (Figure 48a) are viewed as homogeneously interpenetrating subphases, the electronic conductor having relatively high electrical conductivity, while the ionic conductor has finite ionic resistivity $\rho = 1/\sigma_i$. At the interface between these phases, oxygen reduction occurs at a rate proportional to the local overpotential, resulting in passage of current from the ionic to the electronic phase, $i_y = \eta(x)/k$, where $\eta(x)$ is the local overpotential and k in this case is the interfacial resistance per unit volume (Ω cm^3). Consideration of charge conservation a la classic porous electrode theory[303] leads to the solutions shown in Figure 48c,d. In analogy to the situation shown in Figures 14b and 26a, the composite electrode is found to be co-limited by interfacial resistance and ionic transport in the ionic subphase, exhibiting a maximum utilization region of size $\sim\sqrt{k/\rho}$ and overall resistance proportional to $\sqrt{\rho k}$ for

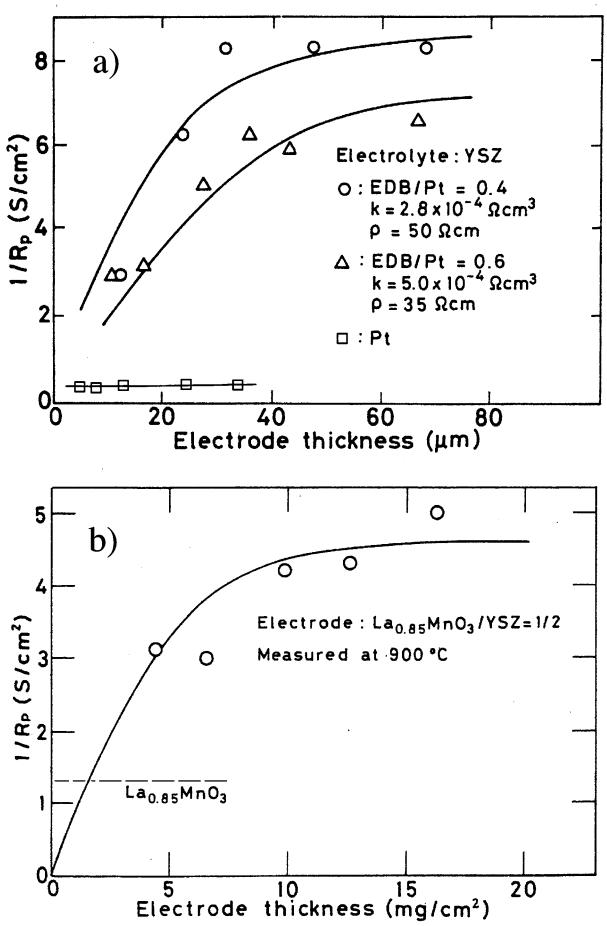

Figure 47. Measured area-specific admittance (reciprocal of the polarization resistance R_p) as a function of electrode thickness for Pt/ESB and LSM/YSZ composite electrodes. Performance of the same electrode materials without an ionic subphase are also shown for comparison. Lines indicate fits to the model shown in Figure 48, as discussed in the text. (Reprinted with permission from refs 300 and 301. Copyright 1991 and 1992 The Electrochemical Society, Inc. and Elsevier, respectively.)

an infinitely thick electrode. As shown in Figure 47, fitting of this model yields values of ρ and k found to be in reasonable agreement with the properties of ESB and YSZ given the uncertainties in the details of the microstructure (interparticle contact, ionic tortuosity, interphase contact area).

What this result shows is that for materials having a small natural active region as a single porous phase (50−500 nm for Pt, perhaps somewhat larger for LM), the use of a composite microstructure can significantly enhance performance, extending the active region to include a much larger fraction of the electrode material (~10 μm). A number of workers have since demonstrated the benefits of this approach for LSM/YSZ, some reporting active regions of similar size (5−10 μm) as single-phase mixed conductors.[304,305] Besides establishing a new paradigm in how to design SOFC cathodes, this approach has also introduced a new set of issues to be considered, including the efficiency of the ionic and electronic transport paths,[24,306−309] quality and quantity of internal interfacial contact between the ionic and electronic subphases,[30,310] functional grading of the materials for structural or other purposes,[36,311−313] and tuning of the microstructure to match the local natural extension region of the electrode material.

As one might expect, interpreting the electrochemical characteristics of composite electrodes is considerably more challenging than understanding their single-phase counterparts. Since work in this area is sparse, we confine this discussion to a few of the salient differences. First, the various physical processes contributing to the overpotential are more difficult to separate. With a single-phase electrode, ohmic losses associated with the electrolyte (and in some cases also interfacial electrochemical kinetics) can be isolated or treated using equivalent circuit analogies independent of how complex the processes occurring in the electrode itself may be. In contrast, as implied by Figure 48, the characteristics of a composite electrode involve an inherent convolution of the ohmic loss in the electrolytic subphase with the electrochemical and chemical losses at the junction between the ionic and electronic (or mixed conducting) subphases. This leads to wide dispersion and overlap among the time scales for these processes, making interpretation of impedance extremely challenging, as recently reviewed by Jørgensen and Mogensen.[31]

Second, the electrochemical characteristics of composite electrodes are generally much more sensitive to the details of the microstructure than single-phase materials.[30,35] Indeed, embedded in the parameter k in Figure 48 are literally *all* the physical processes reviewed in sections 3−5 plus the details of how the two subphases are interconnected. While various authors have attempted to relate" in more detail to the microstructure, modeling is often limited to idealized hypothetical microstructures that may or may not be relatable in a quantitative way to the real system.[307,314] In addition, since composite electrodes work by maximizing surface area and interfacial contact, they are often fired at much lower temperatures than their single-phase counterparts, leading to additional uncertainty as to the geometry and quality of interparticle contact. These details of the microstructure and interfaces, which may be critical to performance, are extremely difficult to quantify using current cross-sectional sampling techniques (SEM, HRTEM, SIMS, AFM).

Finally, due to their high surface area, composite electrodes often incorporate microstructural features competitive or smaller than the active region of a single-phase electrode of the same material. In this situation, we expect chemical transport processes to be largely equilibrated on a local (submicrometer) length scale, leaving dissociative oxygen ab(b)sorption as the only significant chemical resistance. One consequence of this situation is that the electrochemical kinetics contributing to k in Figure 48 may not be the same as those governing the kinetics of a single-phase electrode, even when TPB area is known and properly accounted for. Rather, the mechanism itself may shift toward a different set of co-limiting steps, in particular catalytic reduction, interfacial electrochemical kinetics, and ionic transport in the ionic subphase.

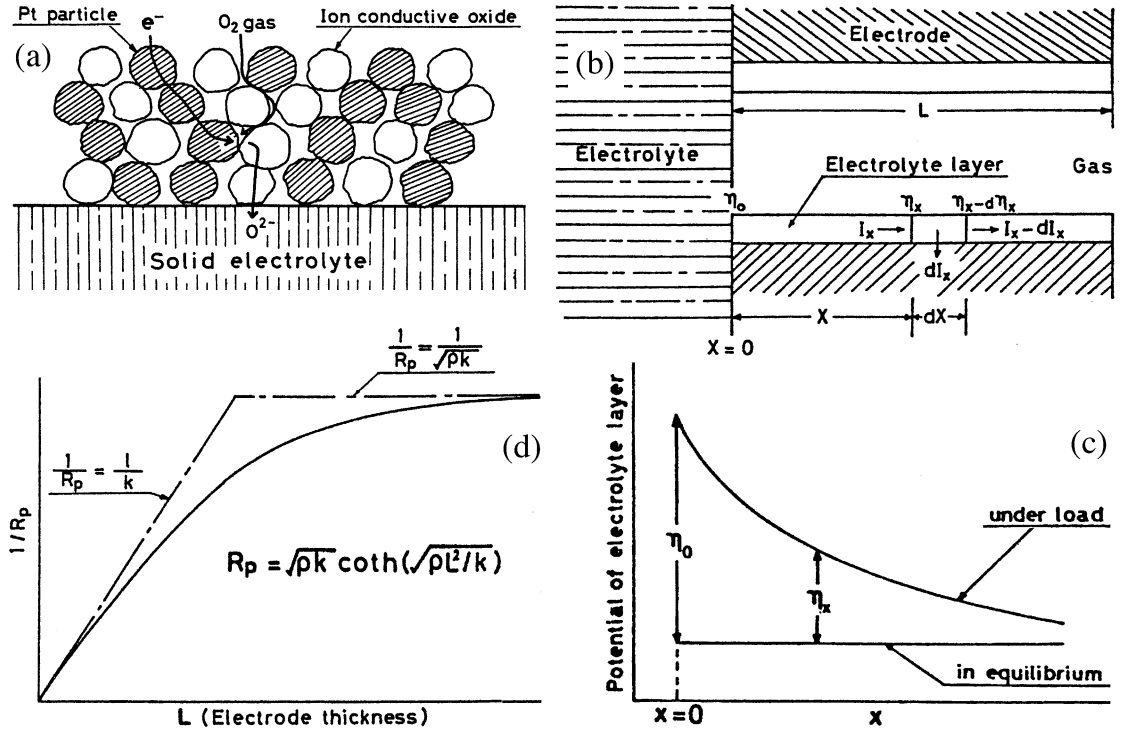

Figure 48. Kenjo's 1D macrohomogeneous model for polarization and ohmic losses in a composite electrode. (a) Sketch of the composite microstructure. (b) Description of ionic conduction in the ionic subphase and reaction at the TPB's in terms of interpenetrating thin films following the approach of ref 302. (c) Predicted overpotential profile in the electrode near the electrode/electrolyte interface. (d) Predicted admittance as a function of the electrode thickness as used to fit the data in Figure 47. (Reprinted with permission from refs 300 and 301. Copyright 1991 and 1992 Electrochemical Society, Inc. and Elsevier, reepectively.)

Despite these uncertainties, however, workers have made impressive advances in cathode performance over the last 5−7 years using composite microstructures. A recent paper by McIntosh et al. reports the area-specific resistance of a 50−50 LSM−YSZ composite (fabricated from powders at 1250 °C) to be about ∼0.2 Ω cm^2, both in a half cell and fuel-cell configurations following polarization.[40] Barnett and co-workers report somewhat higher resistances for LSM/GDC composites (∼1.0 Ω cm^2 at 700 °C[33]); however, it should be noted that these electrodes had never seen a bias and thus may have much higher performance under load (see section 5.4). Electrodes incorporating mixed conductors as the electronic subphase generally have even higher performance. As an example, Figure 49 shows the impedance (as a function of temperature in air) of a low-fired (900 °C) LSCF/GDC composite electrode on YSZ made by Murray and co-workers.[35] This electrode has an ASR of ∼0.03 Ω cm^2 at 700 °C with no polarization history. Huang and co-workers reported cathode resistances of ∼0.1 Ω cm^2 at 700 °C for LSC/YSZ and LSF/YSZ composites made by impregnation techniques.[315,316]

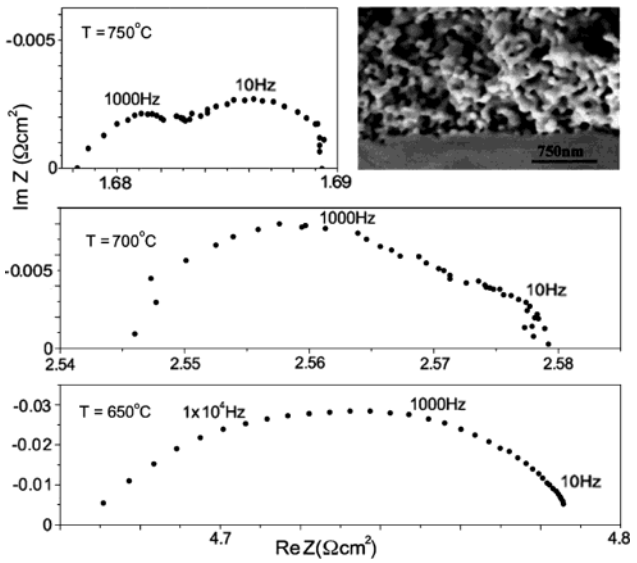

Figure 49. Impedance of a low-fired composite LSCF/GDC electrode on YSZ in air as a function of temperature. (Inset) SEM of the microstructure of the electrode showing very fine porosity but effective interparticle contact. (Reprinted with permission from ref 35. Copyright 2002 Elsevier.)

6.5. Current Constriction Effects

In passing, we should also mention one additional microstructural factor potentially impacting the overall electrode performance: constriction of the ionic current in the electrolyte near the electrode/electrolyte interface. To better understand this effect, consider a circular disk electrode of diameter d immersed in a semi-infinite electrolyte of conductivity σ_i (Figure 50a). It can be shown that the measured IR drop occurs primarily within a distance d of the electrode with a value given by[47]

$$V_{IR} = \frac{I}{2d\sigma_i} \tag{11}$$

where I is the total current. If one views the interface between a solid electrolyte and a porous electrode as

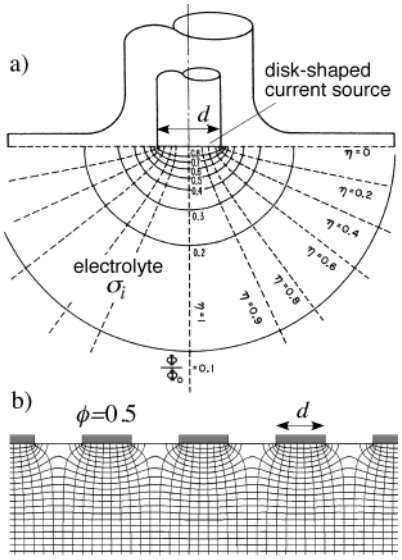

Figure 50. (a) Primary potential distribution surrounding a disk-shaped electrode. (Reprinted with permission from ref 47. Copyright 2004 John Wiley & Sons.) (b) Finite-element calculation of the 2D primary potential profile near an electrode with regular periodic contact to the electrolyte ($\phi = 0.5$). Horizontal lines on the contour plot are lines of constant potential; vertical lines follow the current path.

an array of such small current sources, one expects that as the size of these sources get very small, the *IR* resistance will become increasingly dominated by the constriction of the current near each source rather than the superficial current density of the cell.

Workers have shown theoretically that this effect can be caused both at the microstructural level (due to funneling of the current near the TPB) as well as on a macroscopic level when the electrode is not perfectly electronically conductive and the current collector makes only intermittent contact.[206,244,317] Fleig and Maier further showed that current constriction can have a distortional effect on the frequency response (impedance), which is sensitive to the relative importance of the surface vs bulk path.[318] In particular, they showed that unlike the bulk electrolyte resistance, the constriction resistance can appear at frequencies overlapping the interfacial impedance. Thus, the effect can be hard to separate experimentally from interfacial electrochemical−kinetic resistances, particularly when one considers that many of the same microstructural parameters influencing the electrochemical kinetics (TPB area, contact area) also influence the current constriction.

To facilitate estimates of this effect on the microstructural level, we point out the existence of an important dimensionless group, *J*, that describes the ratio of the current constriction resistance to the electrode resistance.[47,319] If $J \ll 1$, then we expect the constriction effect will be small compared to the electrode resistance, while if $J \geq 1$, the constriction effect is expected to be significant. For example, in the case shown in Figure 50a, *J* is derived by dividing V_{IR} (given by eq 11) by the electrode overpotential $\eta = IR_{electrode}$, where $R_{electrode}$ is the total effective resistance of the disk (in Ω). If we consider a large number of well-separated disks (Figure 50b) and re-express $R_{electrode}$ on a superficial-area-normalized basis, *J* is given approximately by

$$J \approx 0.4\frac{d}{\phi R_{ASR}\sigma_i} \qquad (12)$$

where R_{ASR} is the area-specific resistance of the electrode and ϕ is the fraction of the area through which current must flow at the interface. Applying eq 12 to a bulk-path-dominated electrode (Figure 50b), we can estimate *J* by taking *d* to be the average diameter of the solid−solid contact points while ϕ is the fraction of the electrolyte surface covered by the electrode. For 2D rather than 3D constriction, the situation is similar;[319] thus, for a surface-dominated mechanism, we would take *d* to be the effective width of the TPB while ϕ would correspond the fraction of the electrolyte surface within one-half TPB width of the TPB line.

As an example, consider a porous LSC electrode with an average particle diameter of 0.2 μm operating via a bulk path. If the porosity is 30%, then ϕ will be approximately 0.7. Assuming a superficial electrode resistance of 0.05 Ω cm^2 at 750 °C and an electrolyte conductivity of 0.03 Ω cm^{-1}, then $J \approx 0.01$. Thus, current constriction is probably not an issue in this case. Alternatively, consider a porous LSM electrode of similar morphology and performance, assuming a TPB width of ∼1 nm. In this case ϕ will be approximately 1.4% of the superficial area. Thus, *J* would be ∼0.002. Again, this is a number much smaller than 1. These back-of-the-envelope calculations suggest that microscopic current constriction is not a large effect under most practical situations, and thus most excess ohmic losses reported in the literature arise from more macroscopic current constriction effects (such as insufficient current collection).[206,320] However, it is probably wise for investigators to make estimates of *J* to ensure further analysis is not required for their system.

6.6. Long-Term Degradation

A second form of nonstationary behavior is irreversible long-term degradation of the electrodes, explicitly with either time or time under operation in a given environment. Unfortunately, the literature in this area is neither plentiful nor consistent. In particular, there is a dearth of publications reporting test data past about 100 h due (no doubt) to the extreme cost of conducting long-term testing. As a result, degradation has remained primarily a subject of concern for industrial developers who have the resources needed to tackle this issue but by the same token are generally loath to publish important, hard-fought trade secrets. Furthermore, of the few reports that have been published, results often vary wildly for seemingly similar material systems. For example, workers have reported fuel cells based on porous LSM cathodes lasting >50 000 h with less than 5% degradation,[321] while others have reported cathode degradation of 1000% in less than 50 h.[322] Given this general lack of consensus as to rates and causes of long-term degradation, we only briefly mention a few of the factors reported to cause acute short-term degradation (100−1000 h).

(1) *Morphological evolution*. Driven in part by parallel studies on nickel sintering and degradation in SOFC anodes,[323−326] one concern has been that LSM (or other ceramic cathode materials) can sinter over time, losing active surface area and thus activity. Several workers have reported morphological changes in LSM electrodes with time or with time under current load, which has been correlated with degradation.[157,214,322,327−329] Why the changes occur and how they effect performance is not very clear. It is also not clear that these changes are all caused by the same thing or that all electrodes are likely to experience these changes.

(2) *Chromium contamination*. As discussed previously, one must always be aware of the possible presence of impurities which could have a variety of effects, including enhancing sintering at operating temperatures. An impurity of particular concern has been chromium, which is often part of the interconnect (bipolar plate) in an SOFC stack either as a $LaCrO_3$ (ceramic interconnect) or as part of an alloy in the case of a metal interconnect. Workers have shown that Cr can be quite mobile in an SOFC environment[330,331] and linked it clearly to degradation.[332] There has also been a considerable amount of recent work that has probed the mechanism by which Cr degrades performance.[182,333−335] It appears that perovskite mixed conductors are less susceptible to the effects of chrome than LSM, possibly because they function by a bulk mechanism, which is less influenced by the contamination of the surface by Cr-containing species.

(3) *Evolution of secondary phases*. Another concern has been continued formation of LZ and SZ secondary phases at the perovskite/YSZ interface as a function of time or current density.[336,337] Accelerated testing, achieved by sustained heat treatments of the electrode, suggests that degradation can occur by this mechanism.[338,339] However, whether such thermal treatments can be meaningfully extrapolated to predict natural degradation processes is unclear.

(4) *Thermal cycling*. Finally, we should also mention the issue of thermal cycling, which is a likely source of stress on cells in a commercial SOFC device due to thermal and chemical mismatches among the various materials.[340,341] Hsiao and Selman have shown that this effect has a primary influence on the interface, causing literal separation of the electrode from the electrolyte.

6.7. Experimental Artifacts in Electrochemical Measurements

As we have seen in the previous sections, our understanding of SOFC cathode mechanisms often hinges on interpretation on the magnitude and time scale of electrochemical characteristics. However, these characteristics are often strongly influenced by factors that have nothing to do with the electrode reaction itself but rather the setup of the experiment. In this section we point out two commonly observed effects that can potentially lead to experimental artifacts in electrochemical measurements: (1) polarization resistance caused gas-phase diffusion and (2) artifacts related to the cell geometry. As we will see below, these effects commonly influence the polarization, leading to experimental errors, or appear as "features" in the impedance or other electrochemical measurements that workers misinterpret as part of the electrode reaction mechanism.

(1) *Gas-phase effects*. In aqueous electrochemistry, a rotating disk electrode is often employed to ensure that that mass-transfer effects do not obscure the measurement of electrochemical kinetics except at very high polarization (limiting current). In contrast, the gas inside the pore network of a GDE is *stagnant* and may be so for some distance outside the electrode due to the presence of additional materials required for current collection and/or mechanical support (mass-transfer distances of 30−1000 μm are not uncommon). In addition, the molar concentration of a gas is $\sim 10^3$ times lower than a liquid. Partially compensating for these factors is the fact that gas-phase diffusion is typically 5 orders of magnitude faster than diffusion in aqueous solution. For example, the binary diffusion coefficient of oxygen in air at 700 °C is ~ 1 cm^2/s compared to the diffusion coefficient of dissolved O_2 in H_2O at 25 °C ($\sim 2 \times 10^{-5}$ cm^2/s). However, these estimates also suggest that at O_2 concentrations of $\sim 10^{-2}$ atm or below we might expect gas-phase diffusion to become significant.

One can roughly estimate the effects of gas-phase diffusion at steady state using a simple 1D diffusion model, which has been employed (in some form) by numerous workers.[171,342,343] This approach yields the following expression for the linearized steady-state chemical resistance due to binary diffusion of O_2 in a stagnant film of thickness L[171]

$$R_{\mathrm{gas}} = \frac{RT}{4F^2} \frac{L V_{\mathrm{m}}}{2 x_{O2}^{\infty} D_{\mathrm{AB}}^{\mathrm{eff}}} \tag{13}$$

where x_{O2}^{∞} (assumed $\ll 1$) is the mole fraction of oxygen in the well-mixed region outside the film layer, $V_{\mathrm{m}} = RT/P$ is the molar volume of the gas, and $D_{\mathrm{AB}}^{\mathrm{eff}}$ is the effective diffusion coefficient which may depend on porosity and tortuosity of the electrode as well as the effects of Knudsen diffusion (note the similarity to eq 7). As an example, for a diffusion layer of 100 μm, an effective diffusion coefficient of 0.1 cm^2/s, a gas concentration of 10^{-3} (total pressure 1 atm), and a temperature of 1000 K, this equation predicts a resistance of $\sim 1\ \Omega$ cm^2.

Thus, not surprisingly, numerous workers have knowingly (or unknowingly) observed this effect in polarization and impedance measurements.[28,70,79,171,184,291,342−347] For materials having a small apparent utilization region l_δ compared to the electrode thickness (e.g., porous Pt or LSM at low polarization), gas-phase effects normally appear as a separate arc in the impedance at low frequency.[70,79,345−347] As an example, Figure 51 shows the impedance of porous LSM/YSZ composite electrodes on YSZ at 950 °C, measured as a function of P_{O_2} using blended gases of O_2 in N_2. An arc with frequency ~ 1 Hz appears below $P_{O_2} = 5\%$ and grows dramatically with decreasing P_{O_2}.[346] Telltale signs that this arc is related to gas-phase diffusion are (1) the admittance associated with this arc is first order in P_{O_2}, (2) when

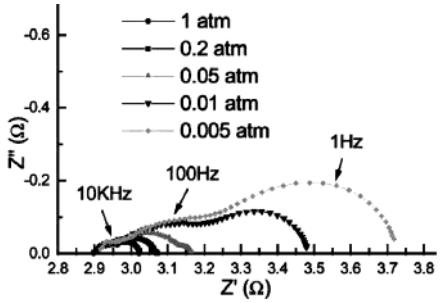

Figure 51. Zero-bias impedance of a 60%/40% LSM/YSZ composite cathode, measured at 950 °C as a function of P_{O_2}.[346] The magnitude of the lowest-frequency arc (~1 Hz) was quantified using equivalent circuit analysis and found to scale inversely with P_{O_2} and only weakly with temperature. (Reprinted with permission from ref 346. Copyright 2001 Elsevier.)

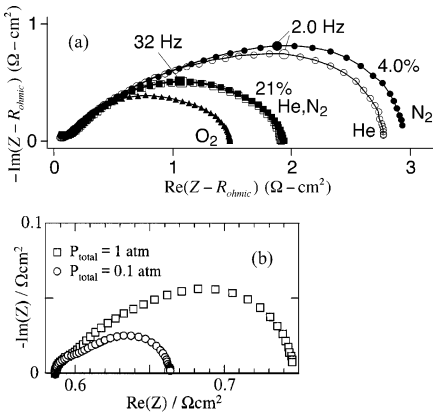

Figure 52. Effect of binary gas-phase diffusion on the impedance characteristics of porous mixed-conducting electrodes at low P_{O_2}: (a) zero-bias impedance of LSC on rare-earth-doped ceria at 1 atm and 750 °C as a function of P_{O_2} using concentrations and balance gases as indicated. (Reprinted with permission from ref 350. Copyright 2000 Elsevier B.V.) (b) Zero-bias impedance of SSC ($x = 0.5$) on SDC at 800 °C and $P_{O_2} = 0.01$ atm as a function of total pressure. (Reprinted with permission from ref 184. Copyright 2001 Electrochemical Society, Inc.)

measured as a function of temperature, the polarization associated with this arc is found to have a very small activation energy, and (3) the very low frequency of the arc, which can generally be understood in terms of the relative chemical capacitances involved, as follows. As discussed in sections 3−5, the chemical capacitance associated with the faradaic impedance is proportional to the linearized storage capacity of adsorbed oxygen on the electrode surface within a distance l_δ of the interface. However, when gas-phase diffusion resistance is present, the relevant oxygen storage capacity involves the entire electrode surface (thickness L) as well as the storage capacity of the gas itself (which may be particularly significant if there is a large stagnant layer outside the electrode). Yoon et al. showed that gas-phase diffusion in the electrode itself and mass-transfer limitations outside the electrode (caused by a flow-rate-dependent boundary layer) appear as separate impedance features due to the relatively large storage capacity of the gas above the cell.[347]

In cases where the utilization region approaches the electrode thickness (e.g., perovskite mixed conductors), it can be harder to discern gas-phase effects as a separate feature since the time scales begin to merge. Some techniques workers have used in this situation include varying the total pressure while keeping P_{O_2} constant[184] (since binary diffusion coefficients scale inversely with P_{total} at low pressure[348]) or replacing the diluent gas (usually N_2 or Ar) with He[28,346,347] (since the binary diffusion coefficient for O_2 in He is about 4−5 times smaller than for O_2 in N_2[349]). As an example, Figure 52a shows the impedance of LSC electrodes on rare-earth-doped ceria at 750 °C as a function of P_{O_2} when a relatively thick (~20 μm) porous silver current collector is used. Replacement of air with 20.9% O_2 in He has little effect on the impedance at zero bias. However, there is measurable difference between 4.0% O_2 in N_2 vs 4.0% O_2 in He. The higher resistance in N_2 is accompanied by a proportionate decrease in characteristic frequency rather than the appearance of a second feature in the impedance. As shown in Figure 52b, Koyama et al. showed similar findings for SSC on SDC at 800 °C and $P_{O_2} = 0.01$ atm by varying total pressure.[184] The similarity in time scale for the chemical vs gas-transport impedances in these cases likely reflects a large utilization length since if the active region is already a significant fraction of the electrode bulk, any fluctuations in solid and gas composition resulting from gradients in gas concentration add little to the already large chemical capacitance.

The results reviewed above suggest that gas-phase diffusion can contribute significantly to polarization as O_2 concentrations as high as a few percent and are not necessarily identifiable as a separate feature in the impedance. Workers studying the P_{O_2}-dependence of the electrode kinetics are therefore urged to eliminate as much external mass-transfer resistance in their experiments as possible and verify experimentally (using variations in balance gas or total pressure) that gas-phase effects are not obscuring their results.

(2) *Cell geometry effects*. Figure 53a illustrates a typical cell configuration used by workers wishing to isolate the polarization losses of a specific SOFC electrode. In this case, the cell consists of a thin (10−500 μm) electrolyte with active (current bearing) electrodes on each side. The reference electrode is placed on the surface of the inactive (unelectroded) portion of the electrolyte, on one or both sides of the cell, some distance away from the edge of the active electrodes. Ideally, the purpose of this configuration is to measure the electrolyte potential along an equipotential surface "somewhere between the two active electrodes". If two reference electrodes are used, they will yield redundant information (differing only in Nernst potential), provided they are placed a distance greater than ~3 electrolyte thicknesses from the edge of the active electrodes and the gas on each side of the cell is well mixed.[350] Assuming this idealization, the total cell voltage losses (V_{total}) can be divided into two parts as shown in Figure 53b: V_A, which contains the overpotential of the first electrode plus some fraction of the electrolyte potential drop, and V_B, which contains the overpotential of the second electrode plus the remaining fraction

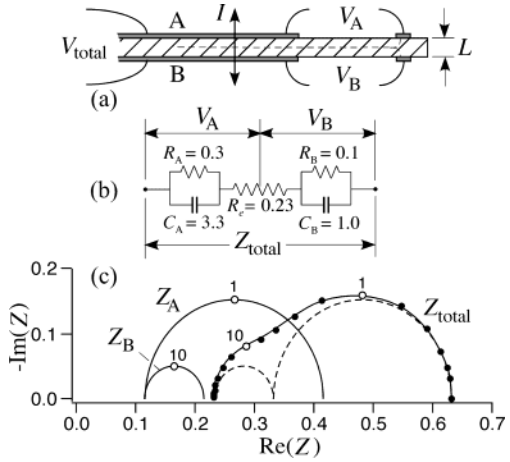

Figure 53. Idealized half-cell response of a thin solid electrolyte cell. (a) Cell geometry including working electrodes A and B and reference electrode(s). (b) Equivalent circuit model for the cell in a, where the electrolyte and two electrodes have area-specific resistances and capacitances as indicated. (c) Total cell and half-cell impedance responses, calculated assuming the reference electrode remains equipotential with a planar surface located somewhere in the middle of the active region, halfway between the two working electrodes, as shown in a.

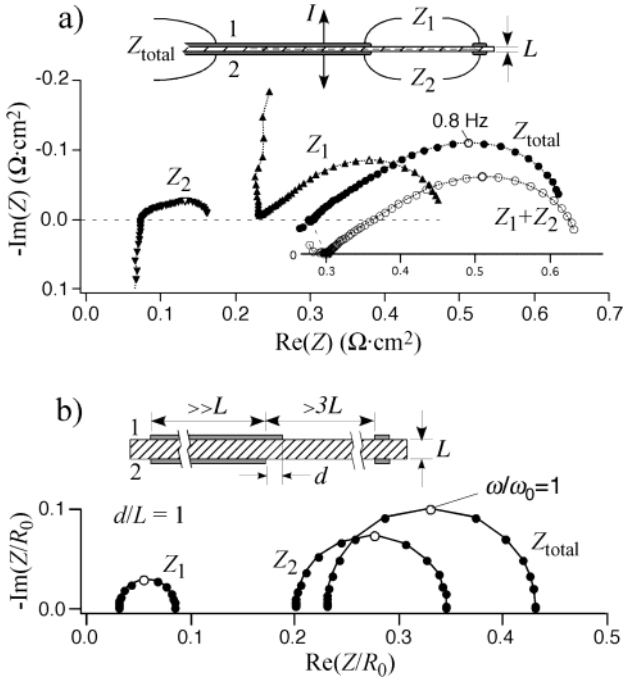

Figure 54. Measured (a) and simulated (b) effect of electrode misalignment. (a) Total-cell and half-cell impedances of a symmetric LSC/rare-earth-doped ceria/LSC cell with nominally identical porous LSC ($x = 0.4$) electrodes, measured at 750 °C in air based on the cell geometry shown.[350] (b) Finite-element calculation of the total-cell and half-cell impedances of a symmetric cell with identical R−C electrodes, assuming a misalignment of the two working electrodes (d) equal to the thickness of the electrolyte (L).[319]

of the electrolyte potential losses. Assuming this division can be achieved, Figure 53c illustrates the resulting separation of the total cell impedance into two ideal half-cell impedances, supposing (for the purposes of example) electrodes with simple linear RC behavior.

Although experimentalists often assume validity of the idealization shown in Figure 53, numerous studies have illustrated the difficulty of making accurate polarization measurements with this type of configuration.[319,350−358] Nagata et al.[351] and Hsieh et al.[352] have shown experimentally that electrode geometries similar to Figure 53 can yield large inaccuracies in the measured steady-state electrode overpotential and impedance. A number of workers have since attempted to simulate these effects.[319,350,353−355] In particular, Winkler et al.[353] used the finite-element method to calculate the primary (infinite frequency) and secondary (zero frequency) d.c. potential distributions for various electrode geometries and reference electrode locations. These calculations showed that a slight *misalignment* of the active electrodes on a thin cell can cause a frequency-dependent displacement of the reference potential, leading to significant inaccuracies in the electrode resistance extracted from a.c. impedance measurements. Adler et al. corroborated these findings[350] and more recently extended FEA analysis to include both the real and imaginary response, allowing determination of distortional effects on the impedance in arbitrary geometries over the entire frequency spectrum.[319]

As an example, Figure 54a shows the zero-bias impedance of LSC electrodes on rare-earth-doped ceria in air at 750 °C measured using a symmetric cell incorporating a traditional reference electrode.[350] Although the two screen-printed electrodes (1 and 2) were processed identically and aligned to an accuracy of ∼0.1 mm, the cell response is highly asymmetric with nearly 80% of the *iR* resistance being apportioned to electrode 2. The two half-cell impedances differ in both shape and magnitude and exhibit anomalous "capacitive" and "inductive" effects at high frequency (that sum to zero in the total impedance). In addition, despite high reproducibility of the total cell impedance from sample to sample, the scatter in the half-cell response among samples is substantial.[350] One explanation for these effects is illustrated in Figure 54b, which shows a finite-element simulation of the half-cell impedance for identical "RC" electrodes, misaligned by a distance d equal to the thickness of the electrolyte ($d/L = 1$). This calculation suggests that the observations in Figure 54a may simply be caused by statistical variation in the alignment of the electrodes (which was subject to the limitations of a manually aligned screen printer in this case).

Furthermore, Boukamp[358] and Adler[319] showed that when the electrodes on opposite sides of a cell are different from each other (as they are in a fuel cell), errors may not only involve a numerical scaling factor but also cross-contamination of anode and cathode frequency response in the measured half-cell impedances. For example, Figure 55a shows the calculated half-cell impedance of the cell idealized in Figure 53a, assuming alignment errors of ±1 electrolyte thickness. Significant distortion of the half-cell impedances (Z_A and Z_B) from the actual impedance of the electrodes are apparent,[319] including "cross-talk"[358] of anode and cathode frequency response (1 and 10 Hz, respectively), as well as a

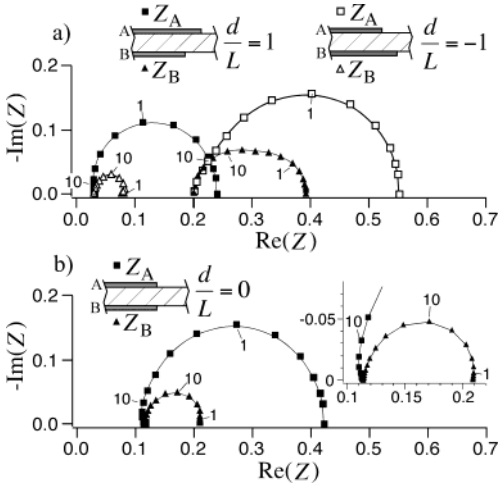

Figure 55. Simulated half-cell impedances of the cell shown in Figure 53, calculated using finite-element analysis.[319] (a) Half-cell responses assuming an electrode misalignment d/L equal to ± 1, as defined in Figure 54c. (b) Half-cell responses assuming perfect electrode alignment ($d/L = 0$).

number of possible inductive artifacts. Figure 55b further shows that distortions of the impedance will occur even when alignment is perfect due to the inherent asymmetry of the potential distribution at intermediate frequency.[319] These results potentially call into question the interpretation of half-cell measurements on all thin electrolytes (particularly very thin, supported electrolytes), not only in terms of measurement error, but also possible misinterpretation of frequency artifacts as "steps" in the reaction mechanism.

A number of different approaches have been developed by workers to combat these problems. One has simply been to avoid half-cell measurements altogether, focusing instead on the response of symmetric cells at zero bias[28] or fuel cells under load where the anode impedance is either small or identifiable by frequency in the impedance spectrum.[40] Another approach has been to use a very thick electrolyte[40] (where alignment is less of an issue), ideally incorporating a reference electrode near the working electrode via a hole in the electrolyte.[353] According to FEA simulations, the thick pellet approach appears to provide good accuracy[353] as well as frequency isolation[319] but is generally limited to lower current densities due to finite compliance voltage and Joule heating of the sample. Workers have also proposed various microelectrode geometries that (in principle) should exhibit excellent frequency isolation.[319,359,360] Early experimental results with this approach appear to be favorable,[361] but more work is needed to develop a truly robust and reliable way of doing half-cell measurements at arbitrary current densities and frequencies.

7. Conclusions and Outlook

The literature reviewed in sections 2−6 represents significant advances made in the last 20 years in our understanding of solid oxide fuel-cell cathodes. At the same time, however, this work has also underscored how *complex* the oxygen reduction reaction is, making it difficult to provide a step-by-step prescription to developers or researchers for the way forward. Rather, here we simply attempt to summarize some of the general conclusions that have emerged from this large volume of work and also highlight areas where future work is likely to make an impact.

One theme that appears to emerge repeatedly in the literature reviewed above is that there is generally no one rate-determining step (RDS) on which to focus our attention. This absence of a RDS appears to arise from two fundamental factors. First, we saw that for oxygen to be incorporated as ionic current (O^{2-}) at the electrode/electrolyte interface, O_2 gas must first be converted to some "electroactive" intermediate form via one or more reaction steps, which we labeled as *chemical* processes (as defined in section 3.2). Since O_2 is a relatively stable molecule even at high temperature, it is perhaps not surprising that these chemical steps are often found to dominate the electrode polarization, even when interfacial electrochemical kinetic resistances are significant. Given that the microstructure is usually a compromise between improved surface area (lower firing temperature) vs improved interfacial contact (higher firing temperature), we are often likely to find optimized electrodes in a mixed regime where electrochemical and chemical contributions to the overpotential are somewhat balanced.

Second, we observed generically that the chemical portion of the reaction mechanism involves an ad(b)sorption step onto (or into) the electrode material, followed by an ambipolar transport step on (or within) the material to the interface (paths a−c−e or b−d−f in Figure 4). As shown in section 3.4, these ad(b)sorption and transport steps tend to be *co-limiting* in a porous microstructure, meaning that both determine the overall rate over a wide range of values of the relevant rate parameters. In section 6.4 we further saw that for composite microstructures (which most state-of-the-art cathodes are) the electrode kinetics also become co-limited by ohmic losses in the ionic subphase. Combining this observation with those in the preceding paragraph, we might expect an optimized composite electrode to be simultaneously limited by at least four physical processes: ad(b)sorption of oxygen, ambipolar transport to the solid−solid interface, interfacial electrochemical kinetics, and ionic transport in the ionic subphase. Conceivably, improvements to *any* of these processes will help overall performance to some degree.

However, as mentioned in section 6, our awareness of this situation is not the same as being able to quantify the contributions of these various physical processes to the performance of a particular electrode under a specific set of conditions or in understanding all the factors that govern the rates of these processes. Unfortunately, due to the inherently convoluted nature of electrochemical and chemical processes, it has proven extremely difficult to isolate and study these processes individually in a complex system. We saw in sections 3−5 that impedance techniques can in some cases be used to isolate the *linearized* resistance of the interface from that of slower chemical steps via time scale. Various workers

have also shown that by accounting for the interfacial double-layer capacitance, one can often quantify the interfacial resistance even when electrochemical and chemical time scales begin to merge. As with all impedance studies, however, these analyses are limited to linearized conditions and subject to the vagaries of modeling the interface as an equivalent circuit. New techniques are needed that have an ability to more unambiguously separate overlapping physical effects in both simple and complex microstructures.

Moreover, despite the many advances in electrochemical measurement and modeling, our understanding of SOFC cathode mechanisms remains largely circumstantial today. Our understanding often relies on having limited explanations for an observed phenomenon (e.g., chemical capacitance as evidence for bulk transport) rather than direct independent measures of the mechanism (e.g., spectroscopic evidence of oxidation/reduction of the electrode material). At various points in this review we saw that high-vacuum techniques commonly employed in electrocatalysis can be used in some limited cases for SOFC materials and conditions (PEEM, for example). New in-situ analytical techniques are needed, particularly which can be applied at ambient pressures, that can probe what is happening in an electrode as a function of temperature, P_{O_2}, polarization, local position, and time.

Throughout the review, we also saw that authors have made substantial progress (particularly in the last 5−7 years) deconvoluting overlapping effects by studying systems of controlled geometry or fabricated microstructures. Hopefully this work will continue and employ new analytical techniques (such as tracer incorporation or local probes of composition and/or thermodynamic potentials) in order to make quantitative measurements of the rate-limiting steps involved. At the same time, it remains important to extend these techniques to commercially relevant microstructures both experimentally and theoretically. Advanced characterization methods such as FIB−SEM, SIMS, and AFM, combined with the many advances made in finite-element modeling, may make it increasingly possible to treat these more complex cases.

One particularly neglected issue appears to be the matching of the microstructure to the important length scales governing the mechanism. Composite electrodes are normally optimized according to the simple paradigm that increased TPB area is a good thing. However, is this always the case? For example, consider a composite electrode consisting of doped ceria and a perovskite mixed conductor. As mentioned in section 6.4, we might expect the mixed conductor, even within the composite, to exhibit a "local" utilization length (l_δ^{local}) determining the extension of the TPB beyond each interparticle contact. If all particles are smaller than this distance, then the perovskite particles will be diffusionally equilibrated locally. In this situation we might not want a high TPB area but rather a very high surface area mixed conductor with more moderately sized ceria particles offering a very efficient ionic transport path. While this is just a hypothetical example, it illustrates how understanding of the mechanism, combined with appropriate new fabrication techniques, might allow a more directed approach to electrode microstructural design.

Another neglected issue, from both a practical and fundamental perspective, is nonstationary behavior, including degradation. Why electrode performances change with time, polarization history, or other factors is very poorly understood but of significant concern to developers. SOFC stack design is very sensitive to the exact performance of the cell, and these stacks are expected to have a service life of at least 5−10 years. Yet the reported performances and degradation rates of SOFC cathodes vary so tremendously from lab to lab that it is difficult to compare, let alone choose, a material system without a substantial independent development effort. If some of these seemingly "random" variables were better identified, it would not only accelerate development but also likely aid fundamental research (by eliminating factors that otherwise obscure what workers are trying to study).

Finally, we have also seen substantial advances in electrode modeling in the last 5−10 years, including new techniques for nonlinear and time-dependent phenomena. These efforts must continue in order to achieve improved *quantitative* linkages among performance, microstructure, and materials properties. However, as mentioned in section 4.7, there is generally a dearth of independent property data for many of the physical processes entering these models. New techniques are needed that can isolate select physical processes, particularly involving the surface of electrode materials. For example, while bulk diffusion in mixed conductors is relatively well understood, it has proven difficult to isolate the rate of surface diffusion independent of the bulk. Also, tracer techniques have allowed us to measure the linearized exchange rate of oxygen on a mixed conductor surface, but it remains largely unknown how the rates of absorption/desorption depend on driving force when substantial displacements from equilibrium are involved.

8. Acknowledgments

The author would first like to acknowledge the many workers who have contributed to this line of research over the last 20 years, whose work has been cited herein. He would also like to thank several individuals for helpful discussions and/or careful readings of the manuscript: Scott Barnett, Roger deSouza, Raymond Gorte, Ronald Imbihl, Allan Jacobson, Juergen Janek, Tatsuya Kawada, Joachim Maier, Augustin McEvoy, Steve McIntosh, Ian Metcalfe, Andreas Mitterdorfer, John Newman, Steven Russek, Brian Steele, Eric Stuve, and Harry Tuller. Preparation of the manuscript was also aided substantially on a logistic level by Ladonna Kennedy, Lai Lu, and Ryan Reed. Finally, the author would also like to thank his department, students, and family for their patience during the preparation and revision of the manuscript.

9. Nomenclature

a (cm^2/cm^3)	surface area per unit volume
α_a, α_c (dimensionless)	anodic and cathodic transfer coefficients
C_i (F/cm^2)	capacitance associated with process or lengthscale i
c_i (mol/cm^3 or mol/cm^2)	bulk or surface concentration of species i
d (cm)	diameter or other characteristic length
δ (dimensionless)	oxygen nonstoichiometry in $ABO_{3-\delta}$
D^* (cm^2/s)	oxygen tracer diffusion coefficient
D_i (cm^2/s)	single component diffusion coefficient for species i
$\tilde{D}$ (cm^2/s)	chemical (ambipolar) diffusion coefficient
ϵ (dimensionless)	porosity
ϕ (dimensionless)	fraction of interface permitting passage of current
f (dimensionless)	a thermodynamic factor $(-\partial\mu_{O2}/\partial\delta)/RT$
F (C/mol)	Faraday's constant (96,487 C/mol)
η (V)	overpotential
I (A)	total current
i (A/cm^2)	current density
i_0 (A/cm^2)	exchange current density
J (dimensionless)	ratio of ohmic constriction to interfacial resistance
k, k^* (cm/s or s^{-1})	surface exchange coefficient
"k" (Ω-cm^3)	volume-specific interfacial resistance in a composite
L (cm)	thickness
l_δ (cm)	utilization length
l_g (cm)	characteristic length of a porous microstructure
μ_i (J/mol)	chemical or electrochemical potential of species i
N_i (mol/area/s)	flux of species "i"
P_{O_2} (bar)	partial pressure of oxygen
ρ (Ω-cm)	resistivity
r_0 ($mol/cm^2/s$)	equilibrium gas−surface exchange rate
r_i ($mol/cm^2/s$)	area-specific reaction rate involving species i
R (J/mol/K)	ideal gas constant (8.314 J/mol/K)
R_i (Ω-cm^2)	area-specific resistance associated with process i
σ_i (Ω^{-1} cm^{-1})	ionic conductivity
T (K or °C)	temperature
t (s)	time
τ (dimensionless)	tortuosity
t_i (dimensionless)	transference number for species i
V (V)	voltage
V_m (cm^3/mol)	molar volume (on a formula-unit basis)
ω (s^{-1})	frequency in radians
x,y (position) (cm)	position
x,y (stoich) (dimensionless)	A-site or B-site stoichiometry parameters
Z (Ω or Ω-cm^2)	impedance

10. Glossary of Commonly Used Acronyms

AFM	atomic force microscopy
CDC	Ca-doped ceria ($Ce_{1-x}Ca_xO_{2-x/2}$)
ESB	erbia-doped bismuth oxide
EIS	electrochemical impedance spectroscopy
FEA	finite-element analysis
FIB−SEM	SEM cross-sectional imaging using focused ion beams
GDC	gadolinia-doped ceria ($Ce_{1-x}Gd_xO_{2-x/2}$)
GDE	gas-diffusion electrode
HRTEM	high-resolution transmission electron microscopy
LCM	$La_{1-x}Ca_xMnO_3$
LM	La_xMnO_3
LSC	$La_{1-x}Sr_xCoO_{3-\delta}$
LSCF	$La_{1-x}Sr_xCo_{1-y}Fe_yO_{3-\delta}$
LSF	$La_{1-x}Sr_xFeO_{3-\delta}$
LSGM	$La_{0.8}Sr_{0.2}Ga_{0.8}Mg_{0.2}O_{2.8}$
LSM	$La_{1-x}Sr_xMnO_{3\pm\delta}$
LZ	lanthanum zirconate ($La_2Zr_2O_7$)
PEEM	photoelectron emission microscopy
SEM	scanning electron microscopy
SIMS	secondary-ion mass spectrometry
SOFC	solid oxide fuel cell
SDC	samaria-doped ceria ($Ce_{1-x}Sm_xO_{2-x/2}$).
SSC	$Sm_{0.5}Sr_{0.5}CoO_{3-\delta}$
SZ	strontium zirconate
TPB	three-phase (or triple-phase) boundary
XPS	X-ray photoelectron spectroscopy
XRD	X-ray diffraction (powder)
YSZ	yttria-stabilized zirconia ($Zr_{1-x}Y_xO_{2-x/2}$)

11. Glossary of Some Commonly Used Terms

chemical (or "pseudo") capacitance	a macroscopically observed capacitive relationship between current and voltage arising from chemical oxidation/reduction of a material or other charge-compensated accumulation of species
chemical (or "ambipolar") diffusion	diffusion of neutral combinations of ionic and/or electronic species under a chemical potential (concentration) driving force
chemical process	a physical or chemical rate process that may occur at a rate independent of current and is driven by a chemical-potential driving force
co-limited reaction	Situation in a porous gas-diffusion electrode wherein the utilization length and steady-state flow of current depends on both kinetic and transport properties
electrochemical kinetic process	a kinetic process involving a net faradaic current across an interface and is driven by an electrochemical potential driving force
mixed conductor	a material containing both mobile ions and mobile electrons (including holes and/or small polarons)
three-phase (or "triple-phase") boundary (*TPB*)	the one-dimensional interface within an electrode microstructure where gaseous, electronic, and ionic subphases meet
utilization length (l_δ)	size of the active region within a porous electrode, established by a balance of reaction and transport rates at steady state (see co-limited reaction)

12. References

(1) Alcock, C. B. *Solid State Ionics* **1992**, *53−56*, 3.
(2) Kilner, J.; Benson, S.; Lane, J.; Waller, D. *Chem. Ind.* **1997**, 907.
(3) Mazanec, T. J. *Solid State Ionics* **1994**, *70/71*, 11.
(4) Mobius, H. H. *J. Solid State Electrochem.* **1997**, *1*, 2.

(5) Singhal, S. C. *Proc. Electrochem. Soc.* **1998**, *97*−*24*, 125.
(6) Badwal, S. P. S.; Foger, K. *Mater. Forum* **1997**, *21*, 187.
(7) Yamamoto, O. *Electrochim. Acta* **2000**, *45*, 2423.
(8) Steele, B. C. H. *Solid State Ionics* **2000**, *134*, 3.
(9) Skinner, S. J. *Int. J. Inorg. Mater.* **2001**, *3*, 113.
(10) Will, J.; Mitterdorfer, A.; Kleinlogel, C.; Perednis, D.; Gauckler, L. J. *Solid State Ionics* **2000**, *131*, 79.
(11) McEvoy, A. J. *J. Mater. Sci.* **2001**, *36*, 1087.
(12) Ormerod, R. M. *Chem. Soc. Rev.* **2003**, *32*, 17.
(13) Yamamoto, O.; Takeda, Y.; Kanno, R.; Tomida, Y. *Nippon Kagaku Kaishi* **1988**, 1324.
(14) Godickemeier, M.; Sasaki, K.; Gauckler, L. J.; Riess, I. *Solid State Ionics* **1996**, *86*−*88*, 691.
(15) Kilner, J. A. *Bol. Soc. Esp. Ceram. Vidrio* **1998**, *37*, 247.
(16) Steele, B. C. H.; Hori, K. M.; Uchino, S. *Solid State Ionics* **2000**, *135*, 445.
(17) Godickemeier, M.; Sasaki, K.; Gauckler, L. J.; Riess, I. *J. Electrochem. Soc.* **1997**, *144*, 1635.
(18) Lane, J. A.; Adler, S.; Middleton, P. H.; Steele, B. C. H. *Solid Oxide Fuel Cells* (SOFC−IV); 1995; pp 584−96.
(19) Maguire, E.; Gharbage, B.; Marques, F. M. B.; Labrincha, J. A. *Solid State Ionics* **2000**, *127*, 329.
(20) Rohland, B. *Mater. Sci. Forum* **1991**, *76*, 149.
(21) Takahashi, T.; Ihara, M.; Yamada, K. *Proc. Electrochem. Soc.* **1995**, *95*−*1*, 1009.
(22) Colomer, M. T.; Steele, B. C. H.; Kilner, J. A. *Solid State Ionics* **2002**, *147*, 41.
(23) Steele, B. C. H. *Solid State Ionics* **1997**, *94*, 239.
(24) Dusastre, V.; Kilner, J. A. *Solid State Ionics* **1999**, *126*, 163.
(25) Schafer, W.; Koch, A.; HeroldSchmidt, U.; Stolten, D. *Solid State Ionics* **1996**, *86*−*8*, 1235.
(26) Liu, W.; Zhang, Z. P.; Xia, C. R.; Xie, J. Q.; Chen, C. S. *J. Inorg. Mater.* **2000**, *15*, 849.
(27) Endo, A.; Fukunaga, H.; Wen, C.; Yamada, K. *Solid State Ionics* **2000**, *135*, 353.
(28) Adler, S. B. *Solid State Ionics* **1998**, *111*, 125.
(29) Murray, E. P.; Barnett, S. A. *Proc. Electrochem. Soc.* **1999**, *99*−*19*, 369.
(30) Jorgensen, M. J.; Primdahl, S.; Bagger, C.; Mogensen, M. *Solid State Ionics* **2001**, *139*, 1.
(31) Jorgensen, M. J.; Mogensen, M. *J. Electrochem. Soc.* **2001**, *148*, A433.
(32) Lu, Z.-G.; Jiang, Y.; Dong, Y.-L.; Zhang, Y.-H.; Yan, J.-W. *Gaodeng Xuexiao Huaxue Xuebao* **2001**, *22*, 791.
(33) Murray, E. P.; Barnett, S. A. *Solid State Ionics* **2001**, *143*, 265.
(34) Barbucci, A.; Bozzo, R.; Cerisola, G.; Costamagna, P. *Electrochim. Acta* **2002**, *47*, 2183.
(35) Murray, E. P.; Sever, M. J.; Barnett, S. A. *Solid State Ionics* **2002**, *148*, 27.
(36) Hart, N. T.; Brandon, N. P.; Day, M. J.; Lapena-Rey, N. *J. Power Sources* **2002**, *106*, 42.
(37) Steele, B. *C. R. Acad. Sci. Serie Ii Fascicule C: Chim.* **1998**, *1*, 533.
(38) Kleitz, M.; Petitbon, F. *Solid State Ionics* **1996**, *92*, 65.
(39) Jorgensen, M. J.; Holtappels, P.; Appel, C. C. *J. Appl. Electrochem.* **2000**, *30*, 411.
(40) McIntosh, S.; Adler, S. B.; M, V. J.; Gorte, R. A. *Electrochem. Solid State Lett.* **2004**, *7*, A111.
(41) Schmid, A., Enke, F., Eds.; Stuttgart, 1923.
(42) Vetter, K. J. *Electrochemical Kinetics, Theoretical and Experimental Aspects*; Academic Press: New York, 1967.
(43) Srinivasan, S.; Hurwitz, H. D.; Bockris, J. O. M. *J. Phys. Chem.* **1967**, *46*, 3108.
(44) Giner, J.; Hunter, C. *J. Electrochem. Soc.* **1969**, *116*, 1125.
(45) Perry, M. L.; Newman, J.; Cairns, E. J. *J. Electrochem. Soc.* **1998**, *145*, 5.
(46) Kleitz, M.; Kloidt, T.; Dessemond, L. *High-Temperature Electrochemical Behavior of Fast Ion and Mixed Conductors*; Roskilde: Denmark, 1993; p 89.
(47) Newman, J. S. *Electrochemical Systems*, 2nd ed.; Prentice Hall: New York, 1991.
(48) Bauerle, J. E. *J. Phys. Chem.: Solids* **1969**, *30*, 2657.
(49) MacDonald, J. R. *Impedance Spectroscopy; Emphasizing Solid Materials and Systems*; John Wiley and Sons: New York, 1987.
(50) Wang, D. Y.; Nowick, A. S. *J. Electrochem. Soc.* **1979**, *126*, 1166.
(51) Wang, D. Y.; Nowick, A. S. *J. Electrochem. Soc.* **1979**, *126*, 1155.
(52) Okamoto, H.; Kawamura, G.; Kudo, T. *Electrochim. Acta* **1983**, *28*, 379.
(53) Hu, H.; Liu, M. *J. Electrochem. Soc.* **1997**, *144*, 3561.
(54) Schouler, E.; Giroud, G.; Kleitz, M. *J. Chim. Phys.* **1973**, *70*, 1309.
(55) Kleitz, M.; Dessemond, L.; Kloidt, T.; Steil, M. C. *Solid Oxide Fuel Cells IV*; 1995; pp 527−536.
(56) van Herle, J.; McEvoy, A. J. *J. Phys. Chem. Solids* **1994**, *55*, 339.
(57) Verkerk, M. J.; Burggraaf, A. J. *J. Electrochem. Soc.* **1983**, *130*, 78.
(58) Lewis, R.; Gomer, R. *Surf. Sci.* **1968**, *12*, 157.
(59) Mizusaki, J.; Amano, K.; Yamauchi, S.; Fueki, K. *Solid State Ionics* **1987**, *22*, 313.
(60) Mizusaki, J.; Amano, K.; Yamauchi, S.; Fueki, K. *Solid State Ionics* **1987**, *22*, 323.
(61) Wang, D. Y. *J. Electrochem. Soc.* **1990**, *137*, 3660.
(62) van Hassel, B. A.; Boukamp, B. A.; Burggraaf, A. J. *Solid State Ionics* **1991**, *48*, 139.
(63) Robertson, N. L.; Michaels, J. N. *J. Electrochem. Soc.* **1990**, *137*, 129.
(64) van Herle, J.; McEvoy, A. J. *Ber. Bunsen-Ges.-Phys. Chem. Chem. Phys.* **1993**, *97*, 470.
(65) Schwandt, C.; Weppner, W. *J. Electrochem. Soc.* **1997**, *144*, 3728.
(66) Kenjo, T.; Shiroichi, N. *Electrochim. Acta* **1997**, *42*, 3461.
(67) Luerssen, B.; Janek, J.; Imbihl, R. *Solid State Ionics* **2001**, *141*, 701.
(68) Janek, J.; Rohnke, M.; Luerssen, B.; Imbihl, R. *Phys. Chem. Chem. Phys.* **2000**, *2*, 1935.
(69) Boukamp, B. A.; Bouwmeester, H. J. M. *Solid State Ionics* **2003**, *157*, 29.
(70) Kamata, H.; Hosaka, A.; Mizusaki, J.; Tagawa, H. *Solid State Ionics* **1998**, *106*, 237.
(71) Gerischer, H. *Z. Phys. Chem.* **1951**, *198*, 216.
(72) Mitterdorfer, A.; Gauckler, L. J. *Solid State Ionics* **1999**, *117*, 187.
(73) Mitterdorfer, A.; Gauckler, L. J. *Solid State Ionics* **1999**, *117*, 203.
(74) Mitterdorfer, A.; Gauckler, L. J. *Solid State Ionics* **1999**, *120*, 211.
(75) Berthier, F.; Diard, J.-P.; Le Gorrec, B.; Montella, C. *Corrosion* **1995**, *51*, 105.
(76) Gland, J. L.; Sexton, B. A.; Fisher, G. B. *Surf. Sci.* **1980**, *95*, 587.
(77) Gorte, R.; Schmidt, L. D. *Surf. Sci.* **1978**, *76*, 559.
(78) Lewis, R.; Gomer, R. *Surf. Sci.* **1968**, *12*, 157.
(79) Verkerk, M. J.; Hammink, M. W. J.; Burggraaf, A. J. *J. Electrochem. Soc.* **1983**, *130*.
(80) Kenjo, T.; Yamakoshi, Y.; Wada, K. *J. Electrochem. Soc.* **1993**, *140*, 2151.
(81) Sasaki, K.; Tamura, J.; Dokiya, M. *Solid State Ionics* **2001**, *144*, 223.
(82) Widmer, S.; Tate, T. J.; Thampi, K. R.; McEvoy, A. J. *Solid Oxide Fuel Cells V*; Aachen: Germany, 1997; pp 451−461.
(83) McEvoy, A. J. *Solid State Ioncs* **2000**, *132*, 159.
(84) Mitterdorfer, A. Ph.D., Swiss Federal Institute of Technology, 1997.
(85) Robertson, N. L.; Michaels, J. N. *J. Electrochem. Soc.* **1991**, *138*, 1494.
(86) Kenjo, T.; Tsukamoto, K. *Solid Oxide Fuel Cells V*; Aachen: Germany, 1997; pp 431−440.
(87) Schouler, E. J. L.; Kleitz, M. *J. Electrochem. Soc.* **1987**, *134*, 1045.
(88) Chao, T.; Walsh, K. J.; Fedkiw, P. S. *Solid State Ionics* **1991**, *47*, 277.
(89) Sridhar, S.; Stancovski, V.; Pal, U. B. *J. Electrochem. Soc.* **1997**, *144*, 2479.
(90) Jacobsen, T.; Zachau-Christiansen, B.; Bay, L.; Jorgensen, M. J. *Electrochim. Acta* **2001**, *46*, 1019.
(91) Shkerin, S. N.; Perfilev, M. V. *Elektrokhimiya* **1990**, *26*, 1468.
(92) Shkerin, S. N.; Perfilev, M. V. *Soviet Electrochem.* **1992**, *28*, 1106.
(93) von Oertzen, A.; Mikhailov, A.; Rotermund, H. H.; Ertl, G. *Surf. Sci.* **1996**, *350*, 259.
(94) Emery, D. A.; Middleton, P. H.; Metcalfe, I. S. *Surf. Sci.* **1998**, *405*, 308.
(95) Bay, L.; Jacobsen, T. *Solid State Ionics* **1997**, *93*, 201.
(96) Svensson, A. M.; Nisancioglu, K. *J. Electrochem. Soc.* **1998**, *145*, 3130.
(97) Luerssen, B.; Janek, J.; Günther, S.; Kiskinova, M.; Imbihl, R. *Phys. Chem. Chem. Phys.* **2002**, *4*, 2673.
(98) Kleitz, M.; Dessemond, L.; Kloidt, T. *Solid Oxide Fuel Cells IV*; 1995; pp 35−44.
(99) van Hassel, B. A.; Boukamp, B. A.; Burggraaf, A. J. *Solid State Ionics* **1992**, *51*, 161.
(100) Ohno, Y.; Nagata, S.; Sato, H. *Solid State Ionics* **1981**, *3/4*, 439.
(101) Takeda, Y.; Kanno, R.; Noda, M.; Yamamoto, O. *Bull. Inst. Chem. Res.* **1986**, *64*, 157.
(102) Raccah, P. M.; Goodenough, J. B. *Phys. Rev.* **1967**, *155*, 932.
(103) Jaya, S. M.; Jagadish, R.; Rao, R. S.; Asokamani, R. *Phys. Rev. B* **1991**, *43*, 13274.
(104) Ishikawa, T.; Park, S. K.; Katsufuji, T.; Arima, T.; Tokura, Y. *Phys. Rev. B* **1998**, *58*, 13326.
(105) Raccah, P. M.; Goodenough, J. B. *J. Appl. Phys.* **1968**, *39*, 1209.
(106) Bhide, V. G.; Rajoria, D. S.; Reddy, Y. S.; Rao, G. R.; Rao, G. V. S.; Rao, C. N. R. *Phys. Rev. Lett.* **1972**, *27*, 1133.
(107) Bhide, V. G.; Rajoria, D. S.; Rao, C. N. R.; Rao, G. R.; Jadhao, V. G. *Phys. Rev. B* **1975**, *12*, 2832.
(108) Ganguly, P.; Kumar, P. S. A.; Santhosh, P. N.; Mulla, I. S. *J. Phys.: Condens. Matter* **1994**, *6*, 533.
(109) Senaris-Rodriguez, M. A.; Goodenough, J. B. *J. Solid State Chem.* **1995**, *118*, 323.

(110) Takahashi, H.; Munakata, F.; Yamanaka, M. *Phys. Rev. B* **1998**, *57*, 15211.
(111) Caciuffo, R.; Mira, J.; Rivas, J.; Seneris-Rodriguez, M. A.; Radaelli, P. G.; Carsughi, F.; Fiorani, D.; Goodenough, J. B. *Europhys. Lett.* **1999**, *45*, 399.
(112) Mizusaki, J.; Tabuchi, J.; Matsuura, T.; Yamauchi, S.; Fueki, K. *J. Electrochem. Soc.* **1987**, *136*, 2082.
(113) Petrov, A. N.; Kononchuk, O. F.; Andreev, A. V.; Cherepanov, V. A.; Kofstad, P. *Solid State Ionics* **1995**, *80*, 189.
(114) Chainani, A.; Mathew, M.; Sarma, D. D. *Phys. Rev. B* **1993**, *48*, 14818.
(115) Torrance, J. B.; Lacorre, P.; Asavaroengchai, C.; Metzger, R. M. *Physica C* **1991**, *182*, 351.
(116) Mizusaki, J.; Sasamoto, T.; Cannon, W. R.; Bowen, H. K. *J. Am. Ceram. Soc.* **1983**, *66*, 247.
(117) Tai, L.-W.; Nasrallah, M. M.; Anderson, H. U.; Sparlin, D. M.; Sehlin, S. R. *Solid State Ionics* **1995**, *76*, 259.
(118) Stevenson, J. W.; Armstrong, T. R.; Carneim, R. D.; Pederson, L. R.; Weber, W. J. *J. Electrochem. Soc.* **1996**, *143*, 2722.
(119) Mizusaki, J.; Yoshihiro, M.; Yamauchi, S.; Fueki, K. *J. Solid State Chem.* **1985**, *58*, 257.
(120) Allnatt, A. R.; Lidiard, A. B. *Atomic Transport in Solids*; Cambridge University Press: New York, 1993.
(121) Mizusaki, J.; Mima, Y.; Yamauchi, S.; Fueki, K.; Tagawa, H. *J. Solid State Chem.* **1989**, *80*, 102.
(122) Petrov, A. N.; Cherepanov, V. A.; Kononchuk, O. F.; Gavrilova, L. Y. *J. Solid State Chem.* **1990**, *87*, 69.
(123) Lankhorst, M. H. R.; Bouwmeester, H. J. M. *J. Electrochem. Soc.* **1997**, *144*, 1268.
(124) Kawada, T.; Suzuki, J.; Sase, M.; Kaimai, A.; Yashiro, K.; Nigara, Y.; Mizusaki, J.; Kawamura, K.; Yugami, H. *J. Electrochem. Soc.* **2002**, *149*, E252.
(125) Lankhorst, M. H. R.; Bouwmeester, H. J. M.; Verweij, H. *Phys. Rev. Lett.* **1996**, *77*, 2989.
(126) Lankhorst, M. H. R.; Bouwmeester, H. J. M.; Verweij, H. *J. Solid State Chem.* **1997**, *133*, 555.
(127) Lankhorst, M. H. R.; Bouwmeester, H. J. M.; Verweij, H. *Solid State Ionics* **1997**, *96*, 21.
(128) Tai, L.-W.; Nasrallah, M. M.; Anderson, H. U.; Sparlin, D. M.; Sehlin, S. R. *Solid State Ionics* **1995**, *76*, 273.
(129) Lankhorst, M. Univerdsity of Twente, 1997.
(130) Lankhorst, M. H. R.; ten Elshof, J. E. *J. Solid State Chem.* **1997**, *130*, 302.
(131) Teraoka, Y.; Zhang, H. M.; Okamoto, K.; Yamazoe, N. *Mater. Res. Bull.* **1988**, *23*, 51.
(132) Teraoka, Y.; Nobunaga, T.; Okamoto, K.; Miura, N.; Yamazoe, N. *Solid State Ionics* **1991**, *48*, 207.
(133) Diethelm, S.; Closset, A.; Nisancioglu, K.; Van herle, J.; McEvoy, A. J.; Gur, T. M. *J. Electrochem. Soc.* **1999**, *146*, 2606.
(134) Kilner, J. A.; Steele, B. C. H.; Ilkov, L. *Solid State Ionics* **1984**, *12*, 89.
(135) Ishigaki, T.; Yamauchi, S.; Kishio, K.; Mizusaki, J.; Fueki, K. *J. Solid State Chem.* **1988**, *73*, 179.
(136) Bouwmeester, H. J. M.; Kruidhof, H.; Burggraaf, A. J. *Solid State Ionics* **1994**, *72*, 185.
(137) Kilner, J. A.; Souza, R. A. D.; Fullarton, I. C. *Solid State Ionics* **1996**, *86*−*88*, 703.
(138) Routbort, J. L.; Doshi, R.; Krumpelt, M. *Solid State Ionics* **1996**, *90*, 21.
(139) van Doorn, R. H. E.; Fullarton, I. C.; de Souza, R. A.; Kilner, J. A.; Bouwmeester, H. J. M.; Burggraaf, A. J. *Solid State Ionics* **1997**, *96*, 1.
(140) De Souza, R. A.; Kilner, J. A. *Solid State Ionics* **1998**, *106*, 175.
(141) De Souza, R. A.; Kilner, J. A. *Solid State Ionics* **1999**, *126*, 153.
(142) Bredesen, R.; Mertins, F.; Norby, T. *Catal. Today* **2000**, *56*, 315.
(143) Ma, B.; Balachandran, U.; Park, J. H.; Segre, C. U. *Solid State Ionics* **1996**, *83*, 65.
(144) ten Elshof, J. E.; Lankhorst, M. H. R.; Bouwmeester, H. J. M. *Solid State Ionics* **1997**, *99*, 15.
(145) ten Elshof, J. E.; Lankhorst, M. H. R.; Bouwmeester, H. J. M. *J. Electrochem. Soc.* **1997**, *144*, 1060.
(146) Lane, J. A.; Benson, S. J.; Waller, D.; Kilner, J. A. *Solid State Ionics* **1999**, *121*, 201.
(147) Kriegel, R.; Pippardt, U.; Voigt, I. *Sep. Purif. Technol.* **2001**, *25*, 127.
(148) Chen, X.; Adler, S. B. Manuscript in preparation.
(149) Fueki, K.; Mizusaki, J.; Yamauchi, S.; Ishigaki, T.; Mima, Y. 10th International Symposium on the Reactivity of Solids; pp 339−343.
(150) ten Elshof, J. E.; Bouwmeester, H. J. M.; Verweij, H. *Solid State Ionics* **1995**, *81*, 97.
(151) ten Elshof, J. E.; Bouwmeester, H. J. M.; Verweij, H. *Solid State Ionics* **1996**, *89*, 81.
(152) Figueiredo, F. M.; Marques, F. M. B.; Frade, J. R. *Solid State Ionics* **1998**, *111*, 273.
(153) Kim, S.; Yang, Y. L.; Jacobson, A. J.; Abeles, B. *Solid State Ionics* **1998**, *106*, 189.
(154) Zhang, C.; Deng, H.; Varon, J.; Abeles, B.; Yang, Y.; Pham, A. Q.; Jacobson, A. J. *MRS* **1994**, 1.
(155) Gharbage, B.; Pagnier, T.; Hammou, A. *J. Electrochem. Soc.* **1994**, *141*, 2118.
(156) Van Herle, J.; McEvoy, A. J.; Thampi, K. R. *Electrochim. Acta* **1994**, *39*, 1675.
(157) Mizusaki, J.; Saito, T.; Tagawa, H. *J. Electrochem. Soc.* **1996**, *143*, 3065.
(158) Masuda, K.; Kawada, T.; Kaimai, A.; Kawamura, K.; Nigara, Y.; Mizusaki, J.; Yugami, H.; Arashi, H. *5th International Symposium on Solid Oxide Fuel Cells*; Achen: Germany, 1997; p 473.
(159) Ioroi, T.; Hara, T.; Uchimoto, Y.; Ogumi, Z.; Takehara, Z. *J. Electrochem. Soc.* **1997**, *144*, 1362.
(160) Ioroi, T.; Hara, T.; Uchimoto, Y.; Ogumi, Z.; Takehara, Z. *J. Electrochem. Soc.* **1998**, *145*, 1999.
(161) Kawada, T.; Masuda, K.; Suzuki, J.; Kaimai, A.; Kawamura, K.; Nigara, Y.; Mizusaki, J.; Yugami, H.; Arashi, H.; Sakai, N.; Yokokawa, H. *Solid State Ionics* **1999**, *121*, 271.
(162) Yang, Y. L.; Chen, C. L.; Chen, S. Y.; Chu, C. W.; Jacobson, A. J. *J. Electrochem. Soc.* **2000**, *147*, 4001.
(163) Fukunaga, H.; Koyama, M.; Takahashi, N.; Wen, C.; Yamada, K. *Solid State Ionics* **2000**, *132*, 279.
(164) Mims, C. A.; Joos, N. I.; van der Heide, P. A. W.; Jacobson, A. J.; Chen, C.; Chu, C. W.; Kim, B. I.; Perry, S. S. *Electrochem. Solid State Lett.* **2000**, *3*, 59.
(165) Yang, Y.; Jacobson, A. J.; Chen, C. L.; Luo, G. P.; Ross, K. D.; Chu, C. W. *Appl. Phys. Lett.* **2001**, *79*, 776.
(166) Ringuede, A.; Fouletier, J. *Solid State Ionics* **2001**, *139*, 167.
(167) Endo, A.; Ihara, M.; Komiyama, H.; Yamada, K. *Solid State Ionics* **1996**, *86*−*88*, 1191.
(168) Adler, S. B. *Solid State Ionics* **2000**, *135*, 603.
(169) Liu, M.; Winnick, J. *J. Electrochem. Soc.* **1997**, *144*, 1881.
(170) Liu, M.; Winnick, J. *Solid State Ionics* **1999**, *118*, 11.
(171) Adler, S. B.; Lane, J. A.; Steele, B. C. H. *J. Electrochem. Soc.* **1996**, *143*, 3554.
(172) Svensson, A. M.; Sunde, S.; Nisancioglu, K. *Solid State Ionics* **1996**, *86*−*8*, 1211.
(173) Abeles, B. *Proc. Electrochem. Soc.* **1997**, *96*−*27*, 1.
(174) Deng, H.; Zhou, M.; Abeles, B. *Solid State Ionics* **1994**, *74*, 75.
(175) Bae, J. M.; Steele, B. C. H. *Solid State Ionics* **1998**, *106*, 255.
(176) Zhou, M.; Deng, H.; Abeles, B. *Solid State Ionics* **1996**, *93*, 133.
(177) Sirman, J.; Lane, J.; Kilner, J. A. Electrochemical Society Meeting, 1997; p 2129.
(178) Steele, B. C. H.; Bae, J.-M. *Solid State Ionics* **1998**, *106*, 255.
(179) Endo, A.; Wada, S.; Wen, C.-J.; Komiyama, H.; Yamada, K. *J. Electrochem. Soc.* **1998**, *145*, L35.
(180) Horita, T.; Yamaji, K.; Sakai, N.; Yokokawa, H.; Weber, A.; Ivers-Tiffee, E. *J. Electrochem. Soc.* **2001**, *148*, A456.
(181) Horita, T.; Yamaji, K.; Sakai, N.; Yokokawa, H.; Weber, A.; Ivers-Tiffee, E. *Electrochim. Acta* **2001**, *46*, 1837.
(182) Jiang, S. P. *Solid State Ionics* **2002**, *146*, 1.
(183) Fleig, J. *Ann. Rev. Mater. Res.* **2003**, *33*, 361.
(184) Koyama, M.; Wen, C. J.; Masuyama, T.; Otomo, J.; Fukunaga, H.; Yamada, K.; Eguchi, K.; Takahashi, H. *J. Electrochem. Soc.* **2001**, *148*, A795.
(185) Svensson, A. M.; Sunde, S.; Nisancioglu, K. *J. Electrochem. Soc.* **1997**, *144*, 2719.
(186) Svensson, A. M.; Sunde, S.; Nisancioglu, K. *J. Electrochem. Soc.* **1998**, *145*, 1390.
(187) Liu, M.; Wu, Z. *Solid State Ionics* **1998**, *107*, 105.
(188) Liu, M. L. *J. Electrochem. Soc.* **1998**, *145*, 142.
(189) Adler, S. B.; Lane, J. A.; Steele, B. C. H. *J. Electrochem. Soc.* **1997**, *144*, 1884.
(190) van Doorn, R. H. E. University of Twente, 1996.
(191) van Doorn, R. H. E.; Burggraaf, A. J. *Solid State Ionics* **2000**, *128*, 65.
(192) Fleig, J. *J. Power Sources* **2002**, *105*, 228.
(193) Fleig, J.; Maier, J. 203 Meeting of the Electrochemical Society, Paris, 2003; p 509.
(194) Fleig, J. *Annu. Rev. Matsci* 2003.
(195) Maier, J. *Solid State Ionics* **1998**, *112*, 197.
(196) Maier, J. *preprint* **1999**, 1.
(197) Maier, J.; Jamnik, J.; Leonhardt, M. *Solid State Ionics* **2000**, *129*, 25.
(198) Kuznecov, M.; Otschik, P.; Eichler, K.; Schaffrath, W. *Ber. Bunsen-Ges.-Phys. Chem. Chem. Phys.* **1998**, *102*, 1410.
(199) Coffey, G. W.; Pederson, L. R.; Rieke, P. C. *J. Electrochem. Soc.* **2003**, *150*, A1139.
(200) Atkinson, A.; Ramos, T. *Solid State Ionics* **2000**, *129*, 259.
(201) Adler, S. B. *J. Am. Ceram. Soc.* **2001**, *84*, 2117.
(202) Mizusaki, J.; Tagawa, H.; Naraya, K.; Sasamoto, T. *Solid State Ionics* **1991**, *49*, 111.
(203) Takeda, Y.; Kanno, R.; Noda, M.; Tomida, Y.; Yamamoto, O. *J. Electrochem. Soc.: Electrochem. Sci. Technol.* **1987**, *134*, 2656.
(204) Mizusaki, J.; Tagawa, H.; Tsuneyoshi, K.; Sawata, A. *J. Electrochem. Soc.* **1991**, *138*, 1867.
(205) Nagata, M.; Hotta, H.; Iwahara, H. *J. Appl. Electrochem.* **1994**, *24*, 411.
(206) Sasaki, K.; Wurth, J. P.; Gschwend, R.; Godickemeier, M.; Gauckler, L. J. *J. Electrochem. Soc.* **1996**, *143*, 530.

(207) Fukunaga, H.; Ihara, M.; Sakaki, K.; Yamada, K. *Solid State Ionics* **1996**, *86−88*, 1179.
(208) van Heuveln, F. H.; Bouwmeester, H. J. M.; vanBerkel, F. P. F. *J. Electrochem. Soc.* **1997**, *144*, 126.
(209) van Heuveln, F. H.; Bouwmeester, H. J. M. *J. Electrochem. Soc.* **1997**, *144*, 134.
(210) Ostergard, M. J. L.; Mogensen, M. *Electrochim. Acta* **1993**, *38*, 2015.
(211) Siebert, E.; Hammouche, A.; Kleitz, M. *Electrochim. Acta* **1995**, *40*, 1741.
(212) Lauret, H.; Hammou, A. *J. Eur. Ceram. Soc.* **1996**, *16*, 447.
(213) Lee, H. Y.; Cho, W. S.; Oh, S. M.; Wiemhofer, H. D.; Gopel, W. *J. Electrochem. Soc.* **1995**, *142*, 2659.
(214) Kuznecov, M.; Otschik, P.; Obenaus, P.; Eichler, K.; Schaffrath, W. *Solid State Ionics* **2003**, *157*, 371.
(215) Mitterdorfer, A.; Gauckler, L. J. *Solid State Ionics* **1998**, *111*, 185.
(216) Poulsen, F. W. *Solid State Ionics* **2000**, *129*, 145.
(217) Chakraborty, A.; Choudhury, P.; Maiti, H. S. *Proc. Electrochem. Soc.* **1995**, *95−1*, 612.
(218) Kim, M. C.; Park, S. J. *Yoop Hakhoechi* **1992**, *29*, 900.
(219) Li, Z.; Behruzi, M.; Fuerst, L.; Stoever, D. *Proc. Electrochem. Soc.* **1993**, *93−4*, 171.
(220) Hammouche, A.; Siebert, E.; Hammou, A.; Kleitz, M.; Caneiro, A. *J. Electrochem. Soc.* **1991**, *138*, 1212.
(221) Tofield, B. C.; Scott, W. R. *J. Solid State Chem.* **1974**, *10*, 183.
(222) Yokokawa, H.; Horita, T.; Sakai, N.; Dokiya, M.; Kawada, T. *Solid State Ionics* **1996**, *86−88*, 1161.
(223) Tanasescu, S.; Totir, N. D.; Marchidan, D. I. *Electrochim. Acta* **1998**, *43*, 1675.
(224) Hammouche, A.; Siebert, E.; Kleitz, M.; Hammou, A. *Proc. Electrochem. Soc.* **1989**, *89−11*, 265.
(225) Hammouche, A.; Siebert, E.; Hammou, A.; Kleitz, M.; Caneiro, A. *J. Electrochem. Soc.* **1991**, *138*, 1212.
(226) Jiang, S. P.; Love, J. G. *Solid State Ionics* **2001**, *138*, 183.
(227) Horita, T.; Yamaji, K.; Sakai, N.; Yokokawa, H.; Kato, T. *J. Electrochem. Soc.* **2001**, *148*, J25.
(228) Brichzin, V.; Fleig, J.; Habermeier, H. U.; Cristiani, G.; Maier, J. *Solid State Ionics* **2002**, *152−153*, 499.
(229) Horita, T.; Yamaji, K.; Ishikawa, M.; Sakai, N.; Yokokawa, H.; Kawada, T.; Kato, T. *J. Electrochem. Soc.* **1998**, *145*, 3196.
(230) Horita, T.; Yamaji, K.; Sakai, N.; Yokokawa, H.; Kawada, T.; Kato, T. *Solid State Ionics* **2000**, *127*, 55.
(231) Horita, T.; Yamaji, K.; Sakai, N.; Xiong, X. P.; Kato, T.; Yokokawa, H.; Kawada, T. *J. Power Sources* **2002**, *106*, 224.
(232) Jiang, Y.; Wang, S.; Zhang, Y.; Yan, J.; Li, W. *Solid State Ionics* **1998**, *110*, 111.
(233) Jiang, Y.; Wang, S.; Zhang, Y.; Yan, J.; Li, W. *J. Electrochem. Soc.* **1998**, *145*, 373.
(234) Jorgensen, M. J.; Primdahl, S.; Mogensen, M. *Electrochim. Acta* **1999**, *44*, 4195.
(235) Jiang, S. P.; Love, J. G.; Zhang, J. P.; Hoang, M.; Ramprakash, Y.; Hughes, A. E.; Badwal, S. P. S. *Solid State Ionics* **1999**, *121*, 1.
(236) Tsukuda, H.; Yamashita, A. 1st European Solid Oxide Fuel Cells Forum, Oct 3−7, 1994, Baden, Switzerland, 1994.
(237) Monceau, D.; Petot, C.; Petotervas, G. *Solid State Ionics* **1991**, *45*, 231.
(238) Petot, C.; Armanet, F.; Klimczyk, H.; Petotervas, G. *Solid State Ionics* **1992**, *50*, 87.
(239) Petotervas, G.; Petot, C.; Monceau, D.; Loudjani, M. *Solid State Ionics* **1992**, *53−6*, 270.
(240) Belova, I. V.; Brown, M. J.; Murch, G. E. *Acta Mater.* **2003**, *51*, 1821.
(241) Brown, M. J.; Belova, I. V.; Murch, G. E. *Phil. Mag.* **2003**, *83*, 1855.
(242) Martin, M. *J. Chem. Thermodyn.* **2003**, *35*, 1291.
(243) Kawada, T.; Sakai, N.; Yokokawa, H.; Dokiya, M.; Anzai, I. *Solid State Ionics* **1992**, *50*, 189.
(244) Tedmon, C. S., Jr.; Spacil, H. S.; Mitoff, S. P. *J. Electrochem. Soc.: Electrochem. Sci.* **1969**, *1969*, 1170.
(245) Lau, S. K.; Singhal, S. C. *Proc. Corrosion* **1985**, *85*, 79.
(246) Takeda, Y.; Hoshino, Y.; Sakaki, Y.; Kawahara, T.; Imanishi, N.; Yamamoto, O. *J. Mater. Sci. Lett.* **1992**, *11*, 1113.
(247) Takeda, Y.; Sakaki, Y.; Ichikawa, T.; Imanishi, N.; Yamamoto, O.; Mori, M.; Mori, N.; Abe, T. *Solid State Ionics* **1994**, *72*, 257.
(248) Takeda, Y.; Ueno, H.; Imanishi, N.; Yamamoto, O.; Sammes, N.; Phillipps, M. B. *Solid State Ionics* **1996**, *86−8*, 1187.
(249) Kostogloudis, G. C.; Tsiniarakis, G.; Ftikos, C. Personal communication, 1999.
(250) Chen, C. C.; Nasrallah, M. M.; Anderson, H. U. *Proc. Electrochem. Soc.* **1993**, *93−4*, 598.
(251) Simner, S. P.; Shelton, J. P.; Anderson, M. D.; Stevenson, J. W. *Solid State Ionics* **2003**, *161*, 11.
(252) Yokokawa, H.; Sakai, N.; Kawada, T.; Dokiya, M. *J. Electrochem. Soc.* **1991**, *138*, 2719.
(253) Yokokawa, H.; Sakai, N.; Kawada, T.; Dokiya, M. *Solid State Ionics* **1992**, *52*, 43.
(254) Labrincha, J. A.; Frade, J. R.; Marques, F. M. B. *J. Mater. Sci.* **1993**, *28*, 3809.
(255) Poulsen, F. W.; Vanderpuil, N. *Solid State Ionics* **1992**, *53−6*, 777.
(256) Vanroosmalen, J. A. M.; Cordfunke, E. H. P. *Solid State Ionics* **1992**, *52*, 303.
(257) Yamamoto, O.; Takeda, Y.; Kanno, R.; Kojima, T. First International Symposium on Solid Oxide Fuel Cells, 1989; p 242.
(258) Ostergard, M. J. L.; Clausen, C.; Bagger, C.; Mogensen, M. *Electrochim. Acta* **1995**, *40*, 1971.
(259) Stochniol, G.; Syskakis, E.; Naoumidis, A. *J. Am. Ceram. Soc.* **1995**, *78*, 929.
(260) Stochniol, G.; Broel, S.; Naoumidis, A.; Nickel, H. *Fresenius J. Anal. Chem.* **1996**, *355*, 697.
(261) Kostogloudis, G. C.; Ftikos, C. *Solid State Ionics* **1999**, *126*, 143.
(262) Yokokawa, H.; Horita, T.; Sakai, N.; Kawada, T.; Dokiya, M. First European Solid Oxide Fuel Cell Forum, Baden-Baden, 1994; p 425.
(263) Horita, T.; Yamaji, K.; Negishi, H.; Sakai, N.; Yokokawa, H.; Kato, T. *Solid State Ionics* **2000**, *136−137*, 897.
(264) Clausen, C.; Bagger, C.; Bildesorensen, J. B.; Horsewell, A. *Solid State Ionics* **1994**, *70*, 59.
(265) Mitsuyasu, H.; Eguchi, K.; Arai, H. *Solid State Ionics* **1997**, *100*, 11.
(266) Wiik, K.; Schmidt, C. R.; Shamsili, S.; Einarsrud, M. A.; Grande, T. *High Temp. Electrochem.: Ceram. Met., Proc. Risoe Int. Symp. Mater. Sci., 17th* **1996**, 491−496.
(267) Wiik, K.; Schmidt, C. R.; Faaland, S.; Shamsili, S.; Einarsrud, M.-A.; Grande, T. *J. Am. Ceram. Soc.* **1999**, *82*, 721.
(268) Bertrand, G. L.; Caboche, G.; Domenichini, B.; Dufour, L. C. *Surf. Interface Anal.* **2000**, *30*, 561.
(269) Kuscer, D.; Holc, J.; Hrovat, M.; Bernik, S.; Samardzija, Z.; Kolar, D. *Solid State Ionics* **1995**, *78*, 79.
(270) Bae, J. M.; Steele, B. C. H. *Solid State Ionics* **1998**, *106*, 247.
(271) Dusastre, V.; Steele, B. C. H. Personal communication, 1997.
(272) Appel, C. C.; Bonanos, N. *J. Eur. Ceram. Soc.* **1999**, *19*, 847.
(273) Uchikoshi, T.; Sakka, Y.; Hiraga, K. *J. Electrocer.* **1999**, *4*, 113.
(274) De Souza, M. F.; De Souza, D. P. F. *J. Mater. Sci.* **1999**, *34*, 6107.
(275) Steele, B. C. H. *Solid State Ionics* **2000**, *129*, 95.
(276) Kawada, T.; Sakai, N.; Yokokawa, H.; Dokiya, M. *Solid State Ionics* **1992**, *53−6*, 418.
(277) Manning, P. S.; Sirman, J. D.; Kilner, J. A. *Solid State Ionics* **1996**, *93*, 125.
(278) Manning, P. S.; Sirman, J. D.; De Souza, R. A.; Kilner, J. A. *Solid State Ionics* **1997**, *100*, 1.
(279) Horita, T.; Yamaji, K.; Sakai, N.; Ishikawa, M.; Yokokawa, H.; Kawada, T.; Dokiya, M. *Electrochem. Solid State Lett.* **1998**, *1*, 4.
(280) Bozo, C.; Guilhaume, N.; Herrmann, J. M. *J. Catal.* **2001**, *203*, 393.
(281) Putna, E. S.; Bunluesin, T.; Fan, X. L.; Gorte, R. J.; Vohs, J. M.; Lakis, R. E.; Egami, T. *Catal. Today* **1999**, *50*, 343.
(282) Lu, C.; Worrell, W. L.; Vohs, J. M.; Gorte, R. J. *J. Electrochem. Soc.* **2003**, *150*, A1357.
(283) van Hassel, B. A.; Boukamp, B. A.; Burggraaf, A. J. *Solid State Ionics* **1992**, *53−6*, 890.
(284) van Hassel, B. A.; Burggraaf, A. J. *Solid State Ionics* **1992**, *57*, 193.
(285) Kim, J. H.; Choi, G. M. *Solid State Ionics* **2000**, *130*, 157.
(286) Boukamp, B. A.; Raming, T. P.; Winnubst, A. J. A.; Verweij, H. *Solid State Ionics* **2003**, *158*, 381.
(287) Kahlich, M. J.; Gasteiger, H. A.; Behm, R. J. *J. Catal.* **1999**, *182*, 430.
(288) Liu, H. C.; Kozlov, A. I.; Kozlova, A. P.; Shido, T.; Iwasawa, Y. *Phys. Chem. Chem. Phys.* **1999**, *1*, 2851.
(289) Schubert, M. M.; Hackenberg, S.; van Veen, A. C.; Muhler, M.; Plzak, V.; Behm, R. J. *J. Catal.* **2001**, *197*, 113.
(290) Fabry, P.; Schouler, E.; Kleitz, M. *Electrochim. Acta* **1978**, *23*, 539.
(291) Lane, J. A.; Middleton, P. H.; Fox, H.; Steele, B. C. H.; Kilner, J. A. 2nd International Symposium on Ionic and Mixed Conducting Ceramics, 1994; pp 489−504.
(292) Sahibzada, M.; Benson, S. J.; Rudkin, R. A.; Kilner, J. A. *Solid State Ionics* **1998**, *115*, 285.
(293) Chavan, S. V.; Tyagi, A. K. *Thermochim. Acta* **2002**, *390*, 79.
(294) Longo, V.; Meriani, S.; Ricciardiello, F. *J. Am. Ceram. Soc.* **1981**, *64*, C38.
(295) Sorokina, S. L.; Skolis, Y. Y.; Kovba, M. L.; Levitskii, V. A. *Zh. Fiz. Khim.* **1986**, *60*, 310.
(296) Tsai, T.; Barnett, S. A. *Solid State Ionics* **1997**, *98*, 191.
(297) Tsai, T.; Perry, E.; Barnett, S. *J. Electrochem. Soc.* **1997**, *144*, L130.
(298) Simner, S. P.; Bonnett, J. F.; Canfield, N. L.; Meinhardt, K. D.; Sprenkle, V. L.; Stevenson, J. W. *Electrochem. Solid State Lett.* **2002**, *5*, A173.
(299) Simner, S. P.; Bonnett, J. R.; Canfield, N. L.; Meinhardt, K. D.; Shelton, J. P.; Sprenkle, V. L.; Stevenson, J. W. *J. Power Sources* **2003**, *113*, 1.

(300) Kenjo, T.; Osawa, S.; Fujikawa, K. *J. Electrochem. Soc.* **1991**, *138*, 349.
(301) Kenjo, T.; Nishiya, M. *Solid State Ionics* **1992**, *57*, 295.
(302) Austin, L. G.; Ariet, M.; Walker, R. D.; Wood, G. B.; Comyn, R. H. *Ind. Eng. Chem. Fundam.* **1965**, *4*, 321.
(303) Newman, J.; Tiedemann, W. *AIChE J.* **1975**, *21*, 25.
(304) Juhl, M.; Primdahl, S.; Manon, C.; Mogensen, M. *J. Power Sources* **1996**, *61*, 173.
(305) Mogensen, M.; Skaarup, S. *Solid State Ionics* **1996**, *86*−*88*, 1151.
(306) Tanner, C. W.; Fung, K. Z.; Virkar, A. V. *J. Electrochem. Soc.* **1997**, *144*, 21.
(307) Virkar, A. V.; Chen, J.; Tanner, C. W.; Kim, J. W. *Solid State Ionics* **2000**, *131*, 189.
(308) Kim, J. D.; Kim, G. D.; Moon, J. W.; Lee, H. W.; Lee, K. T.; Kim, C. E. *Solid State Ionics* **2000**, *133*, 67.
(309) Kim, J.-D.; Kim, G.-D.; Park, J.-A. *Han'guk Seramik Hakhoechi* **2000**, *37*, 227.
(310) Mogensen, M.; Primdahl, S.; Jorgensen, M. J.; Bagger, C. *J. Electroceram.* **2000**, *5*, 141.
(311) Figueiredo, F. M.; Frade, J. R.; Marques, F. M. B. *Solid State Ionics* **2000**, *135*, 463.
(312) Figueiredo, F. M.; Marques, F. M. B.; Frade, J. R. *J. Electroceram.* **2001**, *7*, 47.
(313) Xia, C.; Rauch, W.; Wellborn, W.; Liu, M. *Electrochem. Solid State Lett.* **2002**, *5*, A217.
(314) Sunde, S. *J. Electroceramics* **2000**, *5*, 153.
(315) Huang, Y.; Vohs, J. M.; Gorte, R. J. Submitted for publication.
(316) Huang, Y.; Ahn, K.; Vohs, J. M.; Gorte, R. J. Submitted for publication.
(317) van Heuveln, F. H.; van Berkel, F. P. F.; Huijsmans, J. P. P. *High-Temperature Electrochemical Behavior of Fast Ion and Mixed Conductors*; Roskilde: Denmark, 1993; p 53.
(318) Fleig, J.; Pham, P.; Sztulzaft, P.; Maier, J. *Solid State Ionics* **1998**, *113*−*115*, 739.
(319) Adler, S. B. *J. Electrochem. Soc.* **2002**, *149*, E166.
(320) McIntosh, S.; Vohs, J. M.; Gorte, R. J. *J. Electrochem. Soc.* **2003**, *150*, A470.
(321) Singhal, S. C. *Solid Oxide Fuel Cells V*; Aachen: Germany, 1997; pp 37−50.
(322) Choi, J. H.; Jang, J. H.; Ryu, J. H.; Oh, S. M. *J. Power Sources* **2000**, *87*, 92.
(323) Minh, N. Q. *J. Am. Ceram. Soc.* **1993**, *76*, 563.
(324) Iwata, T. *J. Electrochem. Soc.* **1996**, *143*, 1521.
(325) Murata, K.; Shimotsu, M. *Electrochem.* **1999**, *67*, 789.
(326) Primdahl, S.; Mogensen, M. *J. Appl. Electrochem.* **2000**, *30*, 247.
(327) Umemura, F.; Amano, K.; Michibata, H.; Kimura, A. *Denki Kagaku* **1995**, *63*, 128.
(328) Choi, J. H.; Jang, J. H.; Oh, S. M. *Electrochim. Acta* **2001**, *46*, 867874.
(329) Jiang, S. P.; Love, J. G. *Solid State Ionics* **2003**, *158*, 45.
(330) Hilpert, K.; Das, D.; Miller, M.; Peck, D. H.; Weiss, R. *J. Electrochem. Soc.* **1996**, *143*, 3642.
(331) Quadakkers, W. J.; Greiner, H.; Hansel, M.; Pattanaik, A.; Khanna, A. S.; Mallener, W. *Solid State Ionics* **1996**, *91*, 55.
(332) Badwal, S. P. S.; Deller, R.; Foger, K.; Ramprakash, Y.; Zhang, J. P. *Solid State Ionics* **1997**, *99*, 297.
(333) Matsuzaki, Y.; Yasuda, I. *Solid State Ionics* **2000**, *132*, 271.
(334) Matsuzaki, Y.; Yasuda, I. *J. Electrochem. Soc.* **2001**, *148*, A126.
(335) Jiang, S. P.; Zhang, J. P.; Zheng, X. G. *J. Eur. Ceram. Soc.* **2002**, *22*, 361.
(336) Lee, H. Y.; Oh, S. M. *Solid State Ionics* **1996**, *90*, 133.
(337) Tu, H. Y.; Takeda, Y.; Imanishi, N.; Yamamoto, O. *Solid State Ionics* **1997**, *100*, 283.
(338) Brant, M. C.; Dessemond, L. *Solid State Ionics* **2000**, *138*, 1.
(339) Brant, M. C.; Matencio, T.; Dessemond, L.; Domingues, R. Z. *Chem. Mater.* **2001**, *13*, 3954.
(340) Khandkar, A. C.; Elangovan, S.; Liu, M.; Timper, M. *Thermal Cycle Fatigue Behavior of High-Temperature Electrodes*; Ceramatec, Inc.: 1994.
(341) Hsiao, Y. C.; Selman, J. R. *Solid State Ionics* **1997**, *98*, 33.
(342) Primdahl, S.; Mogensen, M. *J. Electrochem. Soc.* **1998**, *145*, 2431.
(343) Primdahl, S.; Mogensen, M. *J. Electrochem. Soc.* **1999**, *146*, 2827.
(344) Deng, H.; Zhou, M.; Abeles, B. *Solid State Ionics* **1994**, 1.
(345) van Herle, J.; McEnvoy, A. J.; Thampi, K. R. *Electrochim. Acta* **1996**, *41*, 1447.
(346) Kim, J. D.; Kim, G. D.; Moon, J. W.; Park, Y. I.; Lee, W. H.; Kobayashi, K.; Nagai, M.; Kim, C. E. *Solid State Ionics* **2001**, *143*, 379.
(347) Yoon, S. P.; Nam, S. W.; Kim, S.-G.; Hong, S.-A.; Hyun, S.-H. *J. Power Sources* **2003**, *115*, 27.
(348) Bird, R. B.; Stewart, W. E.; Lightfoot, E. N. *Transport Phenomena*, 2nd ed.; John Wiley and Sons: New York, 2002.
(349) *Perry's Chemical Engineers' Handbook*, 50th ed.; Perry, R. H., Green, D. W., Maloney, J. O., Eds.; McGraw-Hill: New York, 1984.
(350) Adler, S. B.; Henderson, B. T.; Wilson, M. A.; Taylor, D. M.; Richards, R. E. *Solid State Ionics* **2000**, *134*, 35.
(351) Nagata, M.; Itoh, Y.; Iwahara, H. *Solid State Ionics* **1994**, *67*, 215.
(352) Hsieh, G.; Mason, T. O.; Garboczi, E. J.; Pederson, L. R. *Solid State Ionics* **1997**, *96*, 153.
(353) Winkler, J.; Hendriksen, P. V.; Bonanos, N.; Mogensen, M. *J. Electrochem. Soc.* **1998**, *145*, 1184.
(354) Figueiredo, F. M.; Frade, J.; Marques, F. M. B. *Boletin De La Sociedad Espanola De Ceramica Y Vidrio* **1999**, *38*, 639.
(355) Kato, T.; Momma, A.; Kaga, Y.; Nagata, S.; Kasuga, Y.; Kitase, M. *Solid State Ionics* **2000**, *132*, 287.
(356) Myland, J. C.; Oldham, K. B. *Anal. Chem.* **2000**, *72*, 3972.
(357) Oldham, K. B.; Stevens, N. P. C. *Anal. Chem.* **2000**, *72*, 3981.
(358) Boukamp, B. A. *Solid State Ionics* **2001**, *143*, 47.
(359) Hashibon, A.; Raz, S.; Riess, I. *Solid State Ionics* **2002**, *149*, 167.
(360) Fleig, J. *Solid State Ionics* **2003**, *161*, 279.
(361) Adler, S. B. Manuscript in preparation.
(362) Bard, A. J.; Faulkner, L. R. *Electrochemical Methods*, 2nd ed.; John Wiley and Sons: 2001.
(363) Vetter, K. J.; Manecke, G. *Z. Phys. Chem.* **1950**, *195*, 337.
(364) Jimenez, R.; Kloidt, T.; Kleitz, M. *J. Electrochem. Soc.* **1997**, *144*, 582.
(365) Kuo, J. H.; Anderson, H. U.; Sparlin, D. M. *J. Solid State Chem.* **1989**, *83*, 52.
(366) In prior publications (refs 28 and 168) the term "non-charge-transfer" has been used to describe such neutral flows. However, this terminology has sometimes generated unintended confusion and/or controversy, since many chemical processes not resulting in a net flow of current do involve charge transfer at the atomic/molecular level (e.g., chemisorption). To avoid this confusion, the term "chemical" is hereby instated in this review to describe processes that are driven by chemical potential driving forces and may occur at a rate decoupled from the faradaic current while the term "electrochemical" is restricted to processes involving net passage of faradaic (noninterfacially polarizing) current due to an electrochemical potential driving force.
(367) In this case the exchange coefficient k has units of s^{-1} (rather than the usual cm/s) because of the reduced dimensionality of the system, i.e., fluxes are written in terms of surface concentrations rather than volumetric concentration.
(368) For this estimate, values for the surface diffusion coefficient (D) and the surface exchange coefficient (k) in eq 2 were obtained by linearizing Mitterdorfer's rate expressions for surface transport and adsorption/desorption (ref 84) and re-expressing in terms of the driving forces in eq 2.
(369) These expressions for R_{chem}, $C_{l\delta}$, and l_δ have the same meaning as R_{chem}, $C_{chem} = (t_{chem}/R_{chem})$, and δ, respectively, as defined in the original cited articles (refs 171 and 28). However, the nomenclature and parameters used here have been updated both to aid clarity and improve consistency with eqs 3−7. In particular, the length parameter previously symbolized as "δ" in the cited papers has been renamed "l_δ" to avoid confusion with the oxygen nonstoichiometry δ in $ABO_{3-\delta}$. The subscript on the chemical capacitance has also been made more specific to indicate the size of the region disturbed by concentration gradients.

CR020724O